d'Collection

Thesis for the Degree of Doctor of Philosophy

Crashworthiness Assessment of Ship Structures under Collision and Grounding

by

Aditya Rio Prabowo

Interdisciplinary Program of Marine Convergence Design

The Graduate School

Pukyong National University

August 2018

Crashworthiness Assessment of Ship Structures under Collision and Grounding

충돌 및 좌초 사고 시 선박 구조의 내구성 평가

Advisor: Prof. Jung Min Sohn

by

Aditya Rio Prabowo

A thesis submitted in partial fulfilment of the requirements

for the degree of

Doctor of Philosophy

in the Interdisciplinary Program of Marine Convergence Design

The Graduate School

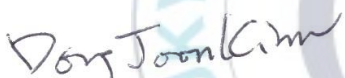Pukyong National University

August 2018

Crashworthiness Assessment of Ship Structures under Collision and Grounding

A dissertation

By

Aditya Rio Prabowo

Approved by:

_____
(Chairman) Prof. Dong Joon Kim

_____
(Member) Prof. Dong Myung Bae

_____
(Member) Prof. Joung Hyung Cho

_____
(Member) Prof. Sung Yong Bae

_____
(Member) Prof. Jung Min Sohn

August 2018

Contents

i

List of Figures

iv

List of Tables

Crashworthiness Assessment of Ship Structures under Collision and Grounding

Aditya Rio Prabowo

Interdisciplinary Program of Marine Convergence Design,

The Graduate School, Pukyong National University

Abstract

Casualties of accidental load type have been found unacceptable in terms of human life losses and financial collapse. Likewise, structural casualties on ships carrying hazardous cargo may trigger further disasters with remarkable consequences, such as pollution of maritime environments due to oil outflow. As responds of these large risks, sustainable developments are addressed since middle of the 19th century to provide safety of ship structures and fundamental international regulations. Taking part in those development efforts, this thesis directs its focus to observe characteristic of the crashworthy steel-based marine structures, as part of passive protection for ship structure against impact. The analysis results, i.e. critical scenario and structural performance are discussed. They will be summarized as reasonable references to provide insight in minimizing impact consequences.

Research in this thesis was begun by conducting several calculations to validate the numerical method applied in the collision and grounding analyses. Experimental tests on reduced scale of 1 side-frame panel from a medium size tanker were modelled and calculated as the benchmark reference for analysis. In the discussion, current solution of the numerical method was compared to data of the experimental results. Result cross-check was addressed to similarity in terms of structural response, and effectiveness of time process.

After verified configuration was obtained, firstly, a series of study was conducted to understand structural behavior under collision based on the fundamental parameters available in the literature. Applied parameters were classified into the external dynamics, such as location, angle and speed, and internal mechanics, i.e. structure and steel types. In the external dynamics, it was found that structural condition was relative better in perpendicular collision than oblique collision. For the internal mechanics, structural design with stiffener and wider

double hull showed the best collision resistance. The later analysis was designed to offer rational reference for establishment speed limit regulation in strait territory. According to the analysis, it can be obtained that the recommended speed for the strait is in range 5~10 kts when a crossing situation (reefer to Collision Regulations-COLREGS description) occurs. Possibility of a new phenomenon during ship-ship collision was also considered. Rebounding of the striking ship was analyzed to compare its influence to crashworthy single and double hulls. Results indicated that, compared to continuous increment of the fully struck assumption, the internal energy and crushing force produced peak point in certain collision time, and then the tendency declined until it reached zero.

Apart of ship collision, in the second part, other accidental load was observed in terms of grounding actions. A comparative study of raking and stranding cases was conducted to obtain information regarding behavior of double bottom against several structural penetrations and obstruction topologies. It was obtained that the double bottom structure was weaker against the stranding than the raking. In terms of the obstruction, a conclusion was taken that wider baseline and steeper angle was capable to inflict more damage on double bottom. Other parameters in grounding were assessed in the next research by applying alternative external parameters, such as elevation and angle. For these parameters, the transition of the damage extent was concluded to take place in the impact elevation 0.0125 m, while contribution of the longitudinal stiffener became remarkable in oblique grounding.

Overall results of this thesis are encouraged to be applied as reasonable reference in future collision and grounding analyses on marine structures.

Keywords: Collision and grounding, crashworthiness criteria, Finite Element Method (FEM), modelling of nonlinear phenomena, external dynamics and internal mechanics, speed limit regulation, rebounding of the striking ship, bottom raking and ship stranding.

I. Introduction

1. Overview and Background

Human race who lives separately on various islands across the globe, has always an urges to interact and engage in trading with his fellow in remote or different islands. High mobility possessed by men has pushed them to explore sea since the beginning of the recorded history. Advance stride of public society and growth of human population, inter-island activity gets significantly increasing. In this situation, role of water transportation mode - ship becomes vital, both to support demands as a public facility, and necessities for product carrier distribution. For millennia, men have built various types of ships, and developed numbers of supporting instruments for voyage operation. In the recent decade itself, modern merchants appear as high technological structures and remarkable diversity of function and type, which are evidences of the developments conducted by naval architects and marine engineers.

| (a) | (b) |

Figure 1.1. Accidental loads on maritime environments: (a) ship collision incident, and (b) a tanker runs aground.

Nowadays, there are growing demands to reduce risk of ship damage due to encounter with accidental loads in their operations. Famous examples of accidental events and their casualties (see illustrations in Figure 1.1) are given as follows: ill-fated maiden voyages of the Titanic during ice collision in 1912, mass destruction of water territory and wide extinction of species after the Exxon Valdez ran aground in 1989, and notable cruise grounding and foundering of the Costa Concordia in the twentieth century (Allianz, 2012). Considering casualties and occurred frequency on maritime environment based on compiled marine accident in Table 1.1 and compiled data by Allianz (2017) in Figure 1.2, collision

and grounding are found as the biggest threat on ships in terms of the accidental loads between two solid entities. Therefore, recorded history of naval architecture cannot deny that these phenomena are behind of drastic revolutions on ship technology and regulation.

Table 1.1. Notable marine accidents in form accidental loads.

Ship Name	Location	Year	Major Casualties
RMS Titanic	Atlantic ocean, US	1912	Life losses
			Environment casualties
Exxon Valdez	Prince William Sound, Alaska	1989	Environmental damage
			Oil spillage
USS Port Royal	Hawaii, US	2009	Structural damage
MV Shen Neng 1	Rockhampton, Australia	2010	Oil spillage
			Reef damage
Costa Concordia	Off Isola del Giglio, Italy	2012	Human life losses
			Structural damage
			Environmental damage
Nora Victoria	Finnoy Island, Norway	2014	Environmental damage
			Oil spillage
			Cargo damage
Hanjin	Sunda Strait, Indonesia	2015	Structural damage
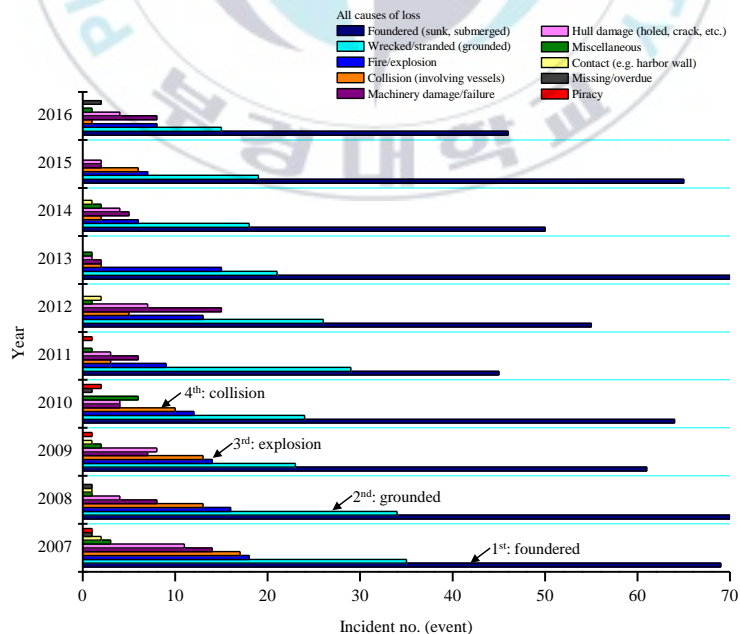
Figure 1.2. Summary of the ship loss due to accidental and non-accidental causes (Allianz, 2017).

With collision and grounding as causes of remarkable casualties, it is clear that subject of rational designs of ship structure against accidental loads can be addressed to highly varying topics, including expected scenario, calculation method and territory regulation. Background of this statement is also supported by relation between improvement of shipping safety and huge consequence of marine pollution. These parties are inextricably linked, and protection of the environment from major disaster, such as shipwreck and oil spill, is rather complex. Means for the protections can be divided into two classes, the active and passive methods. The first one is conducted by deploying navigational instrument, experienced crew and traffic control to prevent an accident from taking place. The second method is effort to minimize the accident's casualties such as by development of crashworthy hull structures and mitigation process. The rational design and passive protection have been heavily connected to assessments of the structural performance under collision and grounding. Even after these developments, these areas still possess many unsolved problems, and nonlinearity characteristic of the accidental loads require sustainable assessment.

Initially, concern of ship structures against accidental loads was addressed on nuclear powered ship by Minorsky (1958). His empirical expression to predict the absorbed energy in collision was later developed by Woisin (1979). Other notable findings for rapid estimation formula were also provided by Zhang (1999). Besides collision phenomena, ship grounding is also concerned as terrible cause of maritime damage. Observation by analytical theory of ship grounding was presented by Simonsen (1997a-b), including its validation on the experimental tests. After several years of these findings, analytical method is extended to assess structural responses of the double bottom over large contact surfaces (Hu et al., 2011), estimating structural resistance in side structure-bulbous bow interaction under side collision (Haris and Amdahl, 2013), and evaluating crushing stages of the local members, such as web and girder during structures encounter collision and grounding (Liu and Soares, 2015).

Advance improvements of the computational instruments make numerical codes are widely used to assess science and engineering phenomena. In cases of the ship collision and grounding, numerical methods is applied to predict structural behavior and damage extent, which one of the most popular methods is the finite element (FE) method. Challenge to define reasonable numerical model rises to be a main topic as analysis using this method is demanded to be solved in reasonable time process, and should be considering effectiveness and reliability (Bathe, 1996). Application of the FE is more inclusive during collision and grounding (Prabowo et al., 2017a-k) are assumed as nonlinear phenomena. Explicit methodology is often preferred, and observation using this strategy is intensively conducted

3

at the same time with rapid evolution of computing technology. Several literatures which also use the FE for solving accidental loads are summarized, and its tendency indicates that this method is well enough to reproduce similar results compared to actual phenomena. To reach this satisfactory, several works as conducted by Sormunen et al. (2016), Calle et al. (2017) and Prabowo et al. (2017l-o), consider experimental test as a benchmark, and/or seek confirmation of the FE setting by conducting calculations using either empirical or analytical method. The research fashion in collaborating such methods is considered as good and recommended methodology since reliability of the main methodology can be guaranteed by cross-checking results.

2. State-of-the-art

Impact phenomena are wide range research opportunity, and several researches have been described in prior sub-chapter. Related to maritime environment, effort to protect sea from various casualties caused by collision and grounding, e.g. oil spill, is divided into two major groups. The first group is the active method which addresses its target to refine navigational instrument to avoid the accidents take place. The second group is called as the passive method which aims to reduce casualties during impact occurs. Most of researches as summarized in Tables 1.2 to 1.4, on the passive method are giving their focus on structural behavior and crashworthiness capability during ship structure under impact load.

Table 1.2. Summary of the past researches on collision and grounding - before 2000.

Source	Considered impact problem	Methodology	Modelled phenomenon	Validation	Remarkable notes
Paik et al. (1994)	Ship grounding	Laboratory test	Load and absorbed energy	-	Damage characteristic and structural response as benchmark
Paik and Pedersen (1995)	Hull panel - indenter interaction	Idealized structural unit method	Collision force, energy and analytical deformed shape	Model test of double-skin plated structures	Behaviour of critical energy
Simonsen (1997a-b)	Ship grounding	Theoretical analysis	Energy, force and damage contour	Laboratory test: double bottom's rupture test	Theoretical model is sufficiently fast to be used in a probabilistic framework to calculate distributions of bottom damage

Table 1.3. Summary of the past researches on collision and grounding - 2000 to 2015.

Source	Considered impact problem	Methodology	Modelled phenomenon	Validation	Remarkable notes
Simonsen and Hansen (2000)	Ship grounding	Theoretical and statistical analysis	Damage distribution	-	Regulations assumed to be proportional to the ship length
Kitamura (2002)	Collision and grounding damage	Finite element analysis	Damage contour and contact force	-	To obtain good accuracy and practicality, the study must be based on the data on the actual Accidents and physical experiments
Wiśniewski and Kołakowski (2003)	Ship collision	Finite element analysis	Energy, crushing force and damage	Laboratory test: impacted plate panel	Large deformations and plastic strains dominate in the struck ship
Ozguc et al. (2005)	Ship collision	Finite element analysis	Internal energy and crushing mode	Laboratory test: double side structure model	Damage induced by collision reduces the ultimate resistance of the ship hull girder
Alsos and Amdahl (2007)	Ship stranding	Finite element analysis	Load, crushing mode, bending moment	Mesh convergence	Buckling of the longitudinal sections severely reduces the capacity of the hull
Alsos and Amdahl (2009)	Panel impact (struck)	Laboratory experiment	Force and damage contour	-	Increasing the stiffness of the panel reduces the ductility of the structure
Alsos et al. (2009)	Panel impact (struck)	Finite element analysis	Force and damage contour	Laboratory test: impacted plate panel	When strain gradients do not dominate, the mesh effect at onset of fracture vanishes
AbuBakar and Dow (2013)	Ship grounding	Finite element method	Force and damage contour	Laboratory test: impacted plate panel	Results demonstrates that FEA is an appropriate tool which can be used to investigate the local and global behaviour of a ship's structure
Yeom and Nho (2015)	Panel impact (struck)	Finite element analysis	Damage contour and load ratio	-	Structural redundancy can be obtained by increasing plate thickness
Yu et al. (2015)	Ship grounding	Theoretical analysis	Energy and damage contour	Finite element method	A simplified model for stiffeners on longitudinal girders was proposed, which captured major observed characteristics of deformation modes

Table 1.4. Summary of the past researches on collision and grounding - after 2015.

Source	Considered impact problem	Methodology	Modelled phenomenon	Validation	Remarkable notes
Liu and Soares (2015)	Ship collision and grounding	Theoretical analysis	Energy, force and damage contour	Finite element analysis and lab. test: girder crushing	A new simplified analytical method is proposed to examine the crushing resistance of web girders
Heinvee and Tabri (2015)	Ship grounding	Finite element analysis	Force and opening width	-	Simplified formulas to evaluate the damage opening size in tanker groundings were derived and presented.
Sormunen et al. (2016)	Ship grounding	Finite element analysis	Energy and damage contour	Field survey: oceanic rock topology	Grounding damage greatly depends on rock surface
Liu et al. (2017a)	Ship collision	Laboratory test and finite element analysis	Energy and force	Laboratory test: impacted plate panel	A new expression to estimate the critical failure strain is introduced
Haag (2017)	Ship grounding	Laboratory test and finite element analysis	Acceleration, force and stress	Laboratory test: impacted plate panel	A novel methodology in measuring hull structures subjected to raking
Baek et al. (2018)	Ship-ship collision	Intelligent supersize finite element method	Residual ultimate hull strength	Actual data of residual ultimate strength	Estimation technique for prevention secondary accident
Cho et al. (2018)	Lateral impact	Laboratory test and finite element analysis	Energy, deflection and damage contour	Laboratory test: impacted plate	Strain-rate is concluded as main cause of scale effect

Review on the presented list concludes that impact engineering in terms of collision and grounding has been widely developed, in crashworthiness criteria (energy, force/load and damage), benchmark data, involved objects/structures and designed scenario, particularly. To achieve satisfactory for the mentioned elements, calculation technique and instrument are perpendicularly improved, such as laboratory test, finite element method and statistical analysis. These methods are usually combined in collision and grounding researches to provide convincing and reliable result, e.g. experimental test and finite element analysis. According to several researches such as Wiśniewski and Kołakowski (2003), Alsos et al. (2009), Liu et al. (2017a) and Cho et al. (2018), experimental test is performed, and the obtained result data is intended as initial benchmark data to verify configuration of finite

element analysis. As alternative, experimental data of pioneer works is judged well enough to be reference data, and can be used to validate simulation by numerical analysis, such as conducted by Ozguc et al. (2005) and AbuBakar and Dow (2013). However, despite of all these achievements, calculation technique by combining a test and computational technique still leave numbers of problem, for example applied mesh in the designed numerical model. It is a fundamental concept that mesh size is important element in numerical calculation as it directly influences the responses (energy and damage). However, in pioneer researches, such Alsos and Amdahl (2007) and Sormunen et al. (2016), application of arbitrary very fine mesh is still considered as the most powerful, but it is clear that computational time is neglected in consideration. Observing in proposed criteria of Bathe (1996), the arbitrary very fine mesh may fulfil reliability conditions (similarity of structural response, etc.), but effectiveness criterion is not obeyed, as can be assessed from research time. Therefore, the current study is addressed to conduct a comparative study to obtain more advance meshing strategy which fulfil both of finite element criteria, and can be widely used in various impact simulations.

Quantification of marine accident has been performed in order to understand complicated phenomena, such collision and grounding. Development of theoretical and statistical methods are conducted on ship grounding such as by Simonsen and Hansen (2000). Advantage from this kind of research is increase possibility to increase active protection (effort to avoid occurrence of the accidental phenomena) by performing fast estimation related to expected damage on the ship under impact. Nevertheless, application of this technique is still less sound in reducing casualties of ship, human life and environment during accident, especially on high-traffic marine territory or so called maritime chokepoints. Therefore, establishment more active regulation on critical territory has to be done in near future. As one of concrete-solid effort to the mentioned idea, through this study, it is newly proposed speed limit regulation for maritime chokepoint. Specific chokepoint and collision scenario in the location are selected for observation and inputted element in the study.

Observation on ship collision as part of impact phenomena has been performed since Minorsky initially proposed empirical formula for high-energy impact in 1958. Main assumption which widely used since then is the striking ship will be fully struck on the target ship after collision process. However, it is also found that possibility of the target ship to experience sinking and capsize after collision, is exist. Besides such events on the target ship, another phenomenon is expected to occur on the striking ship. The proposed idea of ship rebounding is introduced on a part of this dissertation. Significance of this phenomenon on structural crashworthiness is quantified, with expanded ship-ship collision scenarios are

conducted by involving various ships. This scenario approach on collision phenomena is intended to widened knowledge and insight related parties in this research field, as well as to provide constructive yet practical assumption in collision analysis and simulation.

Besides ship collision, concern to other impact phenomena on maritime territory is addressed by analyzing structural condition under grounding action. Basically, according to penetration preference/direction on the ship, the grounding is divided into two main groups, i.e. bottom raking and ship stranding. Pioneer works such as by Heinvee and Tabri (2015) and Alsos and Amdahl (2007) are directing their focus on the raking and stranding cases, consecutively. Nevertheless, direct comparison of two groups in terms of structural casualties and progressive failure has yet performed, since researchers tend to focus on one phenomenon, and explore occurred structural responses during ship experiences such impact actions. In reality, combined observation on raking and stranding is considered important and urgently needed as it is vital stage in estimating passive protection (structural analysis to reduce casualties during impact) of ship structure. Therefore, a comparative study to quantify significance of two elements in grounding action, is to be conducted. Other designed scenarios to quantify effect of encountered oceanic obstruction are analyzed to provide complete crashworthiness assessment.

3. Objectives and Scope of the Research

The scope of this research is primarily to conduct crashworthiness assessment of various ship structures under collision and grounding actions, and to provide new insight and knowledge in terms of scenario variety, numerical calculation and territory regulation related to accidental loads on marine engineering. To satisfy primary scopes of the research, selected specific objectives are set and to be completed within this work.

The first objective is addressed to obtain verified NLFEM procedures for ship collision and grounding analyses. An experimental test of panel resistance against penetration of solid indenter is re-modelled and simulated. Results of test and simulation will be compared to check validity of current configurations.

The second objective is set to understand behaviors of crashworthiness criteria subjected varying scenarios. Parameters in the designed scenarios cover the external dynamics, internal mechanics and numerical factors involved in the FE analysis. Further assessment on full-ship regions is conducted to evaluate damage severity after impact, and they are summarized to provide rational references for proposing an alternatives speed limit in critical strait territory.

The third objective focuses to discover a state-of-the-art in assuming collision scenarios accounting for the side-bow interaction. A terminology of *rebounding* is selected to be the main idea. Significance of the new scenario is to be compared with the existing assumptions.

The fourth objective aims to observe structural crashworthiness accounting for variety of ship grounding scenarios. The proposed impact configurations in the comparative study are designed based on two fundamental concepts, namely raking and stranding.

4. Outline of the Thesis

The thesis is composed into seven chapters which in each chapter, selected topic is discussed according to the designed objectives. Brief description of these chapters are summarized as follows:

1. Chapter I presents initial description of background, and several overviews of related literatures in collision and grounding. Research objectives and scope of the research are described with outline of the overall works.

2. Chapter II is devoted to conduct benchmark analysis according to experimental test data. Implementation of the FE procedures to solve nonlinear phenomena, such as impact is described, which also covers validation of the applied FE configurations.

3. Chapter III gives examples of a number of collision analysis using specific ship region subjected to external dynamics and internal mechanics parameters. Analysis of full-ship regions is conducted in the next stage in order to obtain global response of the selected ship. Results are summarized to present adequate references for proposing alternative speed limit regulation.

4. Chapter IV investigates a new phenomenon in ship collision scenario, namely rebounding of the striking ship. Significance of this subject is to be compared in terms of structural crashworthiness with the existing assumption.

5. Chapter V directs its focus to investigate structural responses based on the fundamental grounding cases. Target member and seabed topology are considered during grounding action occurs on the thin-walled double bottom under raking and stranding cases.

6. Chapter VI contains several conclusions and recommendations for future work in topics of marine-accidental loads.

5. Flow Diagram

Based on described comprehensive background and research objective in the pioneer sections, flow diagram as illustrated in Figure 1.3 is presented to provide better grasp and understanding related to concept and process of the compiled research in this dissertation.
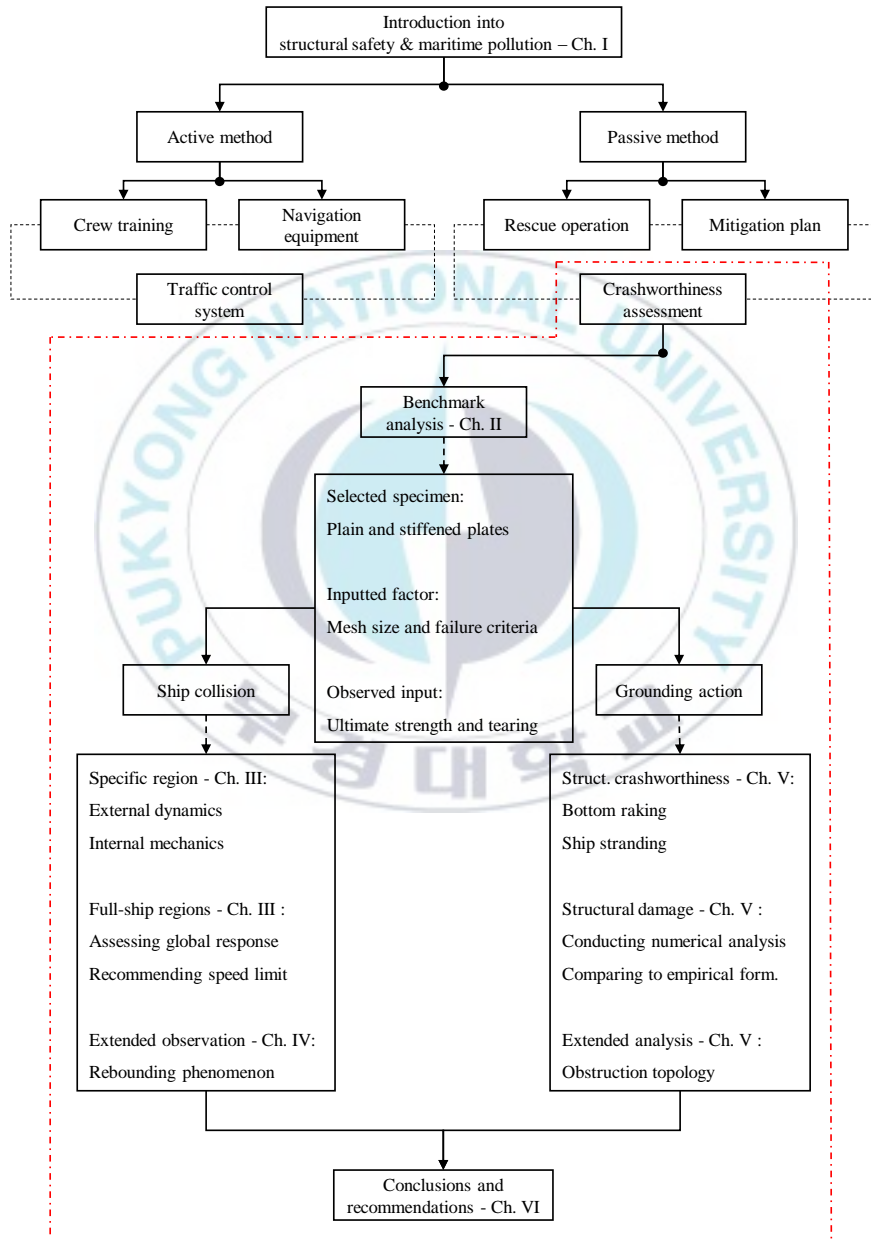
Figure 1.3. Research diagram of the present dissertation.

II. Benchmark Test and Analysis: Plate under Impact Load

Calculation using numerical methodology requires verification to ensure the technique can provide reliable and effective results. Experimental test is adopted in this study to be used as benchmark data which represents actual phenomena. Designed panel structure (see Ozguc et al., 2005; Haris and Amdahl, 2013; Liu et al., 2017a) is preferred since large-scale experiments as conducted in Germany, Japan and The Netherlands (Zhang, 1999) have been considered very costly, and requires large amount of effort with high risk of failure.

1. Test Reference

The numerical simulation methodology in this work will be validated with a benchmark study to ensure that the method can produce reliable results. The study is performed by changing the mesh with respect to collision force and indenter displacement in order to verify the numerical method. Numerical analysis on this chapter is to be conducted based on experimental impact test using a reduced-scaled medium-size tanker panel subjected to the penetration of a rigid indenter (Alsos and Amdahl, 2009). Illustrations of the pioneer test are presented in Figure 2.1. The test is taken as reference for this work as it is highly recommended to validate marine accidental loads, i.e. collision and grounding.

(a)   (b)

Figure 2.1. Experimental setup: (a) initial position of test configuration, and (b) penetration on the panel specimen.

2. Experiment Preparation

The experimental impact test was conducted on the stiffened panel which was set to be laterally impacted by the conical indenter. This test will be re-modelled and calculated using numerical methods. Specimen setup uses two panel types, namely plain and stiffened plates as

the target. Materials of the panel are alphabetically denoted (see Table 2.1) as indicated on manufactured specimen in the actual test. The test will be carried out numerically using the finite element codes ANSYS LS-DYNA (ANSYS, 2017) on a high performance computer with general specification as follows: the 4th Generation Intel Core i7-4790 Processor 4.00 GHz; memory 16 GB RAM; SSD Samsung 850 EVO-sequential read 540 MB/s and included cache 256 MB; graphic card Nvidia Geforce GTX 960 2.0 FB 128 bit). The acting load on the specimen is defined by forcing lateral displacement of the indenter into the center of a panel until approximately 0.234 m. A uniform velocity V is embedded to the rigid-indenter. Friction coefficient is adopting Coulomb coefficient with value $\mu = 0.3$. Details of the setting and preparation of the specimen and indenter for the current analysis are illustrated in technical drawing in Figure 2.2. FE configurations are described as follows: contact is strictly modelled between the rigid indenter and the target specimen, the plastic-kinematic material is applied to the specimen with input density $\rho = 7850$ kg/mm³, Poisson's ratio $v = 0.3$, Young's modulus $E_x = 210000$ MPa and Cowper-Symonds parameters $C_{cs} = 4000$ (1/s) and $P_{cs} = 5.0$. It is widely realized that factor of mesh size in numerical analysis is essential. It will effect both of the reliability (accuracy) and effectiveness (time process). Therefore two methods are investigated to select the most suitable one for the current work, i.e. conducting mesh convergences studies using arbitrary size, and deploying element-length-to-thickness (ELT) ratio as a method to select geometrical mesh.

Table 2.1. Steel properties of the specimen obtained through experiment (Alsos and Amdahl, 2009).

Type	Part name	Grade	σ_Y (MPa)	σ_U (MPa)	n (-)	ε_f (-)
A	Plate	S235JR-EN10025	285	416	0.24	0.35
B	Stiffener	S235JR-EN10025	340	442	0.225	0.35
C	Hollow frame	S235JR-EN10210	390	495	0.18	0.28
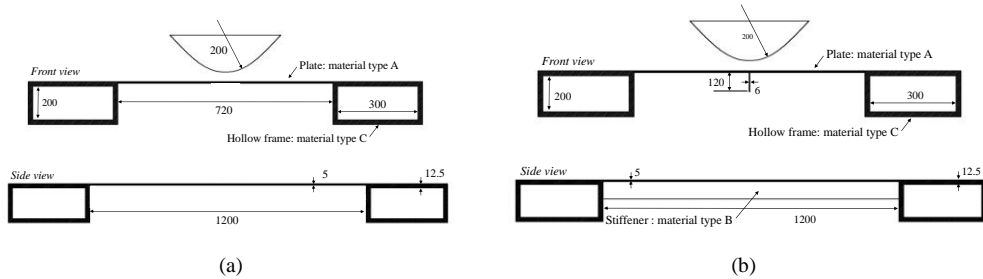
Figure 2.2. Technical drawing of the impact test. The setting is denoted as: (a) plain plate and (b) stiffened plate.

Mesh sizes were chosen as 10, 15 and 20 mm, which illustration of the applied mesh on numerical model is presented in Figure 2.3. Attention to fracture criteria was considered by implementing selected criteria on the geometrical model, namely Det Norske Veritas - Germanischer Lloyd – DNVGL (GL, 2003), Peschmann – PESC (Lehmann and Peschmann, 2002), and combination of Rice-Tracey and Cockcroft-Latham criteria – RTCL (Cockroft and Latham, 1968; Rice and Tracey, 1969; Törnqvist, 2003). The current model was built based on thin-walled concept by deploying shell element. For the constant value of each criterion, uniform strain $\varepsilon_g = 0.056$ and necking strain $\varepsilon_e = 0.54$ would be applied for the DNVGL criterion. On other hands, Peschmann obtained $\varepsilon_g = 1$ and $\alpha = 0.8$ for plate thickness $t = 5$ mm. In case of the RTCL, exponent $n = 0.24$ and strain at $t/l = 1$ at uniaxial test $\varepsilon_n = 0.67$ was applied to the target plate.
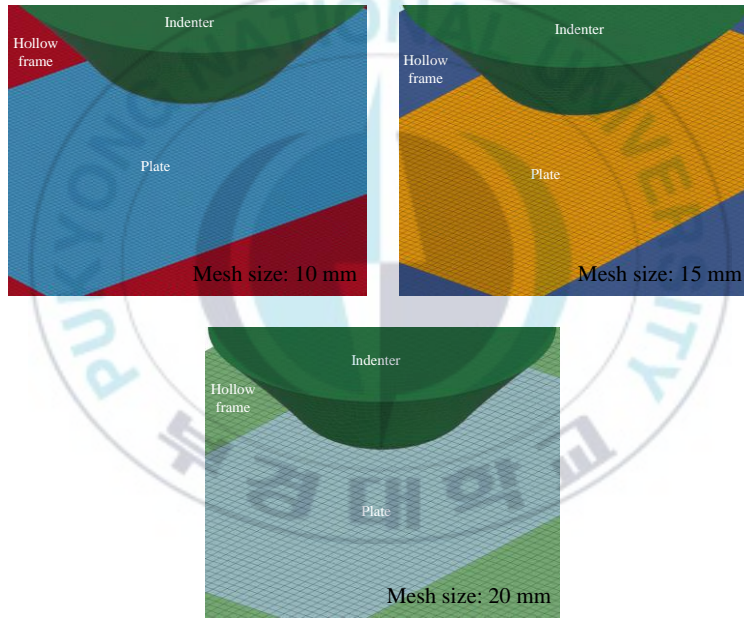
Figure 2.3. Numerical model of the target panel for the present study.

3. Results and Discussion

The results from the present work will be summarized per target specimen type, namely plain and stiffened plates. Comparison will cover force magnitudes during contact between the target specimen and rigid indenter, damage contours on the plate specimen during penetration and allocated time analysis.

3.1. Plain Plate

It can be observed in Figure 2.4 that mesh sizes achieved good correlation compared to the experimental penetration test. Fracture was noted in ranges 0.175-0.2 m of displacement which the most similar was shown by the mesh size 15 mm considering the maximum force and displacement during plate fracture. The results also indicated that predictions of material and structural fractures were mostly influenced by mesh size, especially in terms of the structural response analysis time using the FE method. More refined mesh is unavoidably producing larger element number which is followed by increment of the simulation time. During application of the current mesh size configurations, analyses were successfully finished in time range 10-100 min. The results for mesh size concluded that configuration in the numerical analysis confirmed satisfying tendency compared to the experimental test (Alsos and Amdahl, 2009). Besides structural response and time analysis, solutions of fracture criteria also shared similarity with the pioneer test which fracture on the plate formed similar deformation pattern before fracture and a crescent indentation (Figure 2.5) occurred on three criteria after fracture was experienced. These criteria were verified and could be used in the FE settings for further grounding analysis.
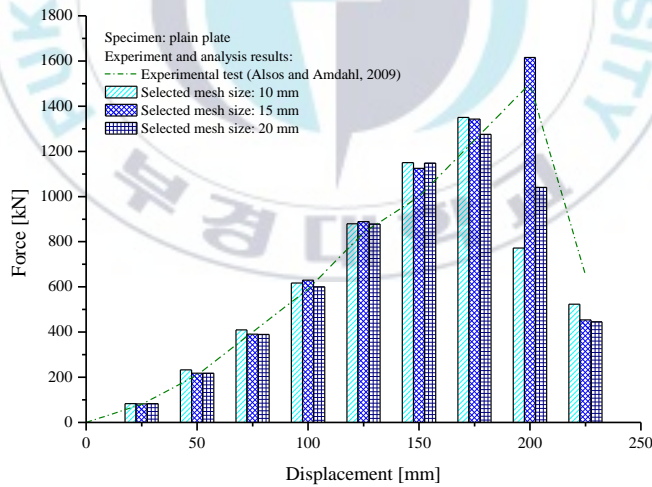
Figure 2.4. Results of the present numerical analysis, and its comparison with the test (Alsos and Amdahl, 2009).

14

Before fracture: test (Alsos and Amdahl, 2009)

After fracture: test (Alsos and Amdahl, 2009)
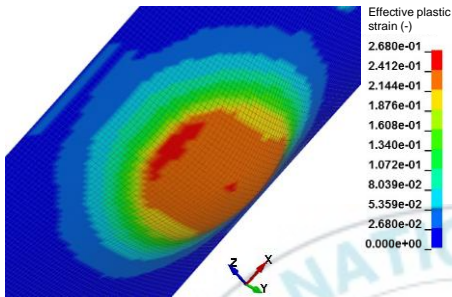
Before fracture: DNVGL
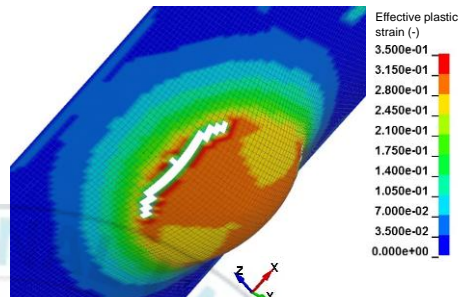
After fracture: DNVGL
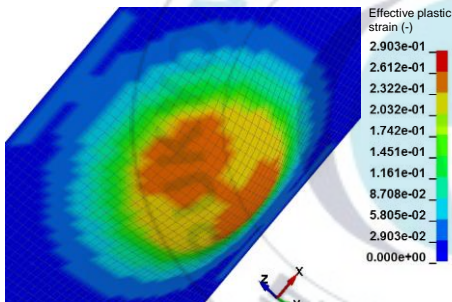
Before fracture: PESC
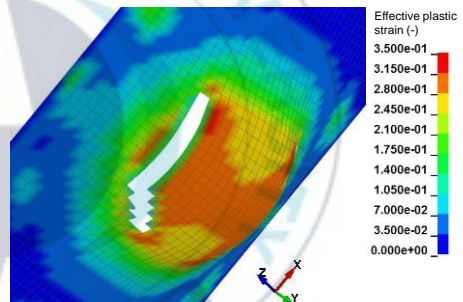
After fracture: PESC
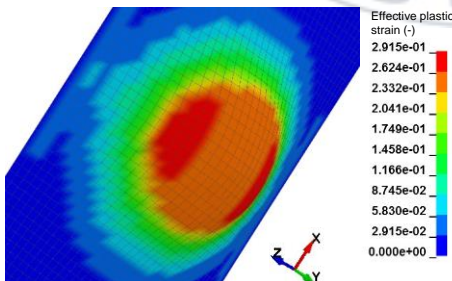
Before fracture: RTCL
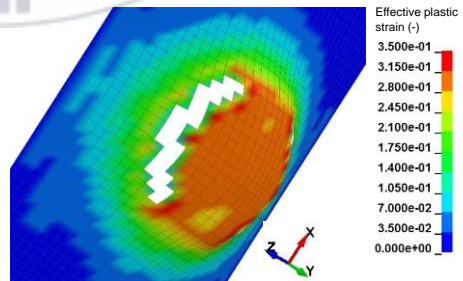
After fracture: RTCL

Figure 2.5. Conditions of the plain plate applied by several fracture criteria.
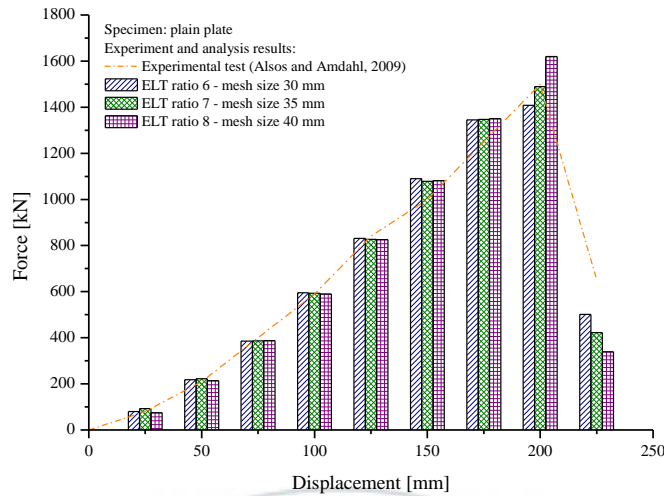
Figure 2.6. Comparison of the test (Alsos and Amdahl, 2009), and current analysis using the ELT ratio.

Table 2.2. Summary of geometrical data and time simulation: plain plate.

Mesh - arbitrary (mm)	Element no. (elem.)	Time (s)	Mesh - ELT ratio (mm)	Element no. (elem.)	Time (s)	Diff. in element (%)	Diff. in time (%)
10	68905	5752	30	7865	255	88.59	95.57
15	31048	1692	35	6049	169	80.52	90.01
20	17285	720	40	4540	109	73.73	84.86

However, considering the simulation time, very fine mesh (15 mm) to be applied to a ship model for grounding analysis can cause very large analysis time. Therefore, another method to select the suitable mesh size according to element-length-to-thickness (ELT) ratio is assessed using the specimen. Applied ratio within range 6-8 is considered in the current study. As the target possessed thickness 5 mm, then element lengths for the selected range are 30, 35 and 40 mm consecutively. Analysis results using the ELT ratio are shown in Figure 2.6. It was concluded that ELT ratio is capable to produce similar tendency compared to the test. Furthermore, according to summary in Table 2.2, analysis cost to mesh the specimen model can be reduced until 88%, and time to calculate meshed geometry by ELT method is significantly faster than the previous one using arbitral very fine mesh selection. Validity of the current benchmark is also checked by conducting mesh convergence on the observed sizes and several expanded mesh sizes. The selected parameter is set to be force in ultimate condition, or limit before failure takes place. Data from the test by Alsos and Amdahl (2009) is compared to the present analysis. Summarized results in Figure 2.7 concluded that convergence state is well achieved with all results close to ratio value 1.

16
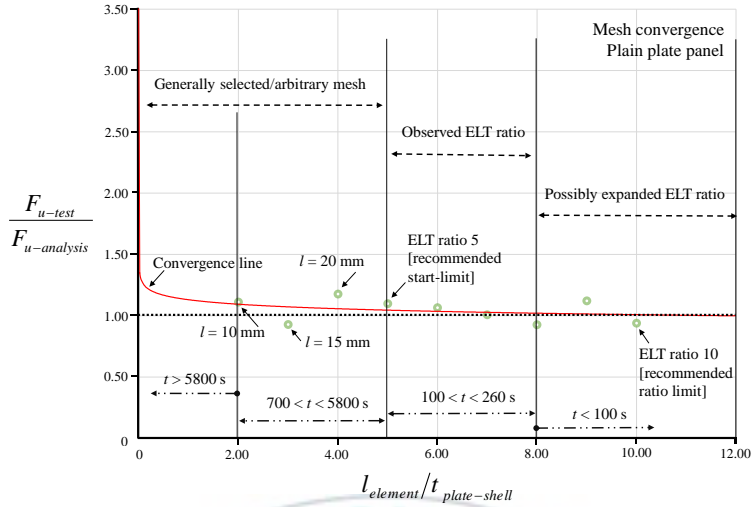
Figure 2.7. Results of the mesh convergence test for the plain plate.

3.2. Stiffened Plate

During the verification of the model with the results of the penetration test (see Figure 2.8), it could be concluded that the solutions of the FE simulation using selected fine mesh sizes were in good agreement with the experimental results. Although there was a difference in magnitude after the force decreased, the overall tendencies allowed us to conclude that the displacement when the force reached its approximate maximum point was satisfactory, with a difference of less than 25 mm between the experiment and simulation. Specifically in terms of the maximum force, the mesh size 20 mm was the most similar with the test, and it was followed by the mesh size 15 mm with minor difference. Considering solutions of the plain plate, result tendency of the stiffened plate can be classified in satisfactory level since the 15 mm is match two specimen types.

As previously conducted, comparative study for mesh size selection is also performed on the solutions of the stiffened plate. It is obtained that, ultimate force (Figure 2.9) and failure displacement of the ELT ratio were judged well enough compared to the test results, which overall comparison indicated better similarity was shown by this method than abritrary mesh size selection. Summary of FE analysis in Table 2.3 also supported this statement that geometrical element of the ELT ratio was reduced almost 89%, and the total time to complete the formed elements differed by more than 95% compared to the arbitrary fine mesh selection. Results of this benchmark indicated that application of the ELT ratio to select mesh size is preferable. Even though size is larger than very fine mesh, the solutions were proven

17

in acceptable level. Verification of the stiffened-plate results is followed by performing mesh convergence to assess significant of ultimate force ratio. Conclusion based on presented results in Figure 2.10 presents satisfactory as value of the generated mesh using ELT ratio is better than arbitrary mesh. Therefore, besides effectiveness aspect (time simulation), other important terms, i.e. reliability of the ELT ratio is successfully proven through this analysis.
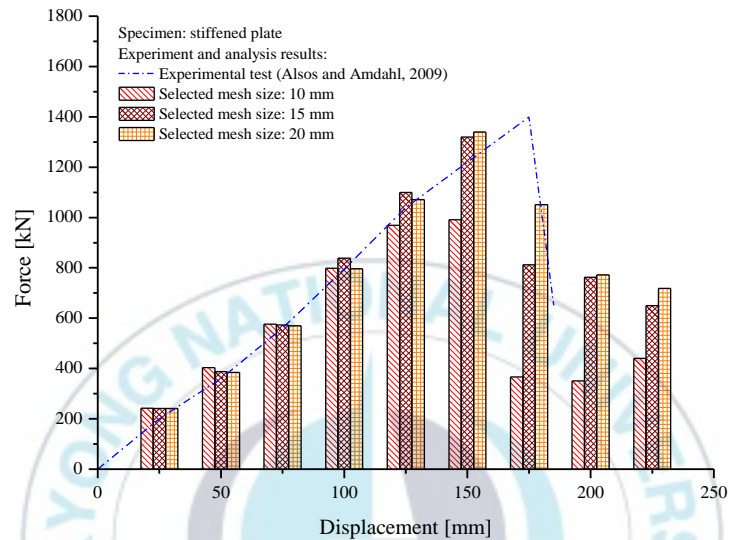
Figure 2.8. Force tendency of stiffened plate against displacement of the indenter.
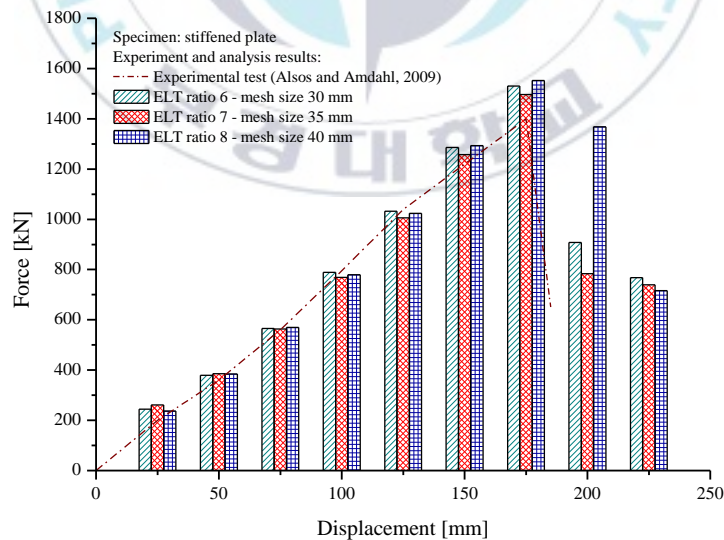
Figure 2.9. Comparison of the ELT method with the experimental test.

Table 2.3. Summary of geometrical data and time simulation: stiffened plate.

Mesh - arbitrary (mm)	Element no. (elem.)	Time (s)	Mesh - ELT ratio (mm)	Element no. (elem.)	Time (s)	Diff. in element (%)	Diff. in time (%)
10	70285	7575	30	8033	241	88.57	96.82
15	31632	2003	35	6622	199	79.07	90.06
20	17615	838	40	4626	110	73.74	86.87
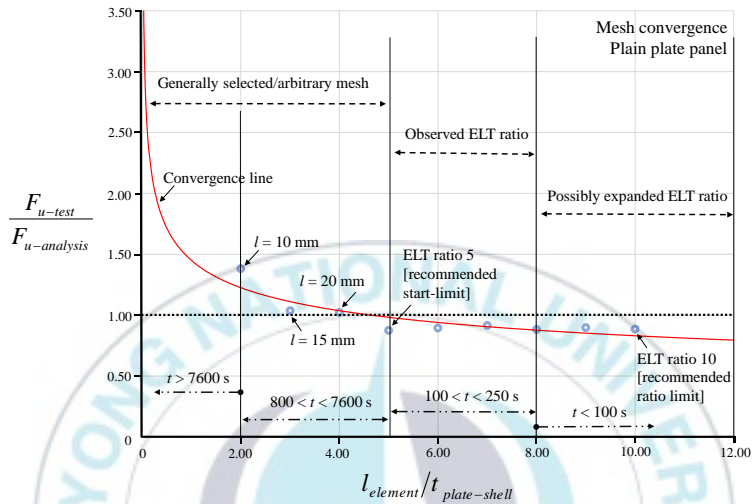
Figure 2.10. Mesh convergence test for obtained results using the stiffened plate.

In other hand, effect of the selected failure criteria to indentation pattern (see Figure 2.11) showed interesting solution. The DNVGL criterion produced similar result to the test until before fracture, which the stiffener of the specimen got torn after the strain limit was achieved. However, such tendency was not found on other criteria. Compared to the DNVGL, stiffener on the indented location was deflected to transverse direction with no tearing was formed on it. Comparing patterns after fracture of the test, the RTCL was the most similar among all criteria.

As comparison in terms of three failure criteria, during plain plate was deployed, the crecent indentation of the DNVGL was the most similar with the PESC and RTCL were also produced similar pattern. However, folding of the stiffener on the second specimen was better modelled using the RTCL and followed by the PESC. It can be obtained that for tearing-oriented indentation, the DNVGL is considered superior among the investigated criteria, while the folding is more suitable to be idealized using the RTCL or PESC criterion.

Before fracture: test (Alsos and Amdahl, 2009)
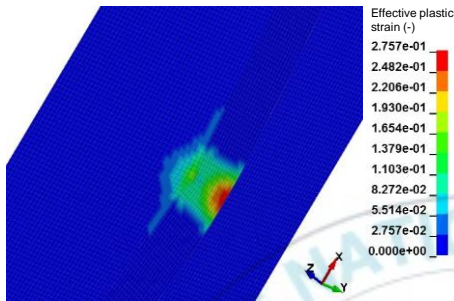
After fracture: test (Alsos and Amdahl, 2009)

Before fracture: DNVGL
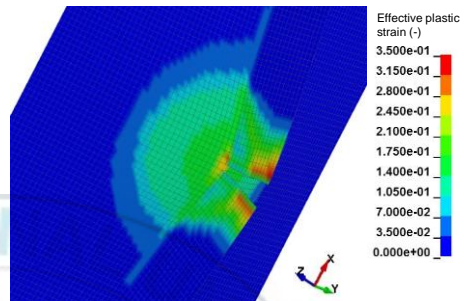
After fracture: DNVGL
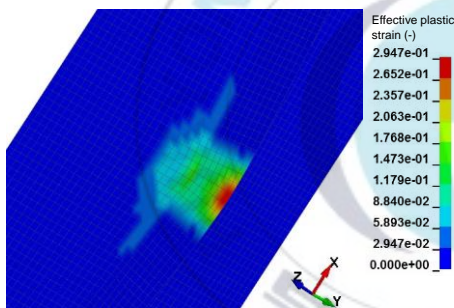
Before fracture: PESC
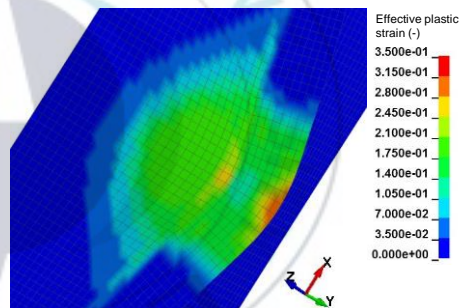
After fracture: PESC
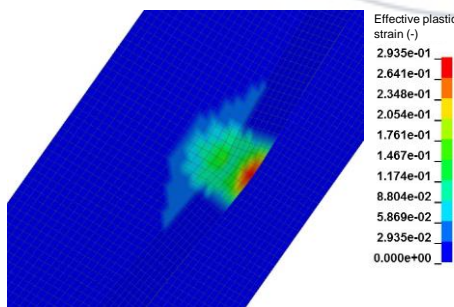
Before fracture: RTCL
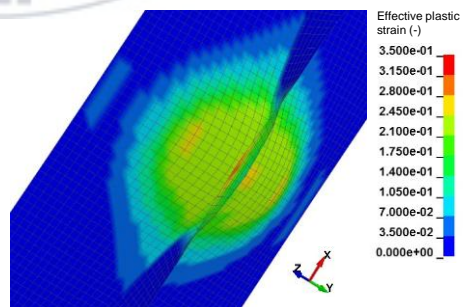
After fracture: RTCL

Figure 2.11. Damage contour on the stiffened plate in event of penetration.

Pioneer works in ship collision such as Ozguc et al. (2005) and Prabowo et al. (2017a) has used the DNVGL for large-scale collision analyses, which the results were evidenced in satisfactory level. Application of the PESC was also perfomed by Lehmann and Peschman (2003) in numerical calculation, while RTCL was included in crashworthy analysis by Törnqvist (2003). Therefore, these criteria can be used as adequate assumption in impact analysis, which the most important one collected based on this study is consequences of applying such criteria on calculation, especially in terms of damage contours on the specimen. Designer has responsible for structural safety, as well as researcher and engineer in marine structures are encouraged to plan benchmark before large-scale structural analysis/simulation is conducted to ensure the configuration and setting inputted in analysis are well verified.

III. Ship Collision

1. Ship Model

A 144 m cargo reefer would be used as the striking ship with rigid body characteristic was implemented on its structures. Furthermore, a Ro-Ro passenger ship with a length of 85 m was used as the deformable struck ship. The main dimension from both of the ships is presented on Tables 3.1 and 3.2. The element of choice was the one point quadrature Belytschko – Tsay element, which was both accurate and effective. The Belytschko – Tsay (BT) shell element as a computationally efficient has become the default shell element formulation. The element-length-to-thickness (ELT) ratio is suggested and should be within the range of 5-10 so that the local stress could be captured well.

Table 3.1. Main dimension of the striking ship.

Type of ship	Cargo reefer
Length over all (m)	144.50
Breadth moulded (m)	19.80
Design draft (m)	5.60
Depth (m)	10.20

Table 3.2. Dimension and structural data of the struck ship.

Type of ship	Ro-Ro passenger
Length over all (m)	85.92
Length between perpendicular (m)	78.00
Breadth moulded (m)	15.00
Design draft (m)	4.30
Depth (m)	10.40
Frame spacing (mm)	600
Width between outer and inner shell (m)	3.50

2. Proposed Configuration and Setting

During collision process, the striking ship will move with velocity 12 kts or 6.17 m/s to proposed target point while the struck ship is set to be fixed in centerline while the ends of the model will be clamped. The fixation is applied on all frames in the end of model. The scenario of collision impact is built based on side collision type with two major parameters, namely structure and material. In term of structure, the component preferences of hull structure is defined based on coming direction of the striking ship, i.e. side shell for transversal component and deck as longitudinal component are used as given in Figure 3.1.
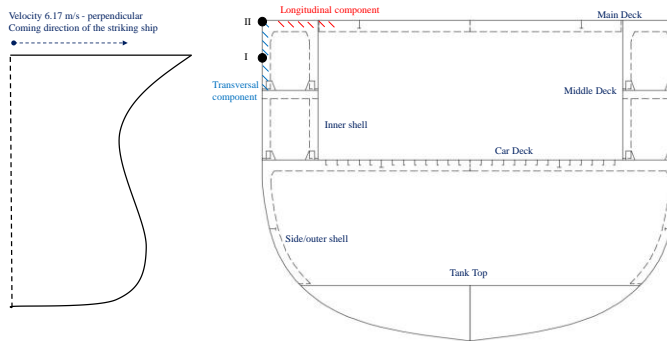
Figure 3.1. Impact scenario model based on component preference parameter.

The structure configurations of double hull with difference on distance between outer and inner shell are also taken as impact model. In material side, the mechanical properties of material especially strength characteristic as introduced by Callister (2007) are adopted for scenario model. Four materials are used with several failure strain values. The material definition in term of kinematic hardening, isotropic hardening and kinematic-isotropic hardening are included in impact models. The detail of scenario models to be applied in the numerical analysis are presented in Tables 3.3 and 3.4.

Table 3.3. Detail of proposed scenario models.

Parameters	Impact Scenario Model		
Structure	Component preference	Transversal component	Side shell
		Longitudinal component	Main deck
	Double hull configuration	Distance of inner-outer shell	3.5 m
			1.5 m
	Strength characteristic	Material type	1010
			1020
			1040
			1080
Material	Failure characteristic	Failure strain	0.1
			0.2
			0.3
	Material definition	Hardening model	kinematic
			isotropic
			kinematic-isotropic

Table 3.4. Chemical composition and mechanical properties for proposed materials.

AISI/SAE or ASTM Number	Composition (wt %)		Strength (MPa)		Ductility (% Elongation)
	Carbon	Manganese	Tensile	Yield	
1010	0.10	0.45	325	180	28
1020	0.20	0.45	380	205	25
1040	0.37	0.60	605	430	33-19
1080	0.75	0.60	800	480	24-13

3. Selected Ship Structures subjected to External Dynamics

The damage resulting from collisions could be reduced through several techniques such as designing appropriate hull structures, ensuring tightness of cargo tanks as well as observation and review on structural behaviors, whilst accounting for all involved parameters. The collision scenario can be influenced by location, angle, velocity and mass as these parts are included in the external dynamics of ship collisions.

3.1. Impact Location

The location of the target point was determined on the side hull of the fore end region exactly between the middle deck and the main deck. In the present work, three collision cases were conducted and simulated using finite element analysis in terms of location. They were denoted as Target I, in which the striking ship collides with the side shell near the location of the middle deck at approximately 9 m from the baseline; Target II in which the striking ship collides with the side shell between the middle deck and the erection deck at 10 m from the base line; and Target III in which the striking ship collides with the side shell between Scenario II and the erection deck at 11 m from the keel (see illustration in Figure 3.2). The striking ship is given a velocity of 6.17 m/s to move to the designated target point on the deformable structure of the struck ship.
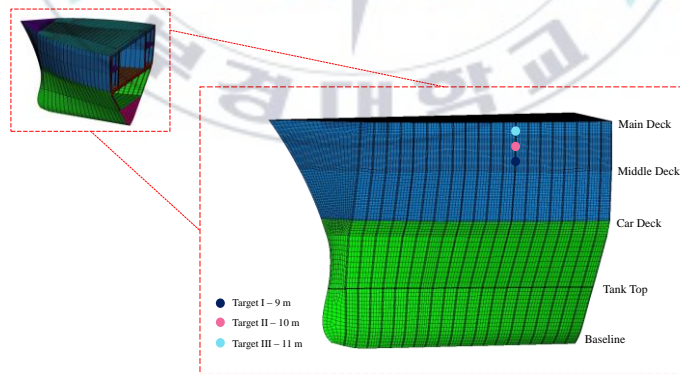
Figure 3.2. Proposed location for target point in collision analysis.

The internal energy in collision analysis was identified as the energy that was needed to plastically deform or even destroy the structure of a struck ship when a collision occurred. Figure 3.3 presented the internal energy of collision simulation. The differences in the graph represented the difference of capabilities between parts of the ship structure when resisting a

striking ship. At the deepest penetration, Scenario III had the smallest energy compared to the other two scenarios. The differences of internal energy between all scenarios were in the range of 12%-24%. Internal energy from Scenario II was found to be bigger than Scenario I with 12.19%, and 24.39% bigger than Scenario III at the end of penetration. The difference between Scenario I and Scenario III was 13.89%.
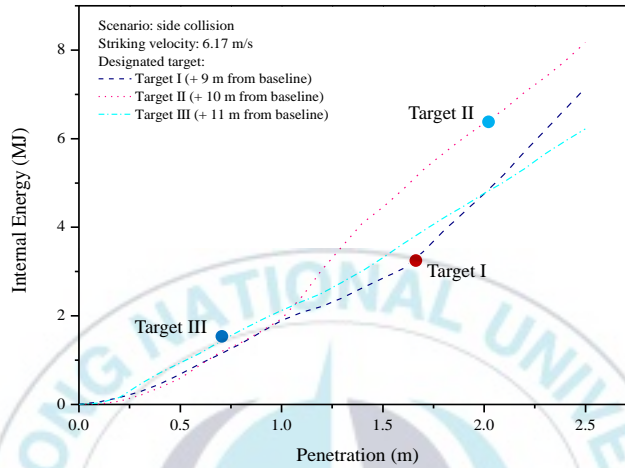
Figure 3.3. Internal energy versus penetration curves for all targets.
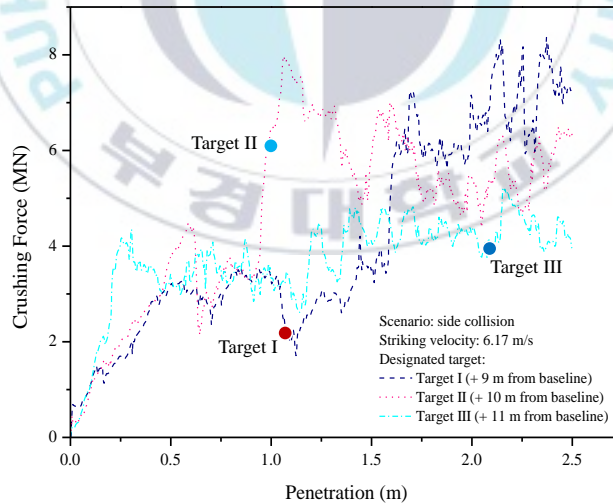
Figure 3.4. History of crushing force during collision process for all locations.

Fluctuation on the force-penetration curve (Figure 3.4) indicated a process of material destruction per depth of penetration. The peak of fluctuation likely occurred during initial tearing, and when destruction on the structural member had already begun. The collision in

Scenario I reached the highest force at the deepest penetration compared to the other scenarios where the contact location of the scenario was near the middle deck, and the side shell which was strengthened by a transverse frame and was also reinforced by the longitudinal deck. The contact force for Scenario III where the collision happened near the erection deck was smaller than the other scenarios.

3.2. Striking Angle

Besides location, the collision angle based on the position of the two ships during the collision was also taken into account. Five different collision angles were used in the simulation, including 30°, 60°, 90°, 120°, and 150°. Illustrations for proposed configuration of the striking angle are given in Figure 3.5.
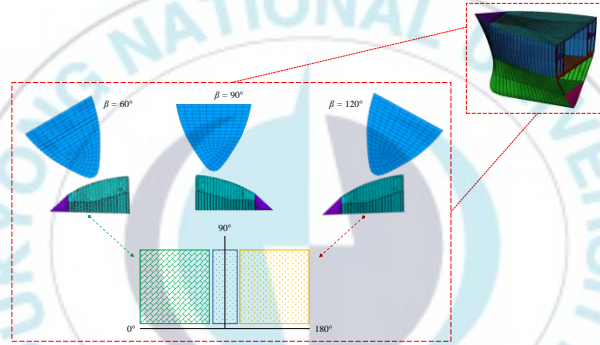
Figure 3.5. Position of collision angle on side collision process.
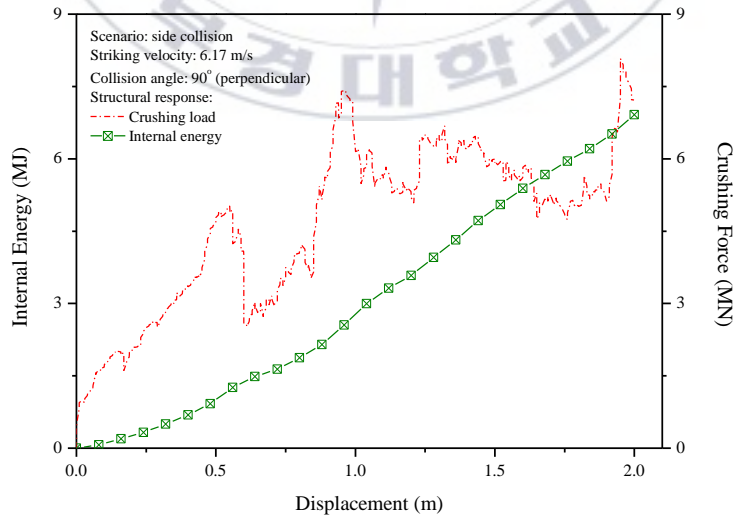
Figure 3.6. Energy and force for perpendicular collision with $\beta = 90°$.

The results of calculation indicated that collisions with a position between struck and striking ship angles below and above 90° (oblique) produced bigger internal energy than collisions in the perpendicular position. In terms of internal energy, the difference between the perpendicular position (Figure 3.6), and 150° (Figure 3.7) was the highest with a difference of approximately more than 48%. The difference between overall simulations is in the range of 30%-50%.
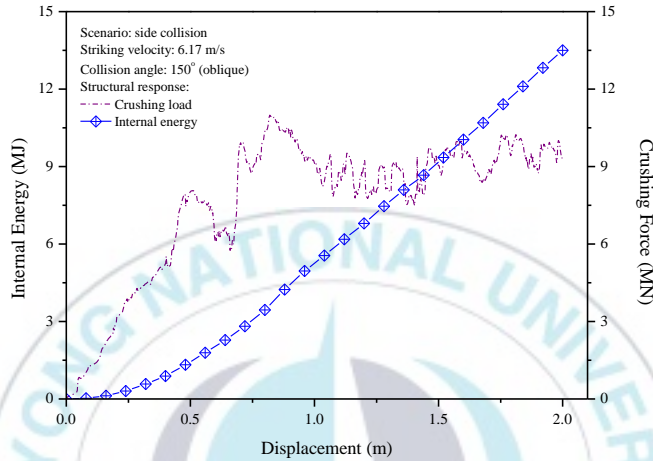
Fig. 3.7. Energy and force for oblique collision with $\beta = 150°$.
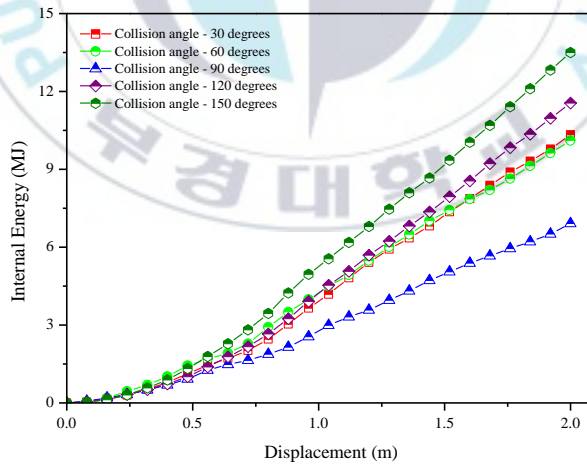
Figure 3.8. Internal energy of striking ship for selected angle cases.

These results were forming a pattern where if the collision angle was closer to 90°, the internal energy was rising but when the collision angle was right on 90°, the energy was found to be smaller. The internal energy would also decrease if the collision angle was

altered to be closer to 0° and 180°. This phenomena occurred because if the collision angle tended to be closer to 0° and 180°, sliding case would take place between the struck and striking ship as they were glancing each other and less penetration would occur during the collision process. The energy pattern of all simulations as presented in Figure 3.8 indicated that the energy in the collision process forming parabolic or quadratic function graph was 90° on the lowest level, and 30° as well as 150° on the highest point.

3.3. Ship Velocity

In the external dynamics of a collision, the ship velocity is one of most influential parameters in relation to the analysis and calculation results. A virtual experiment was conducted to obtain information regarding how the ship velocity affects the structural response after collision. In experiments, the striking ship was moved to the designated contact point on the struck ship with five proposed velocity values. This configuration was already used and verified in the first part of this study. Five velocity values were proposed: 5, 10, 12, 15, and 20 kts or in metric unit were 2.57, 5.14, 6.17, 7.72, and 10.29 m/s. The five forms of internal energy-penetration are presented in Figure 3.9. From these graphs, the velocity can be considered to have a significant effect during the collision process.
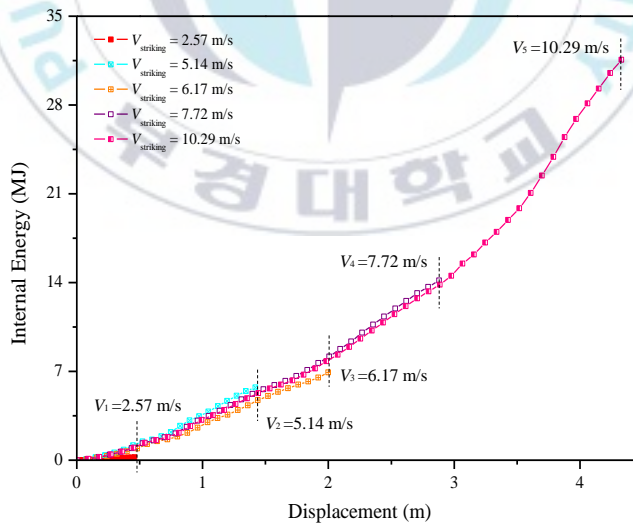
Figure 3.9. Internal energy for all proposed velocities.

As introduced in the velocity formula, for the same time period, the highest velocity will reach the farthest distance. In the study on the velocity influence, the contact point and other

parameters used the same location and parameter. In this case, the velocity formula could be applied. As expected from the velocity formula, as the highest velocity, 10.29 m/s had the deepest penetration. With a striking ship velocity of 10.29 m/s, the penetration reached almost 4.50 m, which allowed the striking ship to penetrate the inner shell of the struck ship. Under this condition, both the struck ship and cargo, especially on the car deck, experienced remarkable damage as a result of the collision with the striking ship. This could also be verified using the force characteristic during the collision process in Figure 3.10. The force behavior after a penetration of 3 m showed remarkable movement, which first occurred in the penetration period of 3-3.5 m and gradually rose until reaching a peak with a value of approximately 23 MN, and decreased after the penetration passed 3.8 m. In this state, the inner shell was completely breached by the striking ship body and immense damage to both the ship and cargo could not be avoided. Starting from depth 4 m until the end of the collision process, the force tended to decline because there was no other structure after the inner shell.
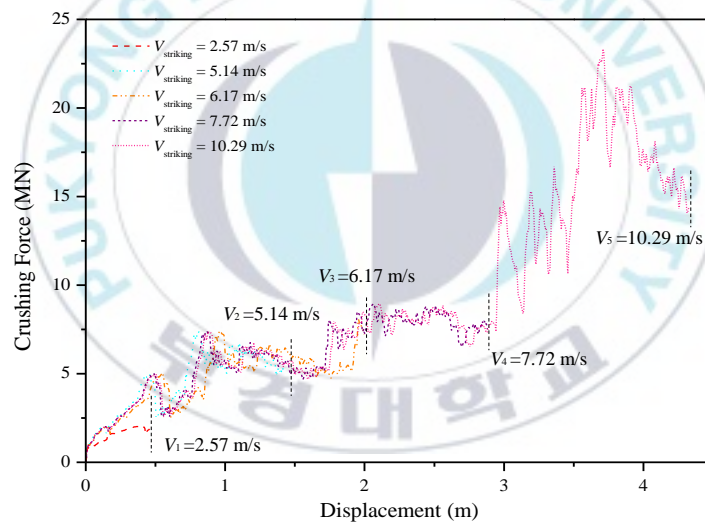
Figure 3.10. Force during collision process as advance penetration occurred.

4. Effect of the Internal Mechanics on the Designated Structures

Internal mechanics on the ship collisions are other important aspects in accidental scenario, besides the external dynamics. Influence of the internal mechanics can be divided into two major classifications, namely structure and material. Discussions in this section aim to study collision responses accounting for inner effects such as common structural type, e.g. single and double hulls, and assumed marine-steel material.

4.1. Structural Parameter

The analysis results of various impact scenario models are presented in this section. First, in term of component preference, the longitudinal structure was proofed provided better resistance subjected to impact load as presented in Figures 3.11 and 3.12. The cross-section based on coming direction of the striking ship was much smaller than side shell which was transversal component. During collision happened to the side shell, large area was more easily deformed due to centralized load on wide cross-section if it was compared with collision on main deck. As a consequences, the internal energy of collision on transversal component was lower but the tearing on side zone was bigger than collision on longitudinal component. Still in structural parameter, the width of the double hull was evidenced affect the internal energy as well as damage extent on both of outer and inner shell. The effect of wide distance between two shells is indeed providing much better defence subjected to side collision. However, amount of carried the carried cargo may be drastically reduced as well as the efficiency of ship itself will be going down. The illustration of damage between two double hull sizes is presented in Figure 3.13.
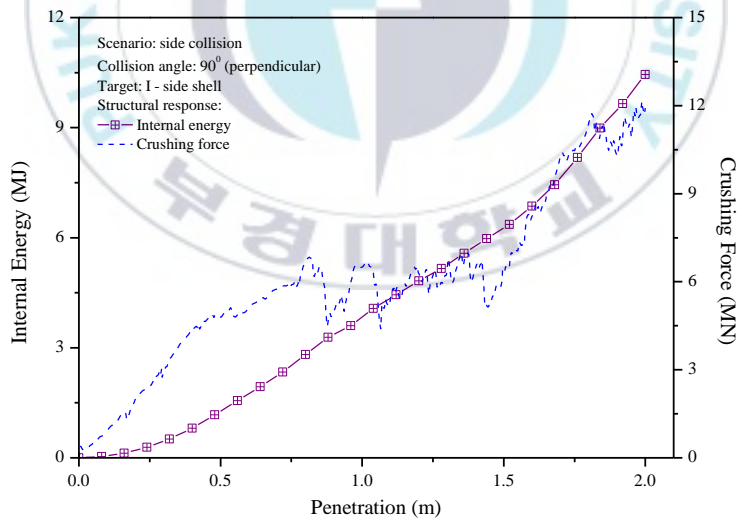
Figure 3.11. Energy and force characteristic of collision on side shell.
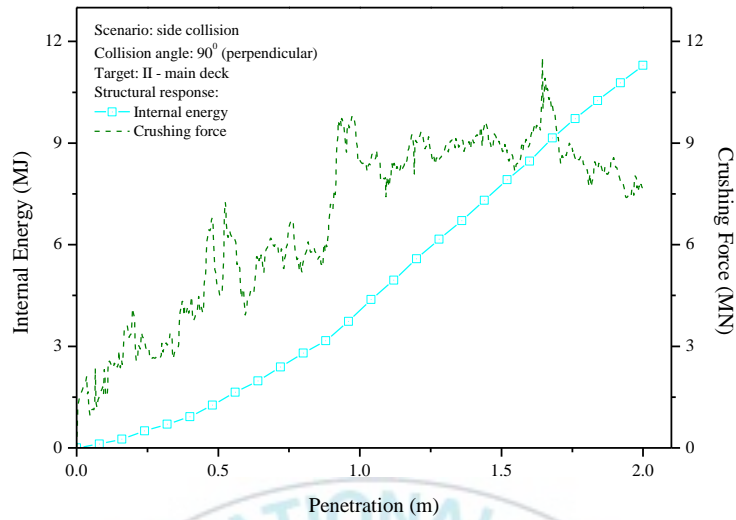
Figure 3.12. Energy and force characteristic of collision on main deck.

(a)   (b)
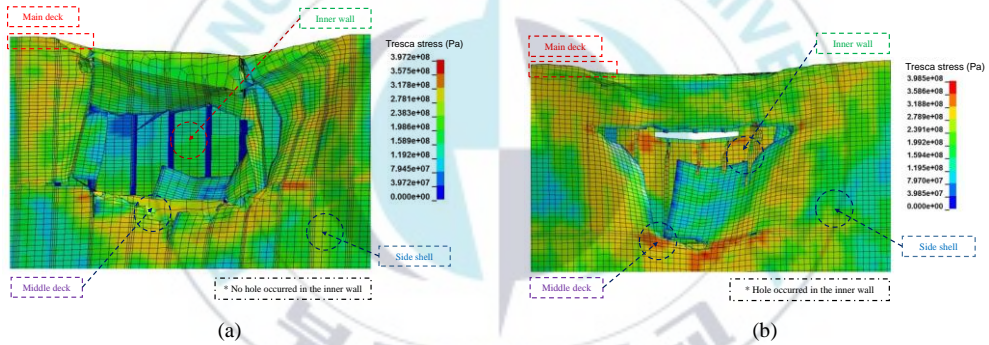
Figure 3.13. Damage on double hull structure: (a) width 3.5 m and (b) width 1.5 m.

4.2. Material Parameter

In terms of material, mechanical properties are clearly affect the results on energy and force as presented in Figure 3.14. The small difference was spotted between material 1010 and 1020 since these materials were coming from same class, plain low-carbon steel. In other hand, during comparison that was performed using 1040 and 1080, the significant result in term of damage extent had clearly happened after collision process.

The effect failure strain to internal energy can be considered significant. With the change 0.1, the product of energy can differ by almost 5 MJ. During the observation on effect of this parameter, the higher failure strain, the less difference in internal energy occurred. Figure

31

3.15 that the difference in term of energy between 0.2 and 0.3 is below 3.5 MJ which is smaller than difference between 0.1 and 0.2.
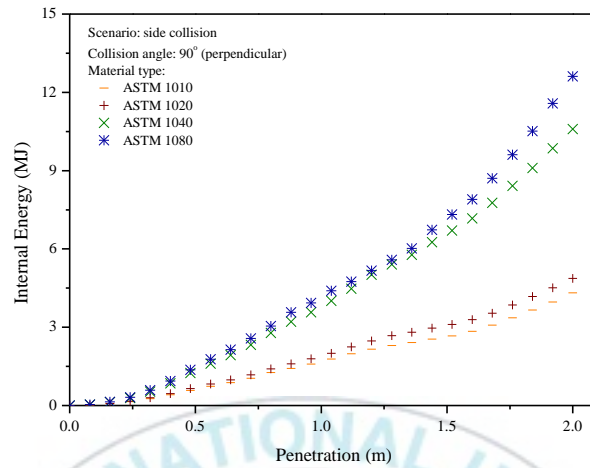
Figure 3.14. Energy characteristic for all proposed material types.
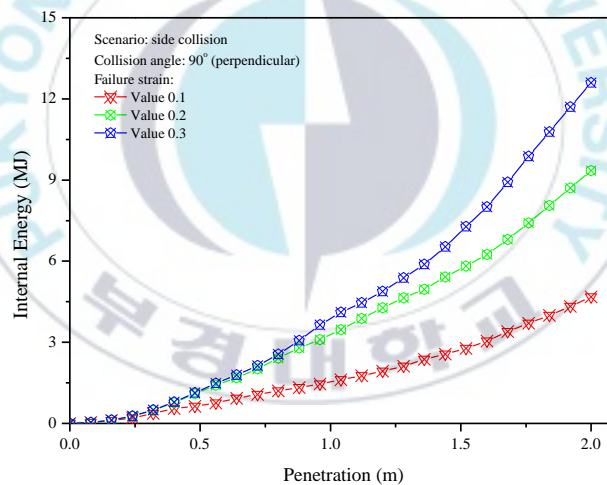
Figure 3.15. Effect of failure strain into energy characteristic.

In hardening parameter, no significant results were found in terms of the damage contours. However, if the damage illustration in Figure 3.16 is observed carefully, the more wrinkling was found during structure was defined as isotropic hardening. This phenomenon occurred because during isotropic hardening was applied on structure, the yield surface expands uniformly in all directions with plastic flow which made the intersection structure between deck and shell experienced more folding than when kinematic hardening was applied onto the structure.
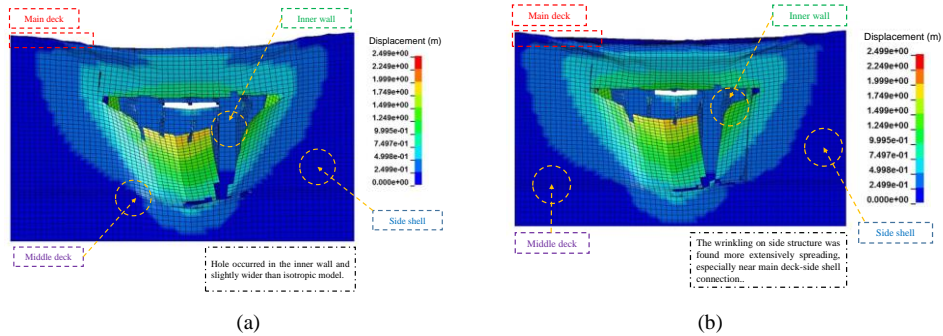
Figure 3.16. Displacement contour subjected to hardening type: (a) kinematic and (b) isotropic.

5. Extended Collision Analysis: Full-Ship Assessment

This study is a continuation of the general assessment of structural behavior in ship collisions, which expands into observations of the damage tendency and speed analysis on full-ship regions. The location and speed are considered as the main parameters in order to evaluate crashworthiness criteria in the event of a collision between two ships. The extent of the damage to the side structure after the collision process is summarized into statistical data that can be used to estimate the critical scenario.

5.1. Scenario Arrangement

The objectives of the main study are as follows: first, to produce reference data from a series of collision analyses, and second, to analyze the resulting data and conclude a speed limit for both ships according to the operational territory. To achieve these purposes, a series of analyses is carried out using more than 30 collision scenarios. To manage the large number of scenarios, the present work is divided into two phases, namely observation on crashworthiness criteria and a discussion of speed limits. All results are used in formulating our conclusions and recommendations in the final part of this research.

Table 3.5. Configurations of the struck ship's hull for each target point.

Region	Point number	Width (m)
After end	1,2	1.5174 - 3.1313
Middle 1	3,4,5,6,7,8	0
Middle 2	9,10,11,12,13,14,15	1.5000
Middle 3	16,17,18,19	2.4979
Middle 4	20,21	3.4108
Fore end	22,23,24,25	3.0812 - 3.5026

The target location is determined along the longitudinal axis of the ship's hull. The coordinate of the target point in each region is the same in terms of the vertical axis: 10.25 m from the baseline. As for the longitudinal axis, the distance between target points is also the same, and 25 target points are deployed to define 25 collision scenarios. The target location is illustrated in Figure 3.17. During the collision, an approximate speed of 12 kts (6 m/s) is used. To assess the speed of the striking ship, four regions of the struck ship are classified (see Table 3.5). In each region, four applied speeds for the striking ship are considered (from 5–20 kts (approx. 2.5–10 m/s) in increments of 5 kts) to observe the capability and behavior of the struck ship's side structure during impact.

(a)

(b)
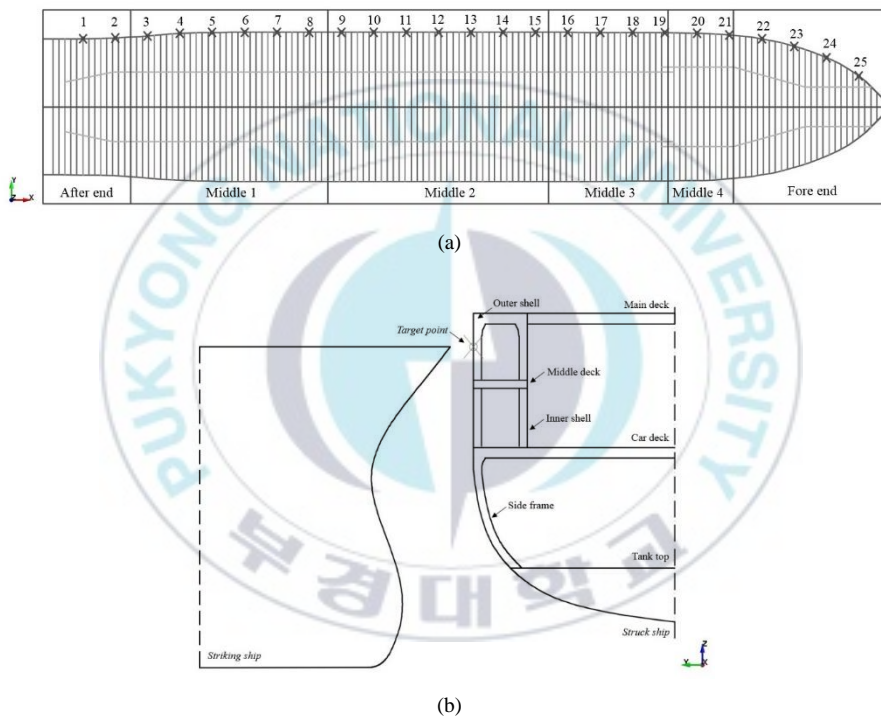
Figure 3.17. The defined collision scenarios for each study: (a) target location and (b) side impact.

5.2. Crashworthiness subjected to Target Location

The analysis in this section was conducted to observe the effect of collision load on the ship's hull in terms of the longitudinal direction (or x-axis, according to the Cartesian coordinate system). As mentioned in the previous section, 25 target points were assigned on the side hull of the struck ship. The different structural preferences in size and arrangement produced nonlinearities in the calculation results.

34

The structural crashworthiness of the side structure is summarized in Table 3.6. As well as a finite element simulation, a statistical analysis was used to determine the tendency of the data. The statistical results indicate that the global data exhibit a high variation in terms of the internal energy, which matches the characteristics of the side structure. The internal energy represents the amount of energy needed to plastically deform the entities involved in an impact. In extreme situations, such as collisions, grounding, and explosions, the energy is not only used to plastically deform the target structure, but also to destroy it. As stated above, this tendency satisfies the correlation between the energy and structural arrangement. The energy in the middle regions has a larger magnitude than at the aft and fore ends, which indicates that the middle regions are harder to destroy during a collision.

The trend in the internal energy along the side hull is shown in Figure 3.18. In these specific regions, the middle region were found harder to be penetrated than other regions. This trend is obtained because in ship design, the middle regions are designed to be stronger than the aft and fore ends to counter the maximum bending moment which occurs in this part. Major fluctuations occur at the aft and fore ends. At the aft end, two target points produced remarkable differences, with point 1 displaying a tear in both shells and point 2 only suffering some displacement of the inner shell. This result is influenced by the arrangement of the side structure at the aft end, where there is a region without a double hull (denoted as the middle 1). Point 2 is closer to the middle 1 and suffered only minor damage to the inner shell after the collision process. In the middle regions, the collision produced relatively stable results in terms of the energy.
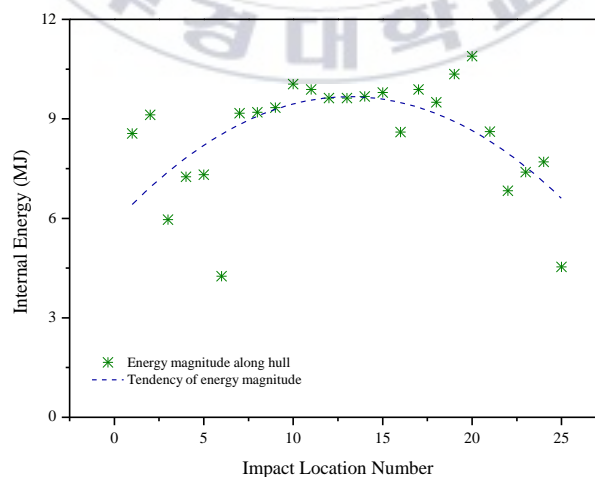
Figure 3.18. Internal energy characteristic along ship hull in longitudinal direction.

Table 3.6. Calculation results based on study of the target locations.

Location no.	$x_{coordinate}$ (MJ)	Internal energy (MJ)	Damage extent					
			Tearing [outer shell]		Disp. (m)	Tearing [inner shell]		Disp. (m)
			Length (m)	Width (m)		Length (m)	Width (m)	
1	-39	8.559	3.345	1.350	2.249	1.687	0.389	1.749
2	-35.75	9.120	4.207	1.932	2.249	0.000	0.000	0.500
3	-32.5	5.958	4.091	2.836	2.249	0.000	0.000	0.000
4	-29.25	7.254	3.725	2.481	2.249	0.000	0.000	0.000
5	-26	7.317	3.234	0.501	1.999	0.000	0.000	0.000
6	-22.75	4.258	1.680	0.408	2.249	0.000	0.000	0.000
7	-19.5	9.172	3.092	0.370	1.999	0.000	0.000	0.000
8	-16.25	9.202	3.346	2.429	1.999	0.000	0.000	0.000
9	-13	9.335	3.227	2.425	1.999	0.000	0.000	0.750
10	-9.75	10.047	3.594	2.474	1.999	0.851	0.094	0.750
11	-6.5	9.887	3.592	2.335	1.999	1.091	0.093	0.750
12	-3.25	9.627	3.839	2.483	1.999	0.735	0.102	0.500
13	0	9.628	4.076	2.486	1.999	0.850	0.093	0.500
14	3.25	9.677	2.992	2.687	1.999	0.000	0.000	0.500
15	6.5	9.794	2.718	0.556	1.749	0.000	0.000	0.750
16	9.75	8.599	4.802	1.215	1.999	0.000	0.000	0.750
17	13	9.889	5.731	1.223	1.866	0.000	0.000	0.746
18	16.25	9.498	5.025	1.159	1.622	0.000	0.000	0.541
19	19.5	10.349	4.536	1.661	1.499	0.000	0.000	0.500
20	22.75	10.894	4.746	1.269	1.399	0.000	0.000	0.700
21	26	8.613	5.204	1.721	1.394	0.000	0.000	0.279
22	29.25	6.833	3.760	2.503	1.749	0.000	0.000	0.250
23	32.5	7.392	2.732	3.389	1.749	0.000	0.000	0.250
24	35.75	7.702	3.014	3.245	1.749	0.000	0.000	0.500
25	39	4.537	2.213	0.734	1.749	0.000	0.000	0.250
Mean		8.526	3.701	1.835	1.910	0.209	0.031	0.521
Standard error		0.346	0.191	0.182	0.051	0.091	0.017	0.074
Standard deviation		1.729	0.957	0.909	0.255	0.453	0.083	0.372
Sample variation		2.991	0.916	0.826	0.065	0.206	0.007	0.139
Confidence level (95%)		0.678	0.375	0.356	0.100	0.178	0.032	0.146

The interaction between damage extent on the outer and inner shells is presented in Figure 3.19. This shows that damage to the outer shell tends to reduce from aft to fore end as the width between the outer and inner shells increases. However, the tendency for damage to the inner shell increases at the middle region and reduces toward the aft and fore end regions. This result matches the safety characteristic of the fore end, where the double hull size is the widest among all regions, and no displacement of the inner wall was observed during and after the collision process.
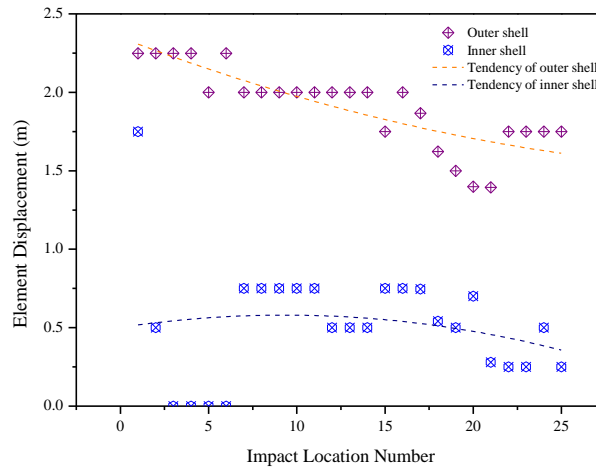
Figure 3.19. Interaction of element displacement at the both of shells.

5.3. Hull Response under Selected Striking Speeds

The striking speed is considered to be a major parameter in terms of the external dynamics. Several striking ship speeds are reviewed to determine the influence of this parameter during impact at different locations. The main considerations are taken from structural crashworthiness criteria, i.e. structural displacement and internal energy. The structural displacement in Figure 3.20 shows a tendency for the outer shell to experience more damage than the inner shell at all striking speeds in the case of side collision. This result satisfies the design criteria against accidental loads for ships, where damage (in this case represented by displacement) to the inner shell must be minimized during a collision.

The lower extent on the inner shell indicates that less damage is experienced by this component, as the major damage has been absorbed by the outer shell. In assessing the displacement to the inner shell, a 15 kts collision speed (approx. 7.72 m/s) produces a displacement of 0.5 m. This value can be used to make a rough estimation that the ship's cargo may be deformed or displaced from its initial location. The displacement of 0.5 m is already considered critical in this study, as this collision model may occur to other regions that have lower double hull spaces than the fore end. Beyond this point, side collision with a striking ship moving at 20 kts (approx. 10 m/s) results in immense damage, with the outer shell suffering displacement of over 4 m and the inner shell being displaced more than 1 m. Confirmation of the energy characteristics at each striking speed show the good correlation between higher energy being produced at higher collision speeds.

37
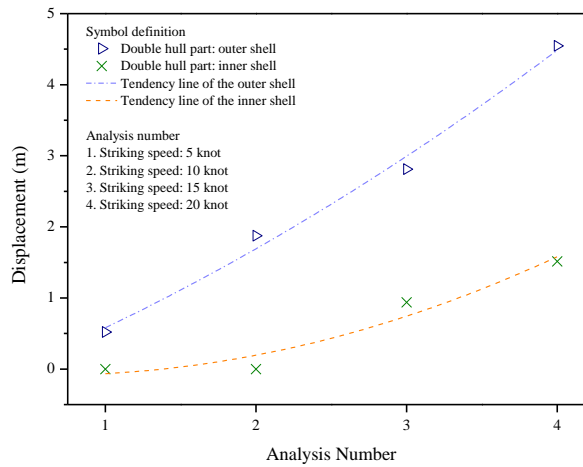
Figure 3.20. The structural displacement on double hull against several striking speeds.
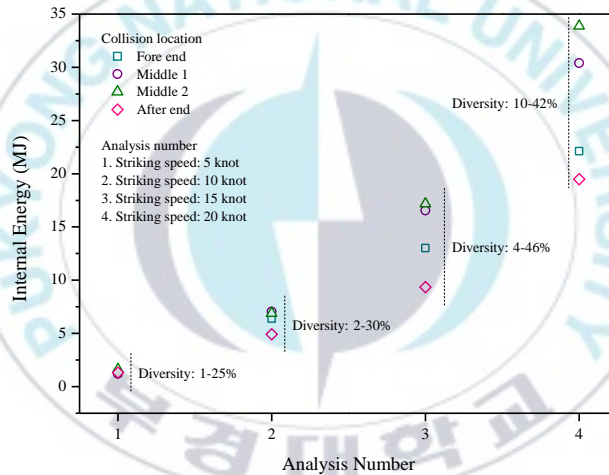
Figure 3.21. The internal energy in study of the striking speed.

As can be observed in Figure 3.21, during low-speed (5 kts) collisions, the resulting energies are similar at the aft end, middle region, and fore end. Based on this study, the low-speed category is defined as 0–5 kts (approx. 2.5 m/s). After exceeding 5 kts, the internal energy starts to diverge, but close similarity remains in the middle and fore end regions. Significant damage occurs in collisions with a striking speed of 15 kts (approx. 7.7 m/s), as the gap between target regions is quite significant with differences estimated at more than 5 MJ. At this speed, the middle regions, which are designed to endure bending and shear loads, still show a degree of similarity. This statement is supported by the detailed internal energy results for each collision model at various striking speeds.

The results of this study indicate that hull strength is a satisfactory characteristic for the resistance capability of the middle regions against an impact load. The strength and structural response of the observed points on the middle regions have to be similar, because a remarkable gap in terms of strength may affect the ship's response when experiencing dynamic loads, e.g. sagging and hogging. The striking speed of 15 kts is considered to be the limit at which the struck ship remains stable following a collision. Even though the middle regions behave similarity until 15 kts, at a speed of 20 kts, the internal energy shows large gaps in the behavior of all regions. Considering the extent of damage in Figure 3.20, the results of the internal energy support the tendency of the displacement level of the outer and inner shells after collision processes. Higher speeds produce greater damage and more internal energy. At the same time, immense damage in the form of displacement is associated with the high energy levels of a 20 kts collision (approx. 10 m/s). Collisions at this speed should be avoided at all costs; otherwise, after-collision disasters such as capsizing, sinking, or even explosions will produce marine casualties (IMO, 1972) in the form of deaths of the crew and passengers, abandonment of the ship, material damage, and severe damage to the environment.

5.4. Concluding Remarks: Speed Limit

The designed scenarios of this study originally refer to a collision incident on the Sunda strait territory approximately three years ago. In this instance, a T-collision occurred between two ships, producing remarkable structural damage on the side structure of the struck ship, i.e. passenger ship. This strait is a major voyage route in the southern seas. The main destinations along this route are Fremantle (Australia), Jakarta (Indonesia), and Singapore. The Sunda strait connects two main islands of Indonesia, namely Java and Sumatra. Ro-Ro passenger ships dominate the route from Merak to Bakauheni, which runs east-to-west. These routes inevitably lead to crossing situations, which may result in impact incidents, i.e. side collisions. The high possibility of crossing situations causing collisions is detailed in the Collision Regulation (COLREGS) (IMO, 1972). Considering the data produced by our numerical analysis, we estimate a speed limit for ships passing through the Sunda strait. Such regulations can be implemented by Indonesia, as the strait is in an exclusive economic zone (EEZ), which allows a country to conserve and manage natural resources, such as by protecting the water environment from pollution due to various causes, e.g. collision incidents (National Government, 1983; Patuzi, 2015; IMO, 2008).

Table 3.7. The internal energy for different regions subjected to striking speeds.

Speed (kts)	Internal energy (MJ)			
	After end	Middle 2	Middle 3	Fore end
5	1.31	1.63	1.21	1.31
10	6.39	6.89	7.04	4.92
15	13.02	17.18	16.54	9.34
20	22.11	33.88	30.40	19.49

Based on the results in the preceding sub-sections, speeds of 0–5 kts tend not to cause any displacement of the inner shell after collision. The displacement of the outer shell is less than 0.6 m at these speeds. During a collision in this speed range, damage to the middle 1 region, which does not have an inner shell, is still considered safe, as the displacement in the outer shell is not remarkable. At 10 kts, the outer shell is displaced by more than 1.5 m, but the inner shell exhibits a similar displacement to that at lower collisions speeds. Confirmation of the internal energy shows a reasonable pattern, as the energy in each region is not scattered significantly. The location study in sub-section 5.1 found large-scale damage at only three locations along the side hull. The safe condition is maintained when the striking ship is moving at 12 kts. However, above 15 kts, both the outer and inner shells suffer large displacements and are subjected to high energies.

The structural crashworthiness at these two speeds is considered remarkable, and such collisions should be prevented. To compare the results with a safety estimation, the recommended safety factor for impact load (Rosato and Rosato, 2003) is applied. The safety factor is a ratio between the yield state and the working stress. The yield state is considered to be the failure state, which occurs during the 15-kts collision, and the working state is determined as the 5 kts collision (i.e. no major damage to either shell after collision). To expand our observations on this factor, the 10-kts collision is included for comparison. The internal energy represents the capability of the structure to resist penetration perpendicular to the experienced stress/force (Bae et al., 2016a-b; Prabowo et al., 2016a-b; 2017a-d). Therefore, the magnitude of the internal energy is used to assess the safety condition of the structures against side collision loads. The results of the striking speed and comparison with the safety factor are presented in Tables 3.7 and 3.8, respectively. The results for the middle 2 and 3 regions are calculated, as these regions are located in the middle ship area which experiences high bending loads and are stronger than the middle 1 and 4 locations, which are near the aft and fore end regions.

Table 3.8. Current safety factor and comparison with the existing value (Rosato and Rosato, 2003).

Location	Calculated factor		Load type					
	5 kts	10 kts	Static short-term	Static long-term	Repeated	Variable change	Fatigue	Impact
After end	10	2						
Middle 2	11	2						
Middle 3	14	2	1 - 2.5	2 - 5	5 - 15	4 - 10	5 - 10	10 - 15
Fore end	7	2						

Based on the presented calculation results in this discussion, most components of the 5 kts striking speed fulfil the safety factors. The 10 kts speed matches the static short-term load, but does not satisfy the impact load factor. Although also included in the static long-term load, this load time does not satisfy the collision load characteristics over short periods of time. This comparison indicates that only the 5-kts striking speed adheres to the proposed factors. However, it is not feasible to apply this speed limit in all conditions when a ship uses the Sunda strait. The 10-kts speed satisfies the factor representing the characteristic of collision load (static short-term load), and can therefore be used as the upper speed limit when crossing situations are expected to occur. Serious attention should be given to navigational instruments and the role of the communication tower in both ports to observe voyage conditions on the strait. During certain dangerous situations, e.g. bad visibility due to fog and limited maneuverability because of the local topology, the lower speed limit of 5 kts is strongly encouraged. This should be implemented by ship crew, port communication tower staff at the Merak and Bakuheni ports, and weather/ meteorology/geophysics monitoring staff in observing and monitoring voyage activities on the Sunda strait. In forming considerations based on absolute safety, the safety of the limiting design should be calculated using a safety factor. There are no hard and fast rules in setting a safety factor. As the occurrence of ship collisions is very nonlinear, the most basic consideration in applying a safety factor is the consequence of failure. There are five additional conditions to be taken into consideration: (1) variation in structural arrangement along the ship's hull; (2) variation in double hull performance; (3) effect of stating material strength properties; (4) type of loading (static, dynamic, etc.); and (5) overall concern for human safety.

IV. Ship Rebounding

1. Introduction

Technological developments have given various communities the opportunity to expand their observations of ocean resources, as commodities and materials such as crude oil, natural gas, fish, etc. are in demand globally. In these conditions, marine structures such as ships become vital, for supplying offshore activity or even transporting export-import products. Furthermore, serious attention has been paid to improvements in ship safety (Goerlandt and Kujala, 2014) and structure (Fang and Das, 2005). During operational and stand-by modes, a ship can be subjected to various loads, which must be resisted to ensure that the objective of ship is fulfilled and the safety of crew, passenger, cargo, and ship itself can be guaranteed. Analyses are conducted before the ship is accepted for construction; these analyses assess the stress and strength of the structure. The output of the structural analysis is the structural response, defined in terms of stresses, deflections, and strengths. Then, the estimated response is compared to the design criteria (Lamb, 2003). However, other loads that cannot be resisted may occur accidentally, which can cause remarkable casualties on the ship and its surroundings. A collision creates an accidental load that is always linked with negative consequences, such as those resulting from the terrible accident of the Doña Paz, in which only 26 out of more than 1400 passengers were reported to have survived. In other cases of collision, environmental damage may occur, such as oil leakage from a tanker vessel (Yip et al., 2011). In addition to being an accidental load, collision is also classified as an impact phenomenon whose occurrence involves significant nonlinearities. Collision scenarios may be limitless, depending on the various influences from materials, structures, etc.

In this work, an observation of structural behaviors affected by several parameters involved in ship collision is conducted. A series of impact scenarios are defined to estimate the behavior of the struck ship during and after impact by the striking ship. Crashworthiness criteria are summarized, and further predictions are presented in the evaluation of results.

2. Review on Numerical Experiment for Collision Phenomena

Advance developments of impact engineering, especially in ship collision are not independent from the improvement of computational instrument which is considered as good calculation method in estimating structural behavior and material response under various

forms of load. Deployment computer to calculate a phenomenon is generally called by numerical experiment – simulation. As indicated by its name, this method is defining real phenomena (physical data i.e. geometry, property, etc.) into the numerical information and then is solved by certain code, for example finite element. This method is judged by researchers suitable for analysis on collision and grounding. The produced results have satisfactory with calculation by other methods such as empirical formula (Minorsky, 1958), simplified expression (Haris and Amdahl, 2013), and even laboratory experiment (Alsos and Amdahl, 2009). After methodology for large-scale simulation is verified by benchmark particulars, the numerical result can be considered as reliable result. This method allows preparation in physical test and experiment can be pressed as low as possible and failure in the experiment can be re-conducted after several refinements.

However, despite of its positive characteristics, challenge rises to obtain numerical solution in reasonable time process. It cannot be denied that time is essential in every method of research, as well as in this method. An accurate result may be obtained by making detail geometry and property as physical reference during pre-processor stage is conducted. This assumption is relative and not always true in numerical study. Bathe (1996) specifically described for finite element method that mathematical (numerical) model should fulfil two main criteria in terms of effectiveness and reliability. Proper consideration in deploying overall ship model is recommended to be conducted before pre-processor stage is performed, since this stage often requires man-hours in making model, defining material part, etc. The other reason is also stated by Bathe that by numerical analysis, user cannot predict the response of physical problem exactly because it is impossible to reproduce even in the most refined mathematical model. Therefore, several researchers in their early works, specifically in collision (Prabowo et al., 2016b; Ozguc et al., 2005) and grounding (Yu et al., 2015; Sormunen et al., 2016), only deployed a partition using a ship region that would be observed under impact instead of full model. As indicated in previous discussion, to ensure reliability of numerical solution using this research method, benchmark is needed. Based on the review, a study which is conducted by several methods to provide satisfactory verification of experiment or investigation. Combination between investigation and real phenomena laboratory test, with deploying numerical experiment in further evaluation is preferred as conducted in several pioneer works. Validation using empirical formula and simplified method is also proved can produce good agreement with other methods.

3. Assessment on Collision Assumption

The previous subsection described pioneering impact engineering works, as well as the implementation of numerical experiments for modelling ship collision. Review based on the presented references concludes that collision analysis is continuously performed to fulfil demand of safety (survivability) during ship operational. The behavior of structures and materials under collision (especially between two ships) can be predicted by other methods, such as empirical formula and analytical methods. Several analyses indicate that during a collision between ships, the striking ship (which penetrates the other ship in a collision) is assumed to be completely-stuck on the struck ship at the end of the collision process. By assessing defined assumptions in pioneer studies, complete-stuck phenomenon can be considered to possibly occur under certain conditions, as follows:

1. The striking ship has a constant velocity. Therefore, during the penetration process, the striking ship can penetrate up to the designated target location without being influenced by the inner structure of the struck ship.
2. The striking ship is significantly larger than the struck ship. However, this factor is relative, as there is another possibility in this assumption, which is that the striking ship will capsize at the end of collision process.
3. A side collision scenario is applied, and the struck ship is set to stand still under impact.

These assumptions are convenient to use, as it is reasonable to assume that this is the worst case for the struck ship, especially in a side collision scenario where the striking ship continues to penetrate the side structure of the struck ship. Nevertheless, this definition ignores the fact that a ship is designed and built to be simultaneously strong and flexible. In an assessment where the striking ship continues to perform a crushing process during collision, the produced results only provide strength characteristics, while the flexural ability of the struck ship to resist penetration is neglected. In order to develop new considerations of collisions between two ships, this work has been conducted to estimate the structural crashworthiness of a struck ship under a dynamic collision scenario with respect to the rebounding phenomenon of the striking ship after penetration occurs. The contributions of structural and material parts in a collision is considered as an internal parameter, while collision velocity and the striking ship represent external factors. Different striking ships are deployed to consider the relationship between ship dimension and penetration location.

4. Preparation and Procedure

4.1 Principal Dimension and Engineering Model

In this work, a series of collision scenarios between two ships are considered, and deployed in the simulation. The ships are defined as follows: the struck ship is the penetrated target, and the striking ship acts as the indenter in the event of ship collision. A deformable structure is applied to the Ro-Ro ship (the struck ship), while rigid characteristics are implemented for the two striking ships, which are a passenger ship and a cargo reefer. These striking ships are chosen by considering their size relative to the struck ship: the passenger ship is smaller and the cargo reefer is larger. The principal dimensions of the striking ships are presented in Table 4.1, and the scantling configuration of the struck ship is given in Table 4.2. Numerical models are shown in Figure 4.1. Since different striking ships are used, the passenger ship will be denoted as the striking-I and cargo reefer denoted as the striking-II in further analysis.

Table 4.1. Principal dimension of the striking ship.

Dimension component	Striking-I	Striking-II
Length over all (m)	67.5	144.5
Breadth (m)	12.8	19.8
Draught (m)	3	5.6
Depth (m)	3.9	10.2

Table 4.2. Principal dimension and scantling of the Ro-Ro ship.

Variable	Value
Principal dimension (m)	
Length over all	85.92
Breadth	15
Draught	4.3
Depth	10.4
Scantling (mm)	
Main frame	L 150 x 90 x 9
Web frame	T 300 x 9 + 125 x 12
Strong beam	T 350 x 10 + 150 x 16
Side shell	12 (lower than car deck) and 10 (upper than car deck)
Inner shell	10
Main deck	8
Middle deck	8
Car deck	15
Tank top	12

(a)

(b)

(c)
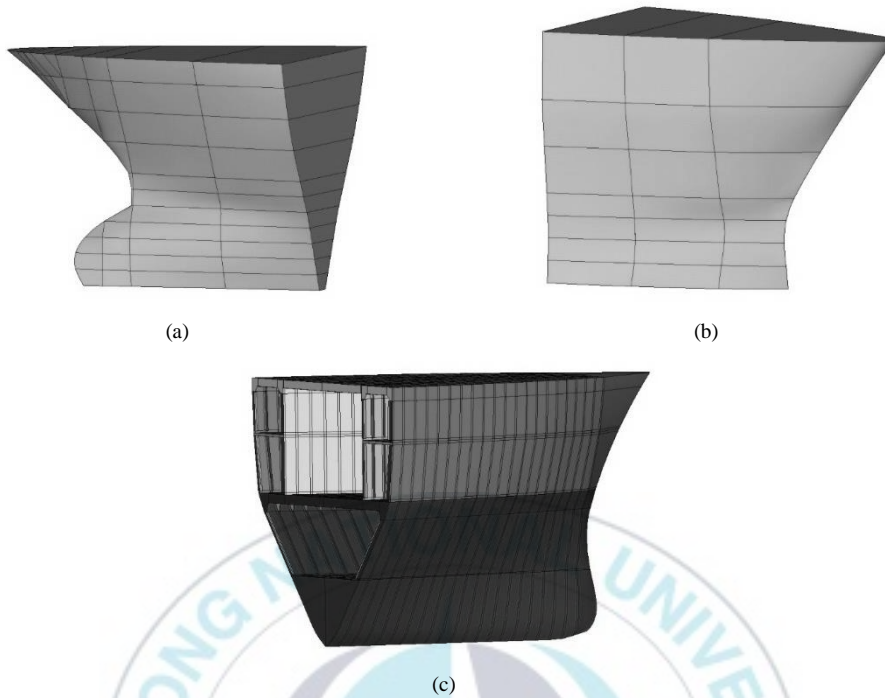
Figure 4.1. Numerical model of the involved ships: (a) striking-I, (b) striking-II, and (c) struck ship.

In the numerical experiment, ship models will be deployed as the involved ships, and will be analyzed in several scenarios by explicit finite element (FE) codes to estimate the structural crashworthiness of those ships in the event of a collision. As a highlight of the collision scenario, varying velocities will be modelled for the movement of the striking ships to the designated target location on the struck ship, which is restrained by the centerline. Fixation is applied to all transverse frames at the end of the struck ship model. In the same location, axial displacement is applied on the shell plating. When contact between two ships occurs, dynamic stress will be produced on the deformable structure as different parameters are applied in each scenario. Several responses are estimated to take place with respect to the applied parameters for both the striking and struck ship. As previously described, ship collision is a very complex process. It involves significant force, extensive damage contours, and crushing of structural members. Rupture is unavoidable in certain cases, and the entire process is highly nonlinear. Unwanted phenomena in such a dynamic system can occur in the form of hourglass and shear locking phenomena. The fully integrated Belytschko-Tsay element formulation is implemented as a countermeasure for all model scenarios.

$$\varepsilon_f \left(l_e \right) = \varepsilon_g + \varepsilon_e \cdot \frac{t}{l_e} \tag{4.1}$$

Table 4.3. Proposed failure strain versus mesh size (GL, 2003).

Stress state	One dimension structure	Two dimension structure
ε_g	0.079	0.056
ε_e	0.76	0.54
Element type	Beam-Truss	Shell-Plate

A plastic-kinematic material is applied on the struck ship—the failure criterion for this type of material is defined based on the failure recommendations of Det Norske Veritas - Germanischer Lloyds (GL, 2003), as shown in Equation 4.1 and Table 4.3. Mesh sensitivity of the overall model is determined to be in the range of 5-10 in terms of element length-to-thickness (ELT) ratio. As two ships undergo contact in a collision process, their friction properties must be defined. Typically, static coulomb friction coefficients in the range 0.2-0.4 are adopted for steel-on-steel contact. Therefore, a coefficient of 0.3 will be implemented for the FE configuration in this work. Further details of the engineering model (i.e. material properties, ship velocities, and target location) will be described in next subsection.

4.2 Scenario Configuration

A series of collision scenarios are defined for the present work in this subsection. The applied parameters in the analyses are considered based on external and internal parameters relative to the struck ship. In terms of external parameters, the velocity and size of the striking ship are considered. Several implemented material properties (based on chemical composition and differences in structural arrangement as affected by the target location) are determined as the internal parameters. This consideration is applied to the simulation based on a review of the mechanics of ship collisions (Zhang, 1999), where the external parameters are evidenced to contribute significantly to the crushing of involved structures. Ships with several structure material and shipbuilding arrangement may be subjected to impact loading, which leads to an assessment of the crashworthiness of a ship structure with several internal configurations (i.e. material and structural arrangement) against side collision.

In the present work, the striking ships are assigned specific velocities in the range of 1-10 m/s. Constant and initial characteristics are defined to demonstrate the contribution of ship velocity to struck and rebounding phenomena in a side collision scenario. In order to evaluate

the capability of the struck ship to resist collision impact in various situations, the velocity range is expanded, so that velocities higher than the recorded velocity of the striking ship are included in the analysis. For another external parameter (as described in the previous subsection) two striking ships are determined based on their size relative to the struck ship. The effect of ship size on structural behavior under impact will be observed and discussed. The size affects the target location of each striking ship, which is illustrated in Figure 4.2 with the assumption that during a collision process, the involved ships are fully loaded.
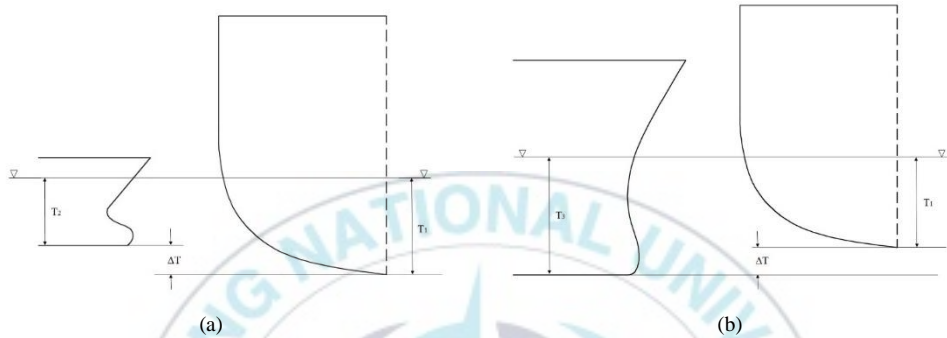
Figure 4.2. Draught gaps between striking and struck ships: (a) with striking-I, and (b) with striking-II.

Table 4.4. Material properties of the proposed steel.

Material	Steel grade	Yield strength (Pa)	Ultimate strength (Pa)	Elastic modulus (Pa)	Density (kg/m³)	Poisson's ratio (-)
Medium-carbon	1030	4.40×10^8	5.25×10^8			
High-carbon	1080	4.80×10^8	8.00×10^8	2.10×10^{11}	7850	0.3
HSLA	AH32	3.15×10^8	4.70×10^8			

Thus, the ships mold until they reach maximum draught. The internal parameters of the struck ship are implemented with consideration of the steel material according to the carbon composition. There are three steels (including medium-carbon, high-carbon, and high-strength low-alloy (HSLA) that are used on the deformable structure. The strength properties of these materials are presented in Table 4.4. In the proposed material model, the strength properties of the three steels will be applied along with the calculated failure strain with respect to mesh size. The structural capability under the influence of several materials will be assessed against collision with the striking ships.

On the other hand, besides affecting draught (the larger ship has a higher draught), the dimensions of the striking ships also contribute to the target location in the vertical direction, which has a different structural arrangement. Striking-I, which is smaller than the struck ship,

impacts the lower part of the side structure of the struck ship. This part is defined to be the side structure between the car deck and tank top. Striking-II is larger than both the struck ship and striking-I, and it impacts the upper part of the struck ship. This part is determined to be the side structure between the main and car decks, where an inner shell is also installed. The ship crashworthiness of the upper and lower parts (which have significantly different structures) subjected to the defined collision scenarios are evaluated and discussed.

5. Comparison of Collision Cases with and without Ship Rebounding

The comparison results between cases with and without rebounding are presented in this subsection. As described in the scenario configuration, the possibility of the striking ship being completely stuck on the target ship exists, and can occur during collision, especially during a side collision. However, the flexibility of the side hull of the struck ship provides another possibility, in which rebounding may happen. Two velocity types were calculated. Their tendencies, shown in Figure 4.3 indicate that for cases with the same parameters i.e. velocity, involved ships, experiment time and other material and structure configurations, different results are obtained.
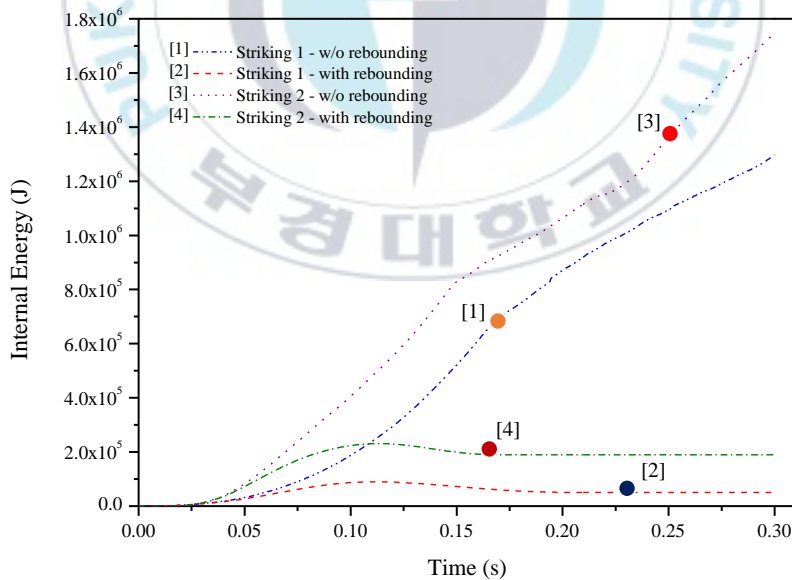
Figure 4.3. Result of internal energy for different applied velocity's characteristic.

The experiment, which was conducted using a constant velocity, produced an internal that increases continuously during a collision event. This behavior matches the applied

characteristics of the striking ship, which was set to constantly penetrate the struck ship during collision. In comparison with previous work (Haris and Amdahl, 2013; Ozguc et al., 2005; Lehmann and Peschmann, 2002; Paik and Pedersen, 1996) that used FE calculations, simplified expressions, and model tests, the energy tendencies in the present work are in good agreement. The initial velocity characteristics, on the other hand, indicated that the energy increases to certain level and decreases after reaching a peak point. This tendency is influenced by the elastic characteristics of the material and structure of the struck ship. During the initial penetration, the striking ship continuously penetrated the struck ship, moving with kinetic energy.
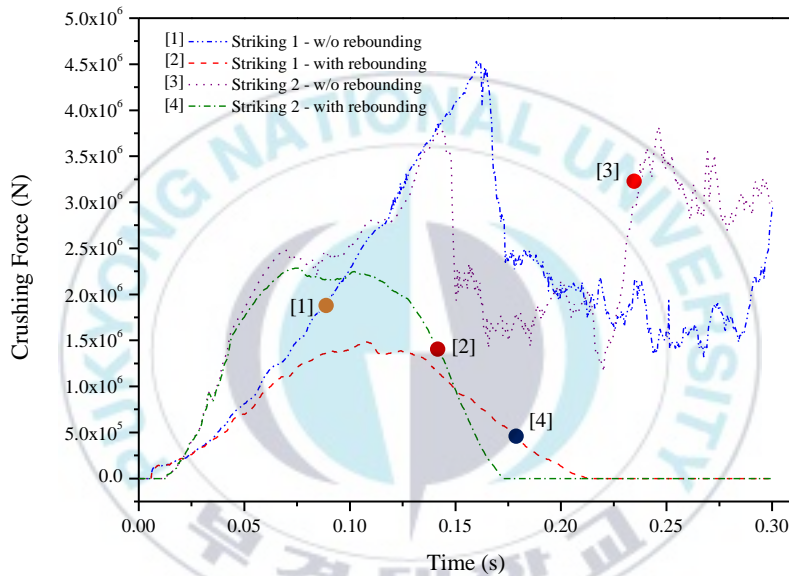
Figure 4.4. Crushing force during ship-ship collision on different targets.

A phenomenon of the deflected striking ship that reached the maximum penetration (in this moment it has zero kinetic energy and its movement is stopped) to opposite direction from the approach direction is called rebounding. A good correlation is also shown in terms of crushing force (Figure 4.4) during collision. The striking ship which using the constant velocity was found capable to perform extensive crushing onto deeper penetration than the initial velocity. High-fluctuation of the crushing force was observed take place along collision period and it completely stuck in the end of impact. The similarity of the characteristics of the two velocities is apparent only for very short durations (approximately 0.03 s). After this time period, the crushing force of the ship with a constant velocity

50

continuously increased; the ship with an initial velocity also increased, but not with the same significant tendency shown by the ship with the constant velocity. Based on this evaluation, it can be concluded that rebounding phenomena can possibly occur during a side collision scenario between two ships; this result demonstrates that the crashworthiness of the target structure can significantly differ during rebounding of the striking ship.

6. Structural Crashworthiness at the Collision
6.1 Striking Ship

This section presents an evaluation of how the striking ship continues to influence the structural behavior of a ship under collision. Several velocities are implemented for the movement of the striking ships towards their designated target locations, based on the sizes of the ships. Indications of rebounding are clearly shown by the internal energy during collision at velocities between 1-8 m/s in a collision scenario between striking-I and the struck ship. The tendencies in Figure 4.5 indicate that over a collision period of 0.075-0.10 s, the striking ship stopped for a moment before experiencing rebounding in the opposite direction.
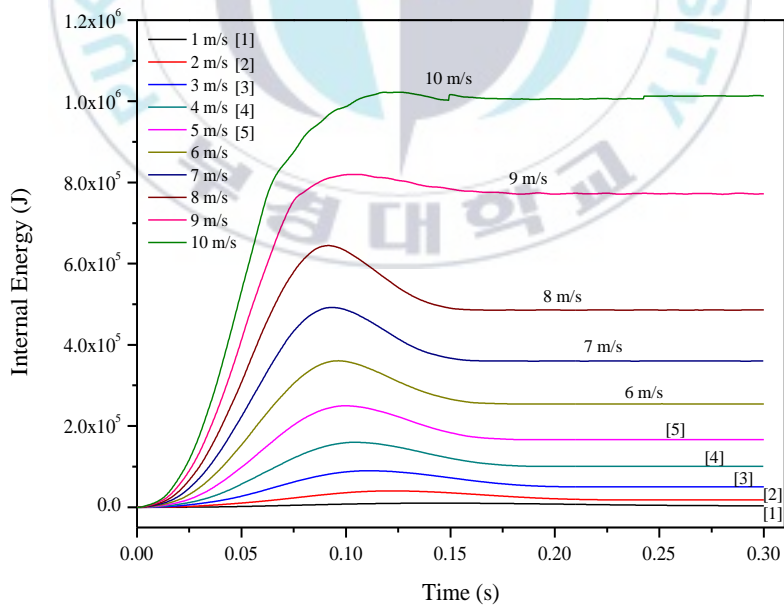
Figure 4.5. Internal energy for selected-ten velocities of the striking-I.
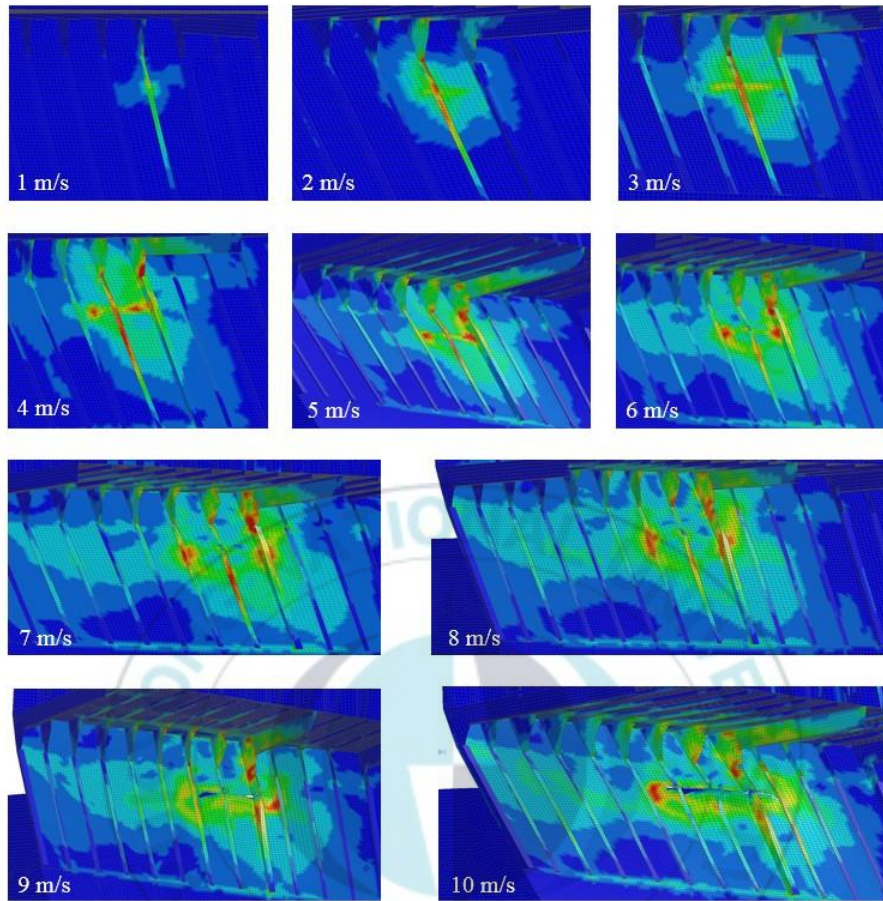
Figure 4.6. Extent of damage on the struck ship after collision with the striking-I.

After exceeding a velocity of 8 m/s, the internal energy does not produce a significant rising and reducing in the form of the hill-shape-like tendency given by 4-8 m/s. In conformation with the extent of the damage, it is observed that for a velocity of 9 m/s, the side shell was torn by the striking ship. A tear on the side structure of the striking ship was explicitly observed, as presented in Figure 4.6. A good correlation was observed at the moment of side plating failure between the internal energy and the extent of crushing force (Figure 4.7), reaching its peak point according to the applied velocity. The higher the striking velocity of the ship, the higher the force that is experienced. For the applied parameters, the tearing that occurred when the side plating ruptured influenced the force to significantly decrease over a short time. The conclusion of this behavior is different from for the collision that occurs before the side plating ruptures.
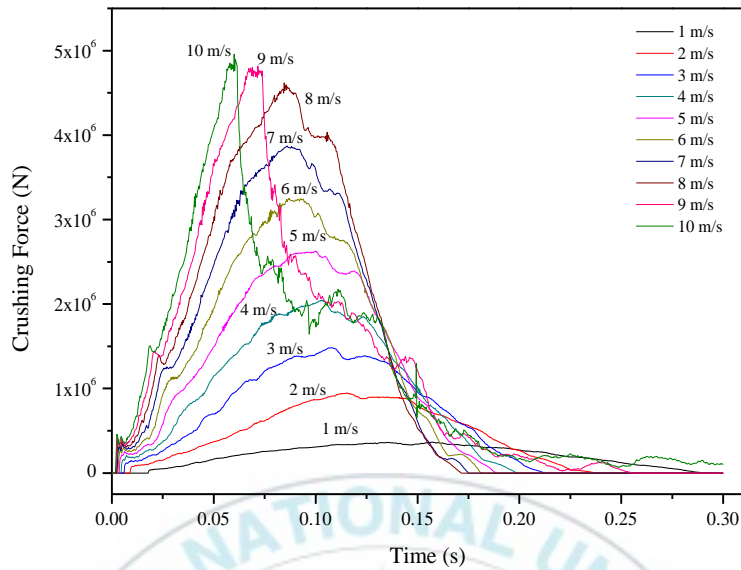
Figure 4.7. Crushing force of the collision scenario with the striking-I.

In the eight initial scenarios, the force decreases after collision, with an applied velocity of 9-10 m/s. In terms of velocities lower than those that produce rupture, the lowest velocity (1 m/s) produces almost no movement in term of internal energy. It is found that the characteristic of very low velocity (in this case can be represented by 1 m/s) in collision with respect to rebounding phenomenon is hard to be observed in term of the internal energy. Therefore, for this velocity, evaluation is performed on the crushing force behavior. In term of force, it is concluded that the force level for 1 m/s is the lowest of the proposed velocities. However, the time period for the force experienced by the struck ship is the longest in the category of no-plating-rupture velocity. For collision velocities in this category, rebounding also takes place. However, since the striking ship moves slowly, the rebounding process takes more time, which makes this behavior occur over a longer period than for ships moving at higher velocities, for which rupture occurs on the side plating. The characterization of structural responses to collision load can also be estimated from force. As velocity in this scenario increases, the force gradually increases over a time period of 0-0.20 s. The faster rate of increase will affect the period of decreasing force in cases where rupture does not occur. This rhythm indicates that the faster the applied velocity, the earlier the striking ship experiences rebounding.

53

During collision with the larger ship (striking-II), the struck ship experienced tearing earlier than it did in the scenario with striking-I. The present collisions indicate that side plating ruptures begin during collisions at a velocity of 6 m/s, occurring on the upper part of the struck ship. The internal energy in Figure 4.8 shows similar tendencies with the energy during rupture in collision with striking-I. From observations of internal energy, it can be estimated that a larger striking ship will produce a smaller rebounding distance than a smaller ship moving with the same velocity. Energy characteristics indicate that there is very little increase at the point at which the internal energy reaches a maximum and then immediately decreases. Hill-shape-like behavior is unlikely to be found in scenarios where a ship that is larger than the struck ship is used as the indenter.
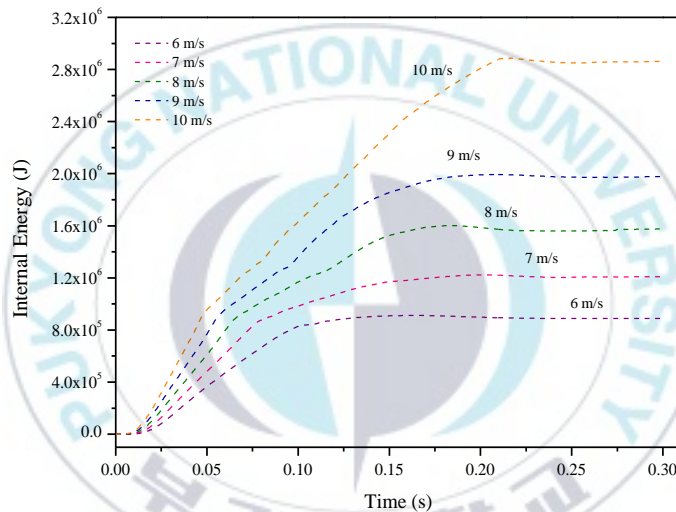
Figure 4.8. Behavior of internal energy under collision with the striking-II.

Higher velocities produce higher levels of internal energy—this response is defined as the energy that is needed to deform or even crush the involved objects for various collision cases. As presented in the literature review, the amount of destroyed volume for the involved structure is predicted to be equally perpendicular to energy. A larger destroyed volume also affects force fluctuation (Figure 5.9) and the tendency that "the tendency of a larger destroyed component to produce more fluctuation" is confirmed. The crushing force for the striking-II scenarios shows that in the initial collision, the tendencies of all velocities are similar, with different magnitudes. In the time range from 0-0.1 s, the side plating does not experience rupture. However, after 0.1 s, the force fluctuates in different patterns for each velocity. This behavior occurs similarly for several applied velocities, however, the extent of

54

penetration will be different (this penetration is followed by the rupture of structural members within the struck ship). Based on these results, it can be predicted that in a scenario where tearing occurs on the struck ship, the energy and force will be larger than for the applied velocity response that produces the greatest rebounding (refers to subsection 4.4).
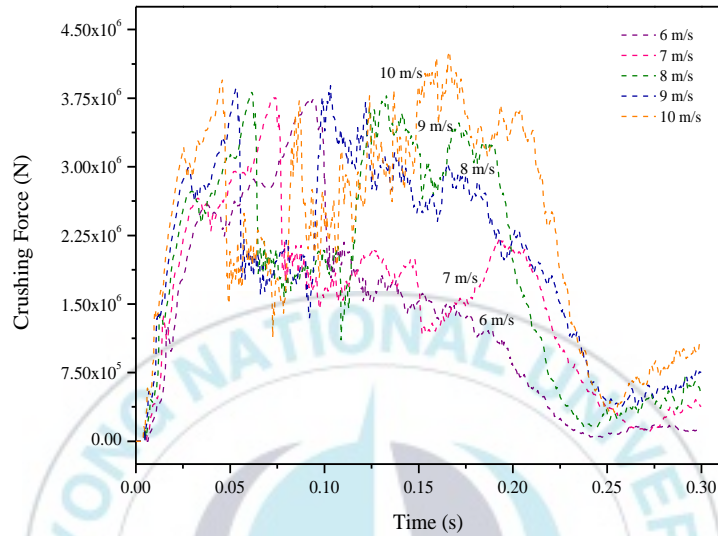
Figure 4.9. Crushing force in five scenarios with the striking-II acts as the indenter.

6.2 Structure Material

Material is an important and inseparable part of ship structure. The application of material to the side structure of a ship can be considered to be a reasonable option for increasing resistance against ship collision. When implementing side structure materials, it can be concluded from crushing force (Figure 4.10) characteristics that medium- and high-carbon steels have similar capacities for resisting collision. It has been demonstrated that an approximately 8% difference in yield strength does not significantly affect structural capabilities. However, a significant distinction is observed between plain-carbon and alloy steels. During the structural rupture occurring at 0.06 s, the low-alloy steel experienced a force magnitude that was 30% lower than that of the high-carbon steel. According to this study, it can be concluded that with a strength gap of 28%, the crushing force shows a significant difference, while the gap indicates that percentage difference of the yield strength and crushing force in the maximum point between two different materials is similar (in this discussion the yield strength differs by 28% and difference of the force in the peak is 30%).
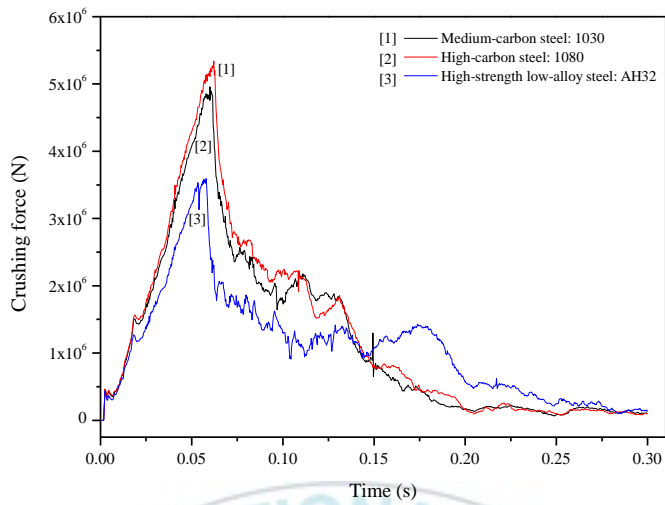
Figure 4.10. Crushing force in collision with the striking-II for different materials.
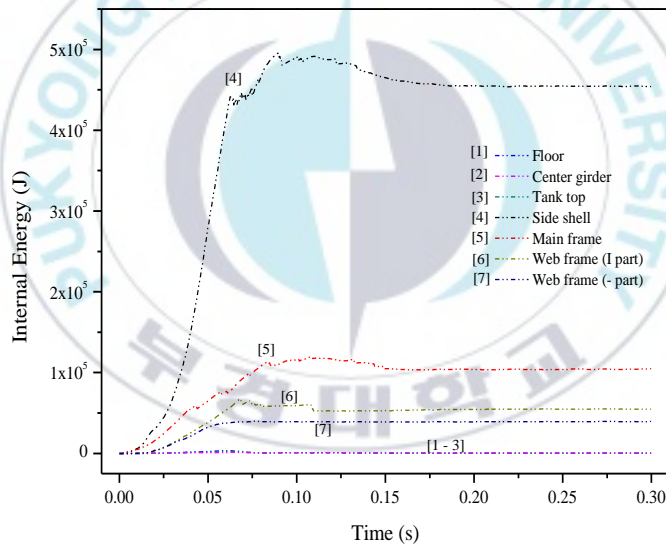
Figure 4.11. Internal energy for each part on the lower part.

With respect to structural arrangements, it can be concluded that the upper structure has a more complex arrangement than the lower structures, as three decks and an inner shell are installed at that location. Taking both the energy formulation and the previous discussion of the internal energy-crushing force relationship, it can be predicted that the internal energy that is required to destroy the lower part will be smaller than that required to destroy the upper part. The energy results for the lower and upper parts are consecutively presented in

Figures 4.11 and 4.12 (for each part connected to the side structure). An evaluation of the internal energy indicates that the outer shell contributed dominantly to side collision resistance. Energy tendencies suggest that the statement "collision to the upper part involves more structural members and leads to higher energy" has been satisfactorily demonstrated.
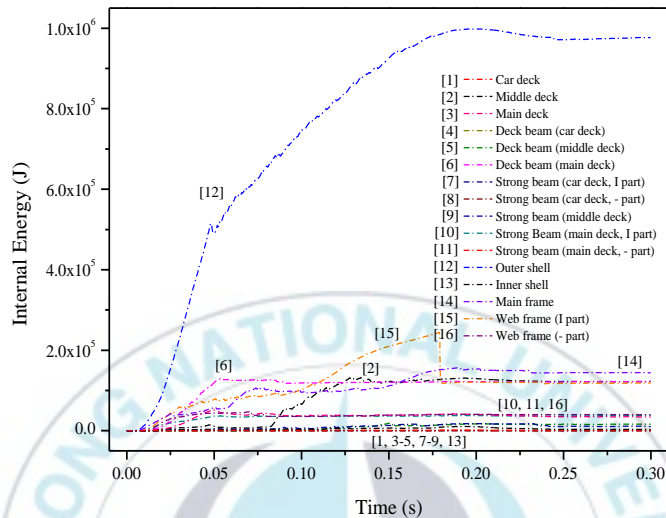
Figure 4.12. Internal energy of structural members on the upper part.

Extent of damage is presented in Figure 4.13 that indicates correlation between the energy and force is successfully confirmed by the occurred damage on the side structure. The material with higher strength will produce less tearing length. Similarity in the force tendency of plain-carbon steel material is shared in term of damage contour.
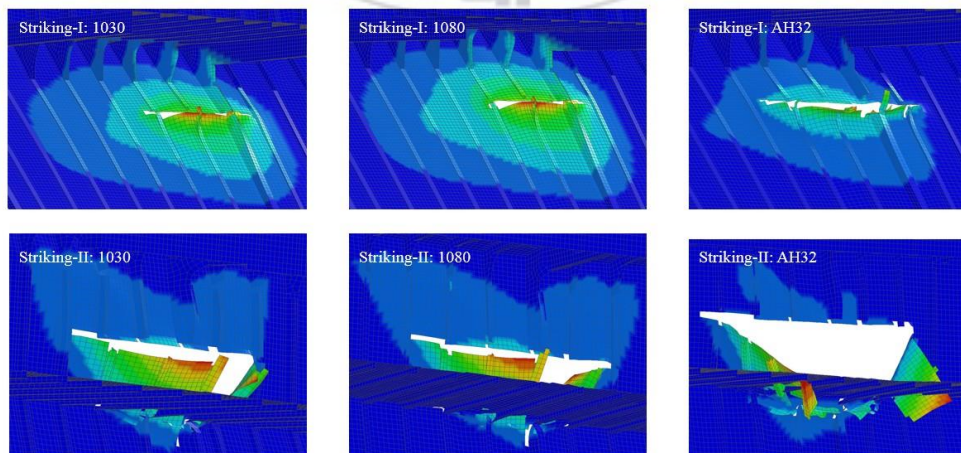
Figure 4.13. Damage extent by different material types respecting the ship size.

7. Overall Discussion on Rebounding of the Striking Ship

In a collision process between two ships, the striking ship may experience rebounding due to the elastic properties of the ship structure and applied material. As briefly discussed for applied velocity, the striking ship experiences a *zero-movement state* when the kinetic energy (Figure 4.14) is reduced to a low point. After passing this state, the striking ship rebounds in the opposite direction relative to the approach direction of earlier penetration.
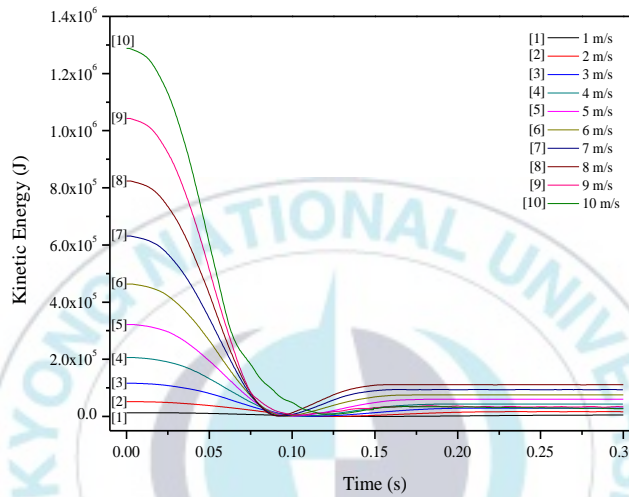
Figure 4.14. Kinetic energy of collision with the striking-I in different velocities.

Table 4.5. Displacement of the outer shell during collision with the striking-I.

Velocity	Displacement (m)				
(m/s)	Side shell	Main frame	Web frame	Tank top	Car deck
1	0.00549	0.00868	0.00000	0.00002	0.00406
2	0.02461	0.03142	0.00418	0.00067	0.01065
3	0.04742	0.05388	0.02805	0.00149	0.02945
4	0.06906	0.07950	0.04817	0.00207	0.03436
5	0.08848	0.10280	0.07417	0.00215	0.04397
6	0.11140	0.12920	0.09349	0.00219	0.05390
7	0.13370	0.15530	0.11210	0.00129	0.04689
8	0.16110	0.18590	0.13630	0.01756	0.05233
9	0.22440	0.28320	0.16550	0.01854	0.06406
10	0.31050	0.35630	0.17310	0.02549	0.07476

This phenomenon is verified by the characteristics of the kinetic energy, which increases after collision at 0.1 s. The rebound of the striking ship also provides a distinction between two groups: prior-to-rupture and after-rupture. In the first group, the striking ship fails to penetrate the side shell until the maximum peak internal energy and crushing force point is

reached. In this group, the tendency of the striking ship to experience rebounding is clear, with the kinetic energy increasing quite significantly after the zero-movement state. However, in the second group, where failure occurs, the time at which the striking ship experiences this state is late, and kinetic energy does not rise to as high a value as the previous group. Almost all of the initial kinetic energy is converted to internal energy, which in this situation destroys the side structure of the struck ship. The rebounding distance is presented in Tables 4.5 and 4.6, with the displacement of related members on the struck ship for different striking ships. More complex structures are involved in the collision with the striking-II, and rebounding distance in certain scenarios is not linear with velocity. This scenario is highly affected by the rupture of the struck ship. As previously described, satisfaction in velocity-rebounding relations is achieved for the prior-to-rupture group. The complexity of the structure that is affected by more-involved members makes the failure of each member happen at a different time. This demonstrates that ship collision involves nonlinear phenomena, as dynamic responses do not always provide a linear correlation between applied parameters and estimated results. The rebounding behavior of the upper structure is confirmed by the tendency of the kinetic energy (Figure 4.15) for the highest velocity. The kinetic energy for a velocity of 10 m/s is observed to be lower than for the collision with an applied velocity of 8 m/s, after the zero-movement state is passed by both velocities.

Table 4.6. Structural response during collision with the striking-II.

Velocity	Displacement (m)							
	Outer shell			Inner shell			Deck	
(m/s)	Side shell	Main frame	Web frame	Side shell	Main frame	Web frame	Main deck	Middle deck
6 m/s	0.28540	0.34250	0.17120	0.11430	0.11430	0.00011	0.06497	0.01106
7 m/s	0.30770	0.46300	0.23000	0.00294	0.00294	0.00294	0.06522	0.00517
8 m/s	0.52230	0.60350	0.36000	0.04583	0.04583	0.04583	0.09221	0.03219
9 m/s	0.54280	0.63490	0.45060	0.10030	0.10030	0.10030	0.07499	0.04434
10 m/s	0.80990	1.04400	0.69290	0.10820	0.10820	0.10820	0.06333	0.07575

With respect to the striking ship, based on displacement of structural members, it can be estimated that striking-II, as the largest ship in the present work, will contribute larger structural responses in terms of acceleration and damage mode than striking-I. As shown in Figure 4.16, the upper structure experienced larger fluctuations in term of acceleration than the lower structure. The double hull structure on the upper part is indicated to provide higher resistance during penetration by the striking ship. Damage modes on the struck ship with

respect to applied velocity are given in Tables 4.7 and 4.8 for striking-I and striking-II, respectively. Based on this data, striking-II has successfully penetrated the side shell with an initial velocity 6 m/s, while (as described in previous discussions) the rupture of the side shell during collision with striking-I occurs later, at an applied velocity of 9 m/s. The correlation between velocity and damage mode is similar to that observed for tearing mode.
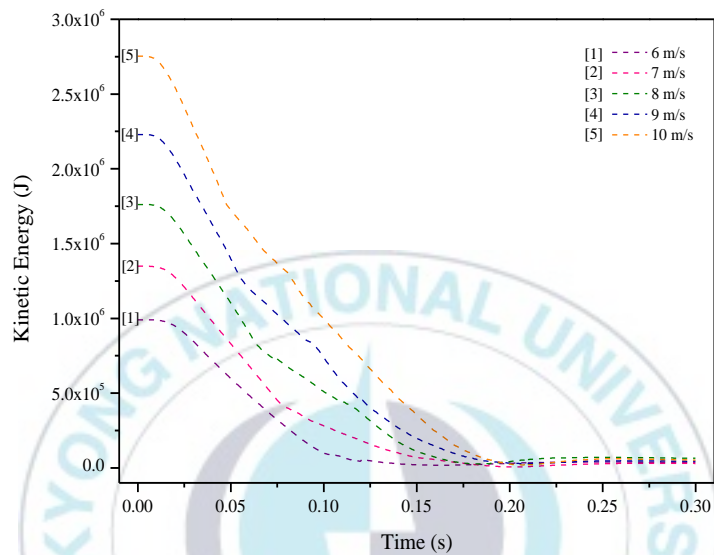
Figure 4.15. Kinetic energy on collision scenario using the striking-II as the indenter.
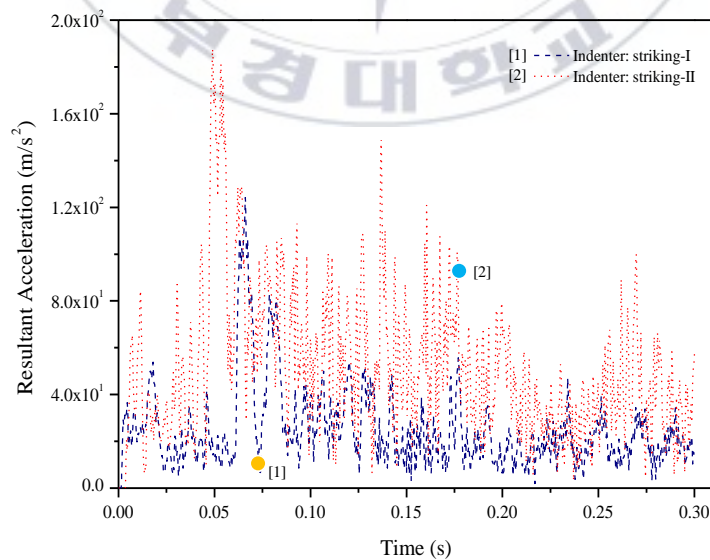
Figure 4.16. Acceleration of the struck ship during collision with velocity 10 m/s.

Table 4.7. Damage mode on side shell in collision with Striking-I.

Type	Velocity (m/s)	Damage on side shell (in length)		
		Tearing (m)	Plastic (m)	Folding (m)
Striking 1	1	0.0000	0.7804	0.0000
	2	0.0000	1.8789	0.0000
	3	0.0000	3.4565	0.0000
	4	0.0000	3.5199	0.0000
	5	0.0000	4.9240	0.5192
	6	0.0000	5.5185	0.8150
	7	0.0000	5.8337	1.4010
	8	0.0000	5.5619	1.9158
	9	1.3831	4.9595	2.2843
	10	1.9435	4.5347	2.7270

Table 4.8. Damage mode on side shell in collision with Striking-II.

Type	Velocity (m/s)	Damage on side shell		
		Tearing (m)	Plastic (m)	Folding (m)
Striking 2	6	1.3387	5.1236	1.9963
	7	1.9803	4.9111	2.0698
	8	2.2733	5.6496	1.9739
	9	2.7616	4.6931	2.0359
	10	3.0840	4.1722	1.1493

This statement is also supported by the structural behavior when different material types are used for the struck ship (Tables 4.9 to 4.11). Low-alloy steel, which has the lowest yield strength, produced the largest tearing of all proposed materials. A tearing length difference of more than approximately 35% was observed in comparison with the high-carbon steel. The rebounding distance in these collision scenarios also shows good agreement with material strength—the higher-strength material will produce a longer rebounding distance.

Crashworthiness can be defined as the ability of a structure to protect its cargo, passengers, crew, or other valuable entities during an impact. Depending on the nature of the impact and the objects involved, several criteria are used to determine the crashworthiness of a structure. In this work, energy, force, acceleration, and damage are presented and discussed. Accounting for crashworthiness and safety, the inner shell is an important component, as it acts as a final defense against side collision. On ships that carry goods that are dangerous when spilled in the ocean (such as crude oil and nuclear products), a double hull system is implemented. The installation of an inner shell is also expanded to the Ro-Ro ship presented in this work. Therefore, besides a discussion of the abovementioned crashworthiness criteria, it is also important to observe the condition of the inner shell after a collision process. It should be ensured that the inner shell is not breached by the striking ship, and that it does not experience significant damage.

Table 4.9. Displacement and damage during collision with the striking-I.

Material type	Displacement (m)					Damage on side shell (in length - m)		
	Side shell	Main frame	Web frame	Tank top	Car deck	Tearing	Plastic	Folding
1030	0.3105	0.3563	0.1731	0.0255	0.0748	1.9435	4.5347	2.727
1080	0.2713	0.3226	0.1505	0.0213	0.0734	1.7576	4.5997	3.6206
AH32	0.4035	0.568	0.4858	0.0226	0.0805	2.7698	3.0084	2.2173

Table 4.10. Displacement during collision with the striking-II.

Material type	Displacement (m)								
	Outer shell			Inner shell			Deck		
	Side shell	Main frame	Web frame	Side shell	Main frame	Web frame	Main deck	Middle deck	Car deck
1030	0.8099	1.0440	0.6929	0.1082	0.1082	0.1082	0.0633	0.0758	0.0170
1080	0.7248	0.8299	0.6197	0.0109	0.0109	0.0109	0.0871	0.0458	0.0046
AH32	0.7924	1.1220	1.2870	0.0321	0.0321	0.0321	0.1268	0.0137	0.0137

Table 4.11. Occurred damage during collision with the striking-II.

Material type	Damage on side shell (in length – (m))		
	Tearing	Plastic	Folding
1030	3.0840	4.1722	1.1493
1080	3.0048	4.3863	1.0735
AH32	3.7268	4.1028	1.1436

The conditions of both the outer and inner shell are presented in Figure 4.17. The results are taken based on a collision with striking-II, which is the largest of the deployed ships. The representation of these results, describing the worst scenarios in this study, is selected based on the internal energy, crushing force, experienced acceleration, and extent of damage. In previous discussions it has been concluded that striking-II produces higher energy levels and force fluctuations, more intense acceleration, and larger tearing on the struck ship. However, as shown, the condition of the inner shell is good-no tearing is found, and all major damage (e.g. plate tearing, folding, and plastic deformation) is experienced by the outer shell.

This tendency is already implicitly described by the internal energy and crushing force that only one significant rising of the energy and maximum fluctuation of the force is only found which indicates that penetration only occurs on the outer shell in early collision. The inner shell is verified to be safe until the end of collision process as the later tendency only presents small rising that represents the striking ship experiences rebounding phenomenon. Before the striking ship reaches the inner shell, its kinetic energy is absorbed by the outer shell; this is verified by the immense damage found in this component.
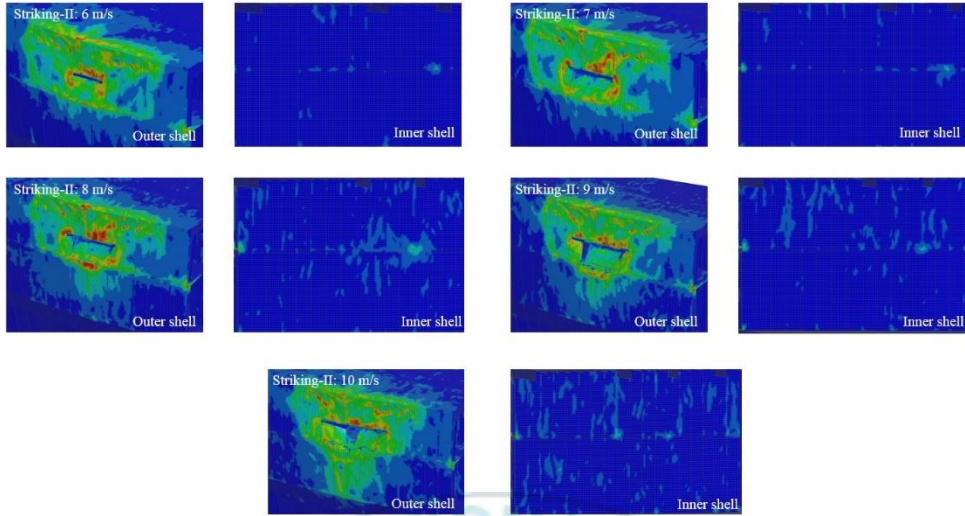
Figure 4.17. Damage of the outer and inner shells under collision with the striking-II.

Table 4.12. Five-highest-magnitude of velocity. Velocities in range 7-10 m/s are referring to Marine Traffic (2017).

Applied velocity		Recorded in operation
(m/s)	(kts)	(kts)
6 [similar to recorded data]	11.6631	Average: 10.30
7 [expanded]	13.6069	Maximum: 11.80
8 [expanded]	15.5508	
9 [expanded]	17.5946	
10 [expanded]	19.4384	

The elastic characteristics of the side structure cause the striking ship to rebound in the opposite direction, which indicates that the inner shell is successfully protected against side collisions in all proposed scenarios in this work. On the lower part, where only an outer shell is installed, tearing is found. However the tearing phenomenon occurs at a higher velocity than the recorded maximum velocity (Marine Traffic, 2017) for striking-I. The highest magnitude is found to be approximately 11.8 kts with an average of 10.3 kts. It can be concluded that if the recorded velocities (Table 4.12) are applied with striking-I, and side collision (with consideration of the striking ship's rebounding) occurs, then the struck ship will not experience tearing. As is described in previous discussions, during a side collision with striking-I, tearing begins when a velocity of 9 m/s is applied to the striking ship. Based on this discussion and using the aforementioned evaluation criteria, it can be concluded that the struck ship has crashworthiness against side collisions, with respect to the rebounding of the striking ship when internal and external parameters are applied to collision scenarios.

8. Concluding Remarks: Ship Rebounding

The results of a series of collision scenarios are summarized in this section. In the initial discussion, it was demonstrated that structural crashworthiness during rebounding phenomena occurring on the struck ship was different than it was for fully stuck cases. During rebounding, internal energy was observed increase to a peak, and then decrease to a certain point; that is, it demonstrated hill-shape-like behavior. This tendency was evaluated differently for fully stuck cases in which energy increased continuously. The rebounding distance of the striking ship was reduced during occurrences of side shell rupture. With respect to other parameters, the velocity and striking ship appear to have the most influence of all parameters during ship collision, especially when the extent of damage and rebounding distance are considered. The size of the striking ship is found to directly affect the target location on the struck ship. In discussion, it is concluded that this parameter will affect an internal parameter (namely, structural arrangement), as significant difference, especially in the vertical direction, influences the positions of the colliding struck and striking ships. The largest striking ship (striking-II) impacts the upper structure, which has more structural members than the lower part, which collides with striking-I. There is a good correlation between internal energy and crushing force for all proposed scenarios. The extent of damage during the internal parameter, i.e. structure material is applied on both of the upper and lower parts suggests good agreement that the rebounding distance is equally perpendicular with the strength of the material. In the same discussion, it can be concluded that there is no significant difference in term of crashworthiness during collision between medium- and high-carbon steels. It is recommended that medium-carbon steel be used as a structural material, since high-carbon materials are more expensive. Because of the carbon content, this steel is difficult to bend or form, especially for a passenger ship, which is dominated by curved shapes.

The conclusion of rebounding phenomena occurs after the striking ship experiences a zero-movement state in a side collision scenario. In this situation, the kinetic energy of the collision is completely absorbed by the struck ship. As applied material on the struck ship has elastic properties, the absorbed energy is deflected in the opposite direction, so that the striking ship undergoes rebounding. This is confirmed by the fact that kinetic energy rises again after the zero-movement state has been passed. The rebounding of the striking ship is obtained reach its farthest distance in one-velocity before rupture occurs (if tearing occurs in the 9 m/s, then the farthest distance will occur in the 8 m/s). This conclusion is summarized

with the assumption the striking ship is applied by the rigid body. Considering that rebounding is reduced when rupture occurs, it can be estimated that when a deformable striking ship is deployed, the rebounding distance will be lower than it is in a scenario using a rigid striking ship.

This phenomenon occurs because the kinetic energy is absorbed not only by the struck ship, but also by the striking ship. This kinetic energy is converted into internal energy that destroys both deformable structures, which is confirmed by the fact that damage occurs on both the struck and striking ship. In this situation, a fully stuck scenario is possible for the striking ship. Verification of the rebounding mechanism described in this study is obtained from Newton's third law of motion that for every action (i.e., the penetration of the struck ship), there is an opposite reaction (i.e., the rebound of the striking ship). The kinetic energy during rebounding does reach the value of the initial penetration, because most of the energy has been converted to plastically deform or even destroy the struck ship as a part of the collision process. The rebounding mechanism discussed in this work can be considered in further studies, especially for collision analyses involving a bulbous bow on the striking ship. Sustainable impact engineering studies for marine structures are highly encouraged, and it is recommended that researchers plan for the verification of an experimental methodology before main analysis is conducted.

V. Grounding Action

1. Introduction

Inspired by an advance development of engineering and technology, maritime societies are shifting their fashion from general rules to specific regulation for each ship. The other factor of this change is affected by rising the demand for safety prediction and wide range of crashworthiness assessment for marine and offshore structures, especially against various accidental load forms. Recently, Lloyd's register report indicated accidental loads in forms of collision and grounding, are still nominated as the highest cause of maritime pollution since early 1900s (Allianz, 2012). Initially, a concern of ship structure against accidental loads was addressed on nuclear powered ship by Minorsky (1958) who later his proposal in empirical formula was developed by several scholars (Woisin, 1979; Paik, 1994; Zhang, 1999). Regarding another cause of marine pollution, grounding is also considered as dangerous as collision. Theory of this phenomenon was described by Simonsen (1997a).

Applications of analytical approach (Paik and Lee, 2005) and actual experiment (Calle et al., 2017) were used to solve thin-walled structural problem. Collaboration of these methods was also considered to evaluate validity of each calculation method, for example by Paik and Seo (2007). Advance development of computational instruments in recent decade presented more acceptable method to conduct structural assessments (Paik and Thayambali, 2003; Leheta et al., 2015). In fields of the impact engineering and marine structures, ship grounding was analyzed using a collaborative strategy of the mentioned approaches, with the computational method Finite Element (FE) was taken as the main methodology. This phenomenon was continuously observed together with another form of impact on marine-steel structures, such as collision by various parties in last five years, and results of the FE were judged reach a satisfaction (Prabowo et al., 2017c-f; Sormunen et al., 2016; Heinvee and Tabri, 2015). Numbers of these works show a trend line that impact phenomena still keep many problems and they still have not been solved. Alsos and Amdahl (2007) state that "Ship grounding is a very complex process. The consequences may be severe and the process is highly nonlinear", and comparative study to assess crashworthiness of marine structures against various impact scenarios is continuously demanded for safety development. Thus there is a need for further research to evaluate the crashworthy of existing structure design.

This work aimed to calculate structural responses and crashworthiness criteria of a double hull tanker under ship grounding using a verified FE methodology. A comparative study on

ship grounding accounting for a variety of the penetration types and selected impact parameters will be conducted as main discussion. Bottom racking and ship stranding were assumed as impact scenarios and to be encountered by the tanker. Effects of the external parameters, such as impact location and obstruction topology will be considered to observe structural responses in details for each scenario. Progressive failures were presented with double bottom damage extent during ship grounding to provide a complete response estimations.

2. Understanding Ship Grounding Phenomena

Accidental loads or so called impact on marine structures have become a top priority due to its characteristic to cause remarkable-disaster scale. Recent statistical evaluation since 2007 by Allianz (2017) concluded that vessels' wrecked/stranded (including grounding) are placed at the second place of top ten vessels loss causes. The ship grounding is stable at this position and it is only surpassed by vessels' foundered for a decade. Remarkable fatalities and high level risks for passenger, environment and carrier are also considered to be important parameters to put ship grounding at this position. A series of oil spillage cases around the world, e.g. disaster of the Exxon Valdez in US territory and the Amoco Cadiz in Europe continent has provided solid evidence for contributions of ship grounding to both maritime and industrial casualties.

Based on its occurrence on ship, grounding is classified into two subcases, such as horizontal slide as referred by raking, and vertical penetration often mentioned as stranding (Figure 5.1). Raking occurs during powered-ship condition or when ship in straight motion during a voyage. Interaction with obstruction can be influenced by heavy fog and a navigational error in estimating topology in a sailing route. Other conditions are experienced such as bad weather and other catastrophic event which effect dynamic motion of the ship. In these conditions, stranding is mostly taking place the pitch and heave due to wave movement and the bottom structure is laterally penetrated by rock or shoal. In terms of the oceanic obstruction, estimation of obstruction topology requires wide insight of seabed contour which its data is actually hard to be accessed. Most of pioneer works use an assumption based on damage of high profile Exxon Valdez accident in 1989 where a pinnacle of seabed opened a large part of ship bottom, for the seabed topology in grounding test and simulation.
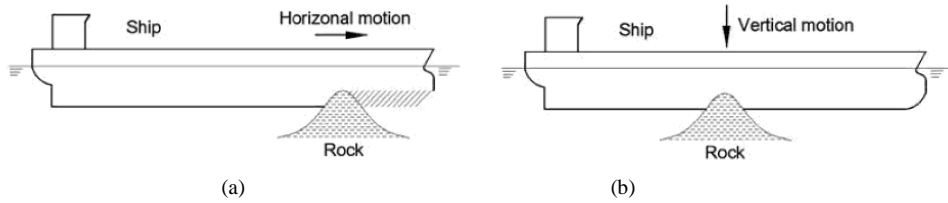
Figure 5.1. The grounding scenario during contact with obstruction: (a) raking and (b) stranding (Liu et al., 2017b).

Shipping safety, cargo protection and marine pollution are strictly linked. Numerous efforts to provide an adequate protection can be classified into two parts. The first part is the active method which is conducted by ensuring shipping/voyage of ships can be well supported using good navigational instruments. Advance radar system, crew training and traffic control regulation are example of this part. The second part is passive method which is presented by developing design crashworthy of marine structures. Famous example of this method is initially announced by applying double hull systems since Oil Pollution Act 1990 (OPA 90). As fast countermeasure of the Exxon Valdez's oil spill due to a grounding phenomenon, double hull system on dangerous-cargo ships is introduced, especially to reduce amount of oil spill. By applying this system to structures, ship will have two inner parts which protect the cargo during impact, namely double side shell and double bottom. The main idea of this system is if ship encounters collision or grounding, the inner shells in side and bottom structures (Figure 5.2a) of the double hull are still intact to reduce or even avoid of oil spillage after ship experiences the impact. Meanwhile, the conventional single hull (Figure 5.2b) will unleash remarkable amount of oil in moment the outer shell is breached by any obstructions. In this situation, chain disastrous events are highly taking place, such as stability loss, reduction longitudinal strength, structural collapse, which lead to life loss of crew and foundered or ship sinking.
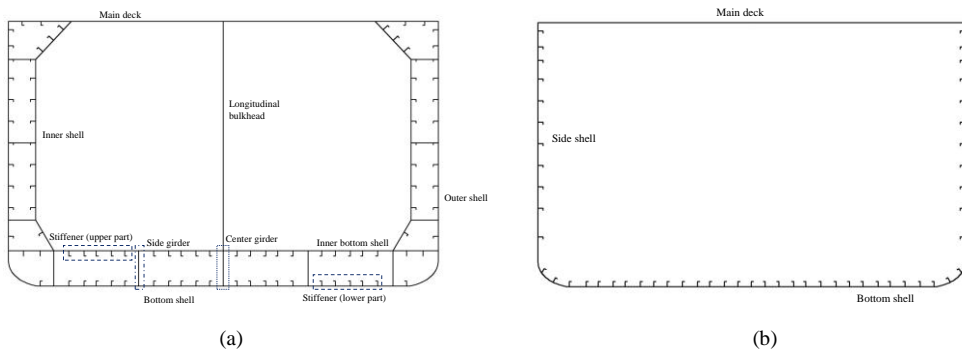
Figure 5.2. The hull design for naval structures: (a) advance double hull and (b) conventional single hull.

3. Grounding Analysis

3.1 Ship Geometry and Assumed Marine Steel

A set of terminology was set to identify the involved entities in the present work. The bottom structure was modelled as a 17000 DWT chemical tanker with given principal dimensions: length overall (L_{oa} = 144 m); breadth (B = 22.6 m); depth (H = 12.5 m) and draft (T = 9.1 m). The geometry model was built in forms of two tank length to reduce interference of the boundary conditions. In following description, this entity was denoted as the *structure*. Table 5.1 shows scantling data and plate thickness for the bottom structure.

Fully integrated shell formulation was applied to the model in order to avoid inaccuracy of deformation due to the hourglass mode. The structure was implemented by a deformable characteristic in order to assess structural damage under several grounding actions. The plastic-kinematic model is used to define the deformable structure, which its formula is shown in Equation 5.1, and the properties in Table 5.2.

Table 5.1. Scantling data of the tanker's double bottom structures.

Components	Configuration (mm)	Components	Configuration (mm)
Center girder	12	Bottom plate – on the keel	14
Side girder	11	Bottom plate	12.5
Bottom stiffener	150 x 90 x 12	Inner bottom plate – upper part of keel	14
Inner bottom stiffener	250 x 90 x 10	Inner bottom plate	13.5
Transverse floor	11	Bilge plate	12.5

$$\sigma_Y = \left[1 + \left(\frac{\dot{\varepsilon}}{C} \right)^{\frac{1}{P}} \right] \left(\sigma_0 + \beta E_P \varepsilon_P^{eff} \right) \tag{5.1}$$

where σ_Y is the yield stress, $\dot{\varepsilon}$ is the strain rate, C and P are the Cowper-Symonds strain rate parameters, σ_0 is the initial yield stress, β is the hardening parameter, Ep is the plastic hardening modulus, E is the elastic modulus, and ε_p^{eff} is the effective plastic strain.

Table 5.2. Properties of the material models in FE simulation: double bottom structures.

Marine steel	Elastic modulus (MPa)	Poisson's ratio (-)	Hardening exp. (-)	Density (kg/m³)	Yield strength (MPa)
AH 36	200000	0.29	0	7850	350
AISI 1030	210000	0.3	0	7850	440

During interaction with oceanic obstruction, heavy damage is expected on the structure, such as rupture of shell, girder crushing etc. Defining failure criterion to acquire precise estimation of damage extent was considered as necessity. In this study, failure was described as a condition of any structural component (plate, stiffener, girder or frame) which surpassed its failure strain limit after experiencing excessive plastic deformation due to contact with an oceanic obstruction. The failure strain value 0.11 was to be applied on the structural geometry, which was taken in considering Amdahl findings (Amdahl, 1995). He stated that typical failure range 0.2-0.35 is too large due to scale effect and material imperfection in collision assessment. In same reference, Amdahl suggested strain value for deformable structure approximately 5%-10%. Besides the failure strain, mesh size was considered as important aspect in impact analysis as it affect the structural deformation. Recommended criterion of the Det Norske Veritas - Germanischer Lloyd (GL, 2003).

As interaction of the structure and obstruction was expected in grounding analysis, it was necessary to consider friction value as part of contact properties. Generally, this value is taken according to Coulomb friction coefficient in the ranges 0.2-0.4 which are previously adopted by Simonsen and Wierzbicki (1998). Variation in the coefficient implementation may occur considering condition of the underwater hull surface conditions, especially bottom and bilge plates. In many cases, the plate surface becomes slippery due spilled oil and marine plant. Assumption of the surface roughness as influenced by manufacturing process, can also be affecting factors. In this study, standard value for steel - rock interaction 0.3 was adopted for the grounding analysis.

3.2 Seabed Topology and Applied Material

Besides description of the structure materials, the seabed detail was also to be presented. This entity would be modelled as the solid-rigid material to idealize hard-grounding situation so that the structure was designed to absorb all impact energy and deformation process. Summary of the obstruction material models for this research is presented in Table 5.3. The seabed would be determined as the obstruction which consisted two topologies of seabed. A conical obstruction is assumed rock and shown in Figure 5.3a to be applied by the Plagioclase feldspar (Christensen, 1996) and used in comparing structural crashworthiness under raking and stranding. In the next analysis, variety of contact surface on the obstruction is considered as an important factor in experienced damage on ship. Therefore, two obstructions with different geometry and configuration than the conical obstruction are

designed and denoted by rock and shoal (see Figures 5.3b-c). The Pyroxene (Christensen, 1996) is to be embedded on these obstructions and deployed in comparative study to assess structural behavior against different obstruction in raking case.

Table 5.3. Properties of the material models in FE simulation: oceanic obstructions.

Seabed mineral	Modulus (MPa)	Poisson's ratio (-)	Density (kg/m^3)
Plagioclase f	67450	0.296	2690
Pyroxene	147000	0.281	4002
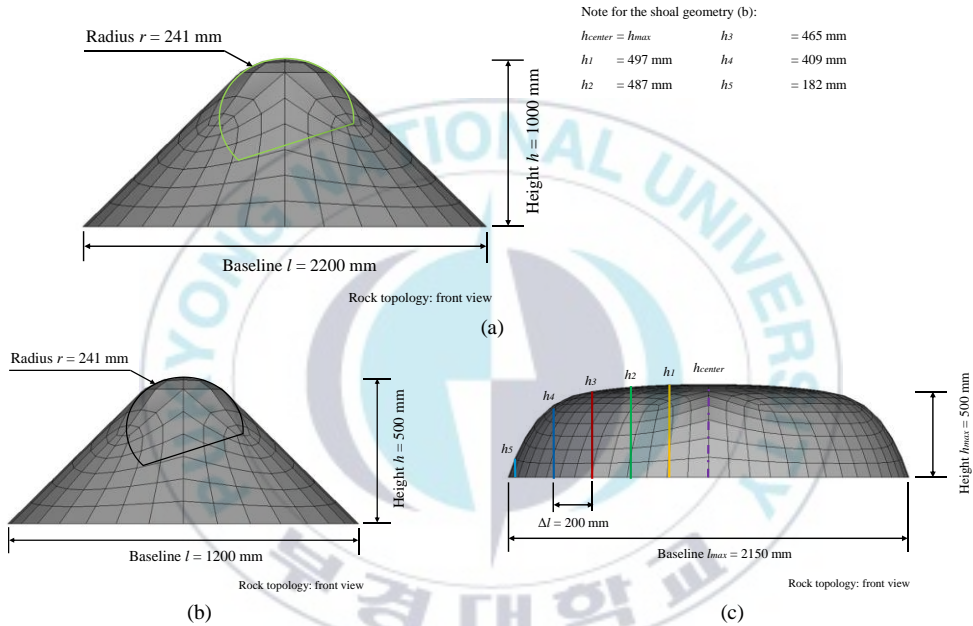
Figure 5.3. Obstruction geometry: (a) conical geometry; (b) and (c) are idealized rock and shoal, consecutively.

3.3 Detail of Grounding Scenarios

The initial grounding analysis was addressed to observe structural behavior of the double bottom under raking and stranding. As shown in Figure 5.4, bottom raking is designed to be experienced by three targets, including center girder, side girder and space between girders. In these scenarios, the conical obstruction was placed in-line to the ship model and applied with uniform velocity 10 m/s. The marine steel AH 36 was to be embedded on the ship geometry, while the analysis time would be terminated in $t_{sim.} = 0.4$ s.

71
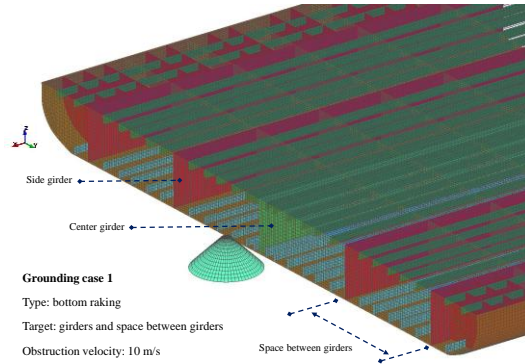
Figure 5.4. Grounding scenario for the first case, bottom raking.
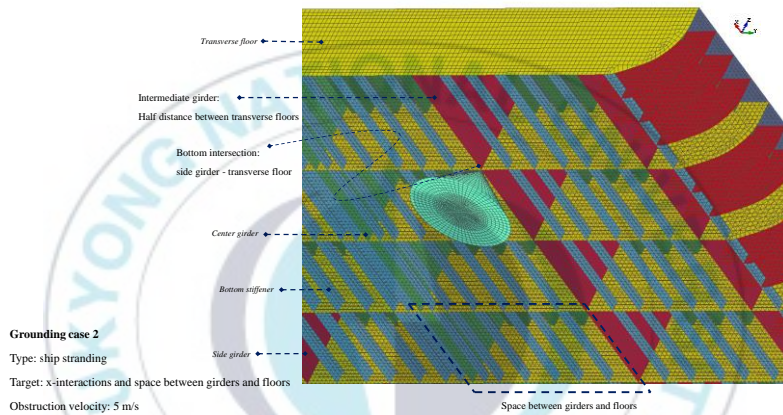
Figure 5.5. Assumed scenario of the second case, ship stranding.

With same setting as bottom raking, next grounding analysis was arranged to observe structural nonlinearities under ship stranding. Different targets were selected due to different location of the conical obstruction. In this scenario, the obstruction was placed below the double bottom, and the structure was penetrated by the obstruction in lateral direction during the position of two entities was inline in vertical direction. The target for this accidental case was determined to be targeting three locations, i.e. x-intersections, and spaces between girders and floors (see Figure 5.5). It was assumed that the stranding takes place during rough sea so that ship experiences slamming and contact with seabed. Therefore, applied velocity in this case is lower than the raking scenario, which velocity 5 m/s is considered in stranding analysis. This assumption is considered reasonable since stranding occurs during heavy storm or violent wave which makes ship slamming and pitching in the vertical accident and contacts with seabed obstruction. In other hand, the raking problem mostly

happens during a ship is sailing forward in powered-condition (Simonsen and Hansen, 2000) which makes applied velocity in raking is generally higher than stranding.

After raking and stranding analyses were performed, comparative study to assess structural crashworthiness against a variety of obstruction types was performed. Under bottom raking scenario as described in prior raking analysis, the rock and shoal topology as described in Figures 5.3b-c were deployed to act as the obstructions. In this comparative study, grounding scenarios were performed by a displacement which controlled behavior of the internal mechanics. The structure was applied by steel AISI 1030 and fully clamped on the inner bottom and bottom shells to restrain its movement during penetration by the obstruction. The raking process was defined as very short loading which the limit of the FE simulation was to be $t_{sim.} = 0.5$ s for the comparative study of raking and stranding. Overall discussions to observe all conducted scenarios, including raking-stranding and rock-shoal cases were presented as summary of this study. Tendency of crashworthiness criteria, assessment on damage mechanism and verification of the FE results using empirical formula were completing the present work.

4. Results and Discussion
4.1 Structural Resistance and Characteristic: Bottom Raking

Observation of the structural response is conducted by assessing structural crashworthiness during the ship against grounding action. Firstly, discussion is addressed to the internal energy. During calculation by FE approach, this criterion was acquired in forms of the internal energy. This energy itself is defined as the amount of energy which is necessary to plastically deform the involved entities in contact. This study presented this criterion in internal energy as it represents absorbed strain energy by the deformed structure in contact, which has same fundamental definition with the internal energy. In grounding scenario, the deformation was fully experienced by the double bottom structure. After three targets on the double bottom collided with the obstruction in the raking case (Figure 5.6), it was found that the center girder absorbed the highest energy level. The highest ranking was followed by the side girder and space between girders in the second and third places, consecutively. Compared to raking case with the side girder, higher energy occurred due to thicker plate of the center girder. Even though both targets was strengthened by a longitudinal girder, plate thickness also contributed to energy absorption in impact. On the third case where the target was the space between two girders, energy on this case was the

lowest. This phenomenon took place since less structural components was located in this location. Based on comparison in these components, it is found that the girders on the double bottom has important role in energy absorption process.
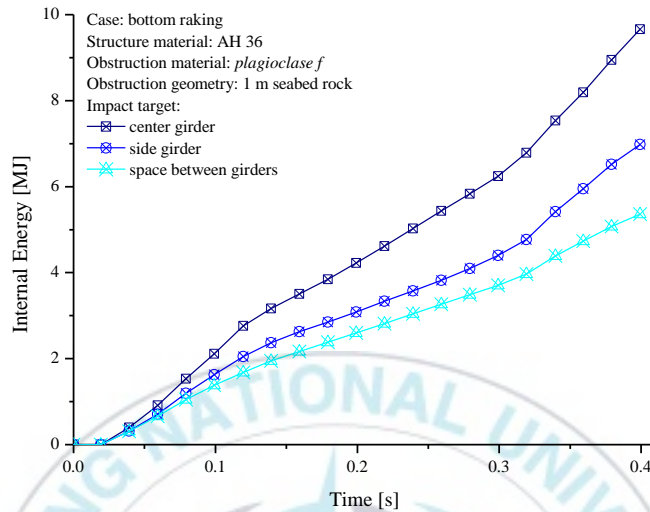
Figure 5.6. Results of the internal energy for three targets in the raking case.
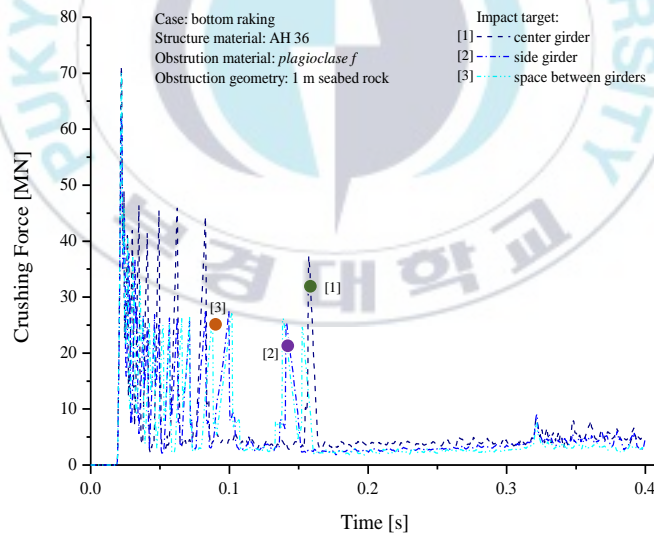
Figure 5.7. Tendency of the crushing force in ship grounding.

Force behavior for the three targets in the raking case (Figure 5.7) concluded that the highest magnitude was achieved by the center girder. This tendency confirmed behavior of the internal energy during structure-rock interaction. The force results also showed high fluctuation in early contact between the structure and obstruction. This fluctuations occurred

as deformation of the structure due to interaction with quite steep angular distance of the obstruction, happened on several structural components in same times, namely lower parts of the bottom shell, and transverse floor. More clear presentation of this phenomenon is presented in a comparative study between two obstructions with different geometric angular distance in next subsection (reefer to Subsection 4.3). After passing the high fluctuation period (in range $t_{sim.} = 0 - 0.15$ s), force fluctuations reduced to certain points in same time of damage expansion on the girders. In other penetration type of ship grounding, namely stranding, it can be expected that the fluctuation style of the crushing force will have significant pattern with the current raking case. This initial statement is highly possible to take place as the obstruction will interact with different structural component on the bottom structure, and penetrate the determined targets in different direction.

Ship grounding involved high internal energy and crushing force during deformation occurred on the bottom structure. In this case, structural crushing and progressive rupture according to penetration sequence are also required to be assessed in analysis. As shown in Figure 5.8, it was concluded that the most deformed component was the bottom plate. This component absorbed the strain energy under raking scenario approximately more than 1.5 and 2.5 MJ during the obstruction contacted with the side girder (left side of Figure 5.8) and center girders (right side of Figure 5.8), consecutively. During impact to the center girder, larger internal energy was presented by the bottom stiffener than the girder. It was caused by the arrangement of the stiffener near the center girder was more narrow so that the stiffener was placed in the second place. Moreover, components on the lower part of the double bottom, including bottom shell, bottom stiffener and center girder were ruptured during interaction with the obstruction. It was obtained that the damage width was similar with the maximum diameter of the rock obstruction on the interaction point (details in Figure 5.9).

This situation was confirmed by the raking case to the side girder, which the girder surpassed the stiffener in terms of the internal energy. This situation took place as influenced by the space between stiffeners in this impacted location, which was wider than the location near the center girder. Therefore, for raking to the side girder, top-three contribution of the structural resistance was presented by bottom plate, side girder, and bottom stiffener. For the transverse floor, after the first floor was breached approximately after $t_{sim.} = 0.10$ s, the constant state was experienced as no energy fluctuations observed.

Failure and penetration sequences:

1. Initial contact between the obstruction, floor, girder, and bottom plate.

2. Half of the obstruction penetrated the structure; and the bottom plate experienced the widest failure as maximum radius of the obstruction entered the structure.

3. The 1st floor was completely breached. After this point, the floor experienced constant state (no deformation).

4. Deformation on the 2nd floor was begun.

5. Bottom stiffener on behind the 2nd floor got pushed and torn by the obstruction.

The impact target was determined on the center girder, which until the end of analysis, effect of the side girder was not found.

Failure and penetration sequences:

1. Initial contact between the obstruction, floor, girder, and bottom plate.

2. Half of the obstruction penetrated the structure. However peak energy did not take place. The cause was the bottom plate on this location was not strengthened as near the center girder (distance between the side girder and stiffener was wider than the location near the center girder).

3. The 1st floor was completely breached and no deformation after this point.

4. Deformation on the 2nd floor was begun.

5. Bottom stiffener on behind the 2nd floor got pushed and torn by the obstruction. Increment of the energy was not as high as the raking case on the center girder, since the less stiffener was located on this location.

Case: bottom raking
Structure material: AH 36
Obstruction material: *plagioclase f*
Obstruction geometry: 1 m seabed rock
Impact target: side girder

Impact target: center girder
Structure component:
— · — center girder
······· side girder
— — — transverse floor
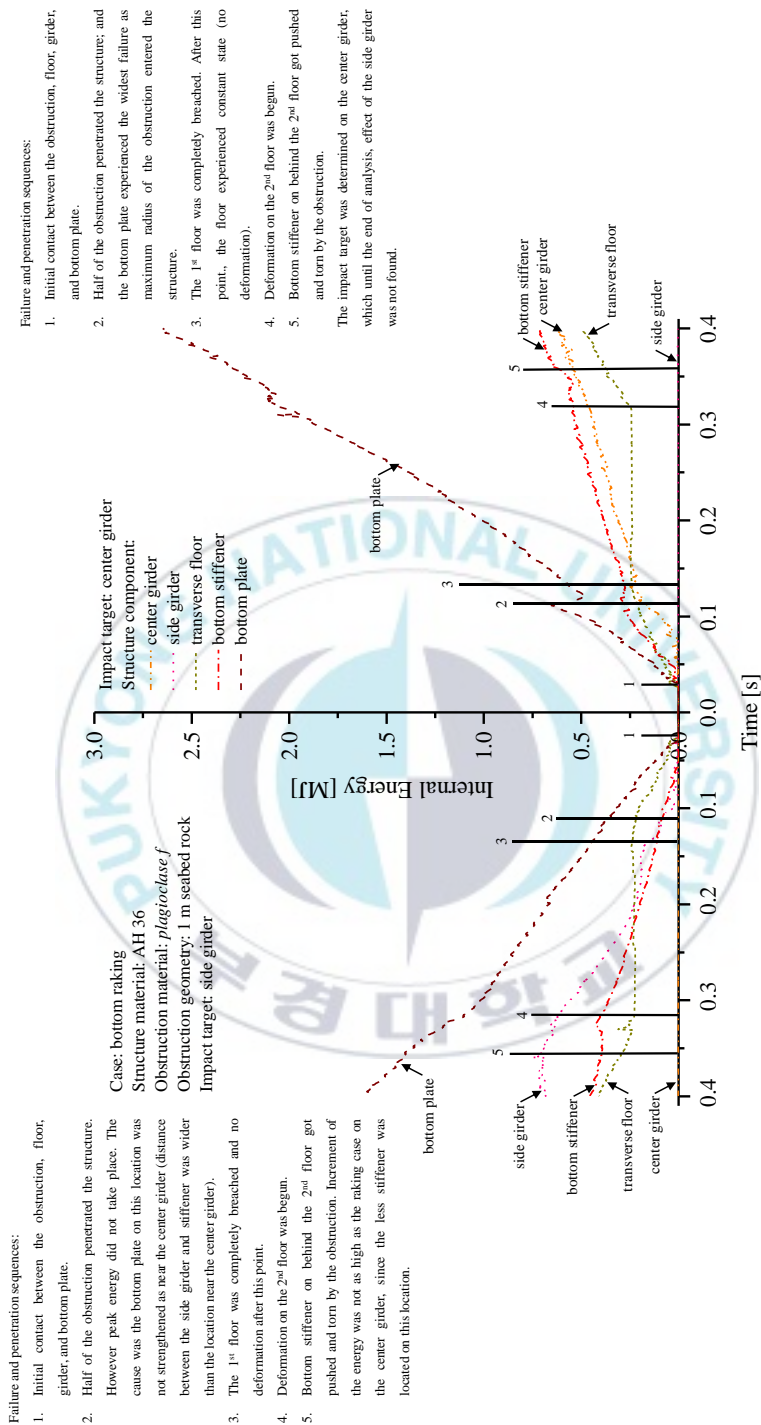— · · — bottom stiffener
— — bottom plate

Figure 5.8. Damage sequence of double bottom in structure-rock interaction.
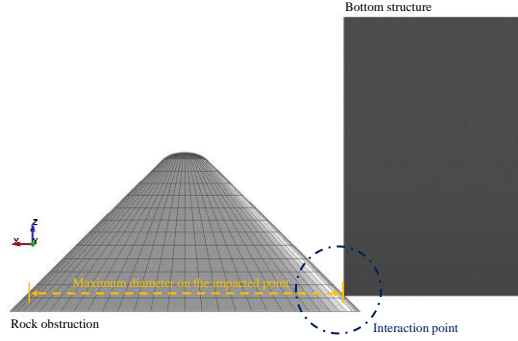
Figure 5.9. Maximum diameter of the obstruction on the interaction point.

It could be predicted from this result that after breached by the obstruction, rupture was focused on the bottom plate, stiffener, and girder, which had no influence to the floor. Fluctuation began to occur again during the second floor experienced deformation process due to advance penetration by the obstruction. It was also noted that, in case of raking to girder, rupture influences to side girder was not spotted until the end of ship grounding.

4.2 Structural Resistance and Characteristic: Ship Stranding

Other case of typical ship grounding occurs in forms of stranding to seabed. Structural deformation is expected if the seabed is formed either by sandbank or hard-rock geometry as analyzed in this work. Internal energy of the stranding case in Figure 5.10a showed difference tendency and level than the raking case (see Figure 5.6). The tendency of the intermediate girder, and space between girders-floors produced increment in range $t_{sim.} = 0.20 – 0.30$ s, which was earlier than the raking case. The energy magnitude of the stranding was also lower which the center girder in raking produced almost 10 MJ (Figure 5.6) in terms of the internal energy, while the girder-floor intersection showed approximately 8.6 MJ (Figure 5.10a). This phenomenon took place as the impact velocity in this case was reduced as assumed in previous sections. However, similar trend was achieved for both cases, which the part of the double bottom strengthened by girder under raking case was the highest as the strengthened structure by girder and floor in stranding case produced higher internal energy than other targets. The energy criterion also confirmed that the longitudinal girder had significant role in providing structural resistance for both longitudinal impact to T-intersection (consisted: transverse floor, bottom plate, and girder) in the bottom raking, and X-intersection (had same components as the raking) in the ship stranding.
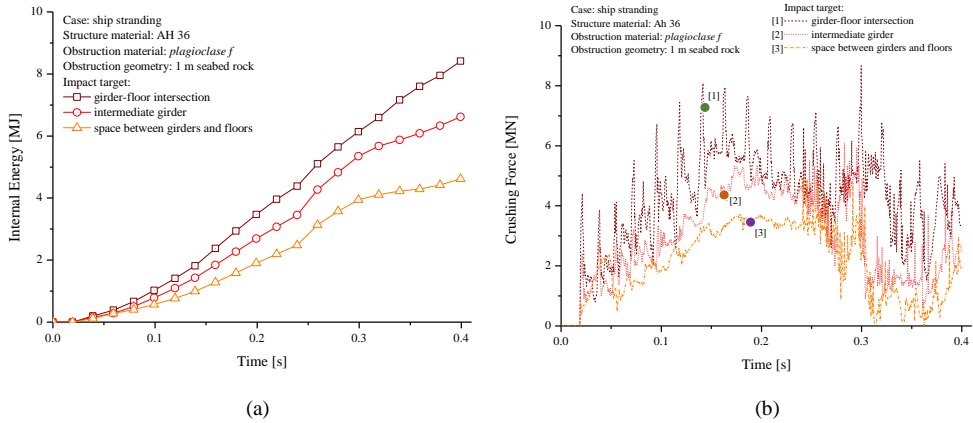
Figure 5.10. (a) The internal energy for three targets in ship stranding. (b) Tendency of the crushing force.

Discussion is continued to the crushing force in the stranding case. Early expectation that stranding scenario case would have different force tendency than the raking, was verified by the fluctuation force in Figure 5.10b. In stranding analysis, peak magnitude occurred approximately in $t_{sim.} = 0.10 - 0.20$ s which in this time span, the obstruction was approaching and surpassed the half-height of the bottom structure. After this point, the force went down as the maximum diameter of the obstruction caused similar damage size on the bottom plate. The crushing force began to increase again as deformation process of the inner bottom shell was started. Overall tendency of the structural crushing produced satisfactory in confirming level of the internal energy for different targets. High fluctuation of the girder-floor intersection indicated better capability in resisting penetration than other targets.

In terms of the crushing of the bottom structure, the initial indentation on the bottom plate was started in $t_{sim.} = 0.05$ s. It was followed by deformation on the lower part of the girder-floor intersection. This component continued to be penetrated together with damage expansion on the bottom shell. After $t_{sim.} = 0.35$ s, the deformation on the inner bottom shell was begun which in other hand, the damage on the bottom shell stopped since it was completely breached by the obstruction. In the end of penetration time, it was found that with the given setting, the tip of the rock seabed successfully penetrated the inner bottom shell. Descriptions of the progressive crush were confirmed by the damage sequence of the structural components in Figure 5.11 which compare behavior of the structural components under stranding occurred on the intermediate girder (left side of Figure 5.11) and girder-floor intersection (right side of Figure 5.11).

Failure and penetration sequences:

1. Initial contact between the obstruction, girder, and bottom plate.
2. Half obstruction penetrated the structure and damage was distributed to wider part of the bottom shell. Bottom stiffener began to deform in this phase.
3. The obstruction surpassed half of the double bottom height. Two bottom stiffeners was torn in penetration.
4. Maximum diameter occurred on the bottom shell. Compared to the stranding case on the bottom intersection, failure on the bottom shell was faster.
5. Deformation on the inner shell was begun.
6. The inner shell was breached by tip of the rock obstruction.

The impact target was determined on the intersection of floor and side girder, which until the end of analysis, effect of the center girder was not found and inner bottom stiffener was very low to resistance.

Case: ship stranding
Structure material: AH 36
Obstruction material: *plagioclase f*
Obstruction geometry: 1 m seabed rock
Impact target: intermediate girder

Impact target: bottom intersection
Structure component:
- - - center girder
.... side girder
--- transverse floor
-·-·- bottom stiffener
·········· inner bottom stiffener
- - bottom plate
-···-··- inner bottom plate

Failure and penetration sequences:

1. Initial contact between the obstruction and intersection which consisted: floor, girder, and bottom plate.
2. The obstruction reached half of the double bottom height. Maximum diameter almost got formed on the bottom shell. Two bottom stiffeners was torn in penetration.
3. Maximum diameter occurred on the bottom shell.
4. Deformation on the inner shell was begun.
5. The inner shell was breached by tip of the rock obstruction.

The impact target was determined on the intersection of floor and side girder, which until the end of analysis, effect of the center girder was not found and inner bottom stiffener was very low to resistance.
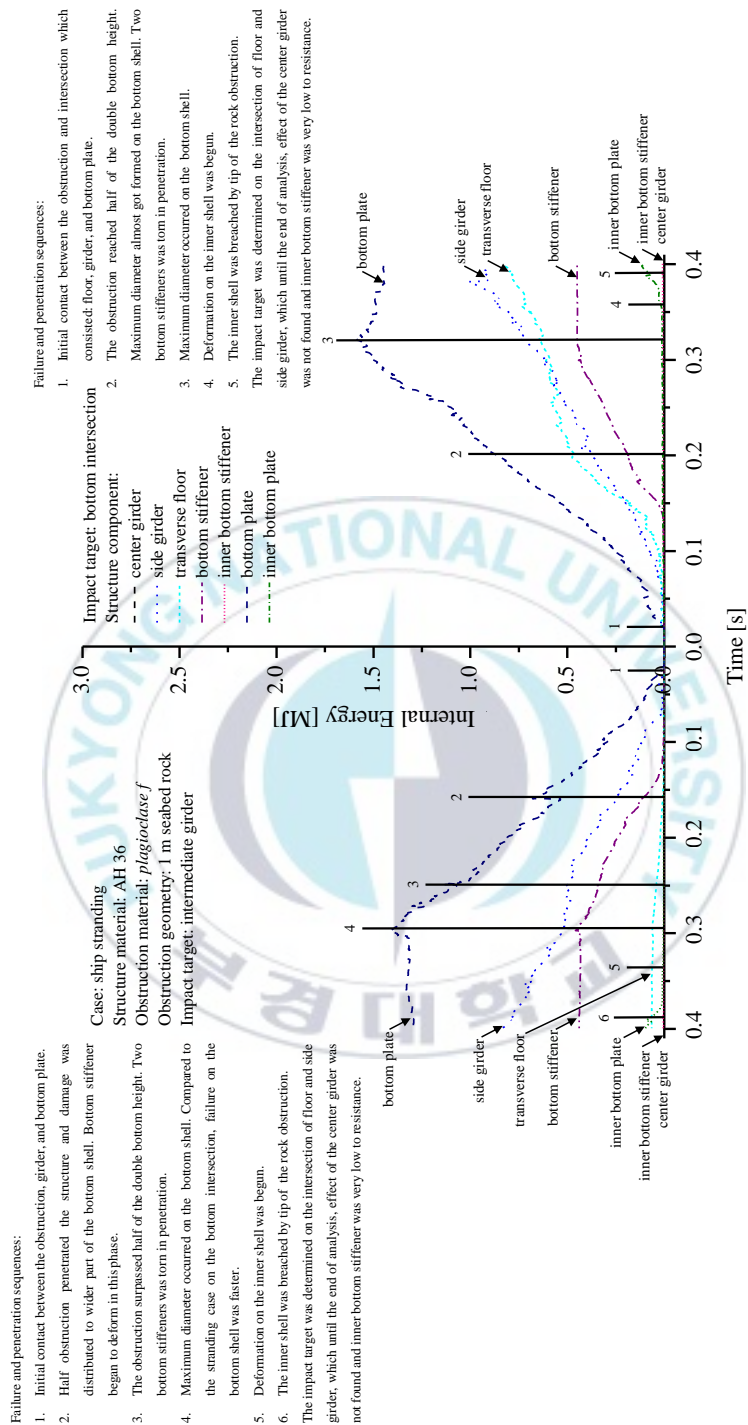

Figure 5.11. Damage sequence on the double bottom structures: ship stranding case.

Both stranding on the intermediate girder and girder-floor intersection produced similar tendency, which the bottom plate was entirely penetrated near $t_{sim.} = 0.3$ s. Nevertheless, internal energy of the bottom plate during interaction with the intermediate girder was lower than in contact with the girder-floor intersection. This tendency was previously found during observation of the overall energy (Figure 5.10a) and crushing force (Figure 5.10b). Main reason of this result is non-existent of the transverse floor on the intermediate girder, which significantly reduced structural resistance against stranding. Assessing final state of the progressive failure in $t_{sim.} = 0.35 - 0.4$ s of stranding to the intermediate girder and girder-floor intersection, the inner bottom shell was found in similar condition, i.e. successfully penetrated by the conical obstruction.

4.3 Effect of the Obstruction Geometry on the Bottom Structure

Assessment of structural crashworthiness is continued by conducting a study which addressed its focus to observe effect of seabed topology as the obstructions. As previously indicated in Subsection 3.3, in order to vary structural responses, time simulation was set to be $t_{sim.} = 0.50$ s, carbon steel material 1030 was applied on the double bottom, and the obstruction would be implemented by the Pyroxene. Raking scenario was chosen to be performed in current comparative study to produce a calculated prediction regarding structural responses against a variety of obstructions, i.e. rock and shoal.
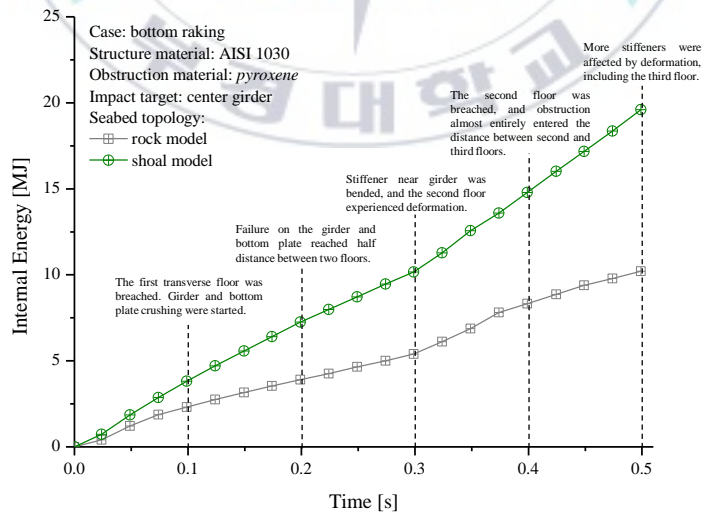

Figure 5.12. Internal energy of the rock and shoal models in the raking case.

In terms of the internal energy (Figure 5.12), the shoal obstruction produced higher level than the rock under bottom raking phenomenon, which an approximation concluded that it was twice higher than the rock. Minor increment in terms of the internal energy after deformation on the second transverse floor began ($t_{sim.} = 0.30$ s) indicated that the rock model had lower magnitude than the shoal. This behavior was verified by the crushing force (Figure 5.13) which steep angular distance on the impact surface for the shoal model produced higher force in both early contact ($t_{sim.} = 0 - 0.05$ s) and after deformation on the second floor was started ($t_{sim.} = 0.3$ s).
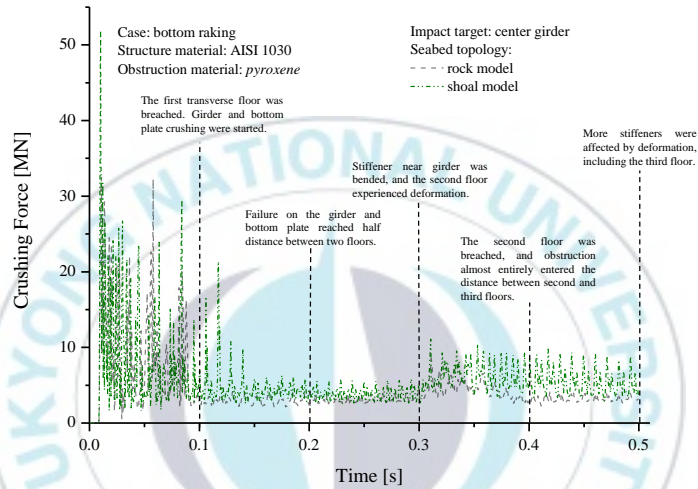

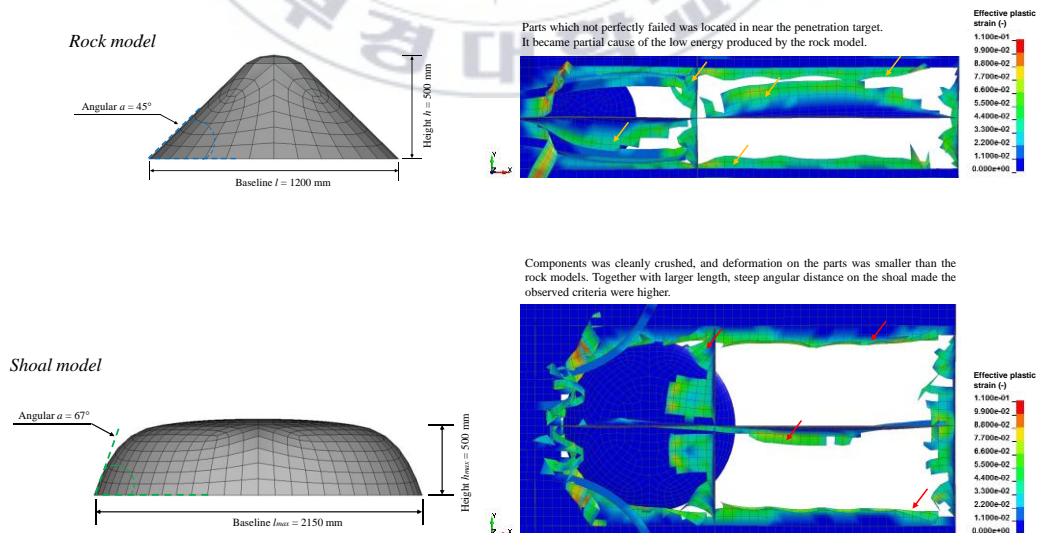Figure 5.13. Crushing force of the selected obstuctions.

Figure 5.14. Configuration of obstruction model and caused damage pattern.

In terms of structural damages, overall progressive failure on the double bottom was quantified in several stages: 1. Crushing of the first floor began, and it was followed by girder and bottom plate; 2. The tearing failures for girder and plate reached half distance of two floors in approximately ($t_{sim.}$ = 0.2 s); 3. Stiffener near girder was bended in crushing process while the second floor experienced initial deformation; 4. The second floor was breached, and obstruction almost entirely entered the next compartment (between second and third floors); 5. More stiffeners were affected by deformation, and the third floor already experienced deformation.

Overall penetration by the shoal also indicated higher tendency of this topology than the rock obstruction. Details of seabed topology concluded that contributions of baseline length l was found significantly in expanding damage range on the double bottom. As rock and shoal obstructions were fully breached the bottom structure, it could be predicted that the occurred damage width for both obstructions was similar and tended to be same with the maximum diameter of the selected obstruction in the interaction point (see explanations related to Figure 5.9). Larger size of the shoal length indicated wider diameter, which furthermore it was evidenced that larger damage extent caused by the seabed shoal than the idealized rock. More specific observation on topological aspect of the obstructions concluded that combination of the formed angular distance between baseline and obstruction increment also affected the damage pattern on the deformable structure. Steeper geometry would be cleanly crushed structural component on the double bottom (Figure 5.14), especially the longitudinal girder which hold critical role in resisting penetration during the raking case. This crushing mode was directly contributed to the observed criteria and structural response.

4.4 Overall Discussion related to Grounding

Development of calculation method in impact analysis and engineering provides several approaches to assess structural response. Early introduction was already addressed that, collaboration of these methods would provide better understanding in crashworthiness results. The benchmark in this study was conducted using combination of laboratory testing data and finite element (FE) simulation. The verified setting and configuration for the ship grounding analysis in this study. In this section, brief comparison of this work was presented by adopting empirical approach to evaluate commonly used method in impact. Several empirical formulas (Equations 5.2 to 5.5) were used to obtain the internal energy in the end

of grounding. Equation 5.2 was taken based on summary of Minorsky analyses on twenty six collision cases of ship accident. This formula was refined by Woisin who introduced low-energy collision equation by included effect of height of broken member and component thickness. In early 2000s, several mathematical forms were developed by Zhang to asses internal energy based on the damage mode. These formulas have same fundamental concept which the energy is equally perpendicular with the amount of damaged structure.

$$E = 4.72R_T + 32.7 \qquad \text{by Minorsky (1958) for high energy collision} \qquad (5.2)$$

$$E = 4.72R_T + 0.5\sum\left(h \cdot t_s^{\ 2}\right) \qquad \text{by Woisin (1979) for low energy collision} \qquad (5.3)$$

$$E = 3.50\left(\frac{t}{d}\right)^{0.67}\sigma_0 R_T \qquad \text{by Zhang (1999) for crushing and folding damage} \qquad (5.4)$$

$$E = 3.21\left(\frac{t}{l}\right)^{0.6}\sigma_0 R_T \qquad \text{by Zhang (1999) for tearing damage} \qquad (5.5)$$

where E = the absorbed energy; R_T = the volume of destroyed material; h = the height of broken or heavily deformed longitudinal members; t_s = the thickness of the members; σ_0 = the flow stress of the material; t = the average thickness of the crushed plate; d = average width of the plates in the crushed cross-section and l = critical tearing length;

Table 5.4. Summary of the energy calculation by the empirical formulas.

Scenario	Target	FE analysis (MJ)	Empirical method			Difference		
			Minorsky (MJ)	Woisin (MJ)	Zhang (MJ)	Minorsky (%)	Woisin (%)	Zhang (%)
Raking	Center girder	9.67	42.144	10.466	15.504	77.055	7.607	37.63
	Side girder	6.993	41.321	9.643	13.262	83.076	27.481	47.271
	Space between girders	5.363	39.944	7.8	10.267	86.573	31.236	47.761
Stranding	X-intersection 1	8.419	41.379	10.519	17.516	79.653	19.956	51.934
	Intermediate girder	6.62	37.917	6.182	7.453	82.542	6.609	11.177
	Space between girders and floor	4.62	36.208	3.723	6.741	87.241	19.409	31.464

Table 5.5. Calculation of the internal energy for the rock and shoal grounding.

Obstruction type	FE analysis (MJ)	Empirical method			Difference		
		Minorsky (MJ)	Woisin (MJ)	Zhang (MJ)	Minorsky (%)	Woisin (%)	Zhang (%)
Rock	10.23	40.445	8.426	14.716	74.707	17.632	30.485
Shoal	19.631	44.431	12.412	22.29	55.817	36.773	11.927

Calculation results by the empirical formula (Tables 5.4 and 5.5) showed correlation with the FE simulation in this work. The most similar was presented by the Woisin and Zhang formulas, consecutively. This tendency was successfully verified that the developed formulas successfully increased accuracy of the empirical calculations in predicting the energy criterion based on damage extent. Confirmation of the Minorsky formula was also acquired based on these results which this formula only suitable for high energy impact. If larger size of the obstruction is considered in future work, the FE energy will be approximately match with Minorsky formula. Compatibility of the collision formula was evidenced by the positive results during comparison was addressed for raking and stranding.

Table 5.6. Structural response and damage extent for the raking and stranding scenarios.

| Scenario | Target | Internal energy | Critical stress | Shear stress | Damage status | | | | | |
| | | | | | Side girder | Center girder | Stiffener | Trans. Floor | Bottom plate | Inner bottom |
		(MJ)	(MPa)	(MPa)	(-)	(-)	(-)	(-)	(-)	(-)
Raking	Center girder	9.67	489.7	282.2	-	crushed	torn	breached	torn	-
	Side girder	6.993	466.7	265.2	crushed	-	folded	breached	torn	-
	Space between girders	5.363	438.8	250.6	-	-	crushed	breached	torn	-
Stranding	x intersection 1	8.419	448.2	254.8	crushed	-	torn	crushed	breached	breached
	intermediate girder	6.62	427.9	246.4	crushed	-	torn	-	breached	breached
	Space between girders and floor	4.62	396.6	223.4	-	-	torn	-	breached	breached

Structural response and damage extent of the bottom structure after several scenarios (Table 5.6) indicated that the crashworthiness criteria were correlated each other, such as internal energy, critical stress (by von Mises approach) and shear stresses. For example, the previous discussion in the raking case concluded the highest resistance was produced by the center girder among of all targets in this case. This statement was validated by the stress level of the side girder and space between girders, which its intensity was lesser than the center girder. Same tendency was found on the stranding case, which the most intense stress was observed on the girder-floor intersection.

Table 5.7. Structural response and damage extent for the rock and shoal geometries.

| Obstruction | Baseline | Angular | Internal energy | Critical stress | Shear stress | Damage status | | | | | |
| | | | | | | Side girder | Center girder | Stiffener | Trans. Floor | Bottom plate | Inner bottom |
	(mm)	(°)	(MJ)	(MPa)	(MPa)	(-)	(-)	(-)	(-)	(-)	(-)
Rock	1200	45	10.23	542	306	-	crushed	torn	breached	torn	-
Shoal	2150	67	19.631	558	322	-	crushed	crushed	breached	torn	-

In case of the comparison between the rock and shoal geometries (Table 5.7), steep angular distance was found more capable to crush the structural component on the bottom structure. This statement was taken as two longitudinal members, namely center girder and stiffener were crushed by the obstruction in raking scenario to the center girder. Based on this result, the worst damage on the bottom structure in raking scenario will occur during the obstruction possesses striking angle 90° on its contact surface.
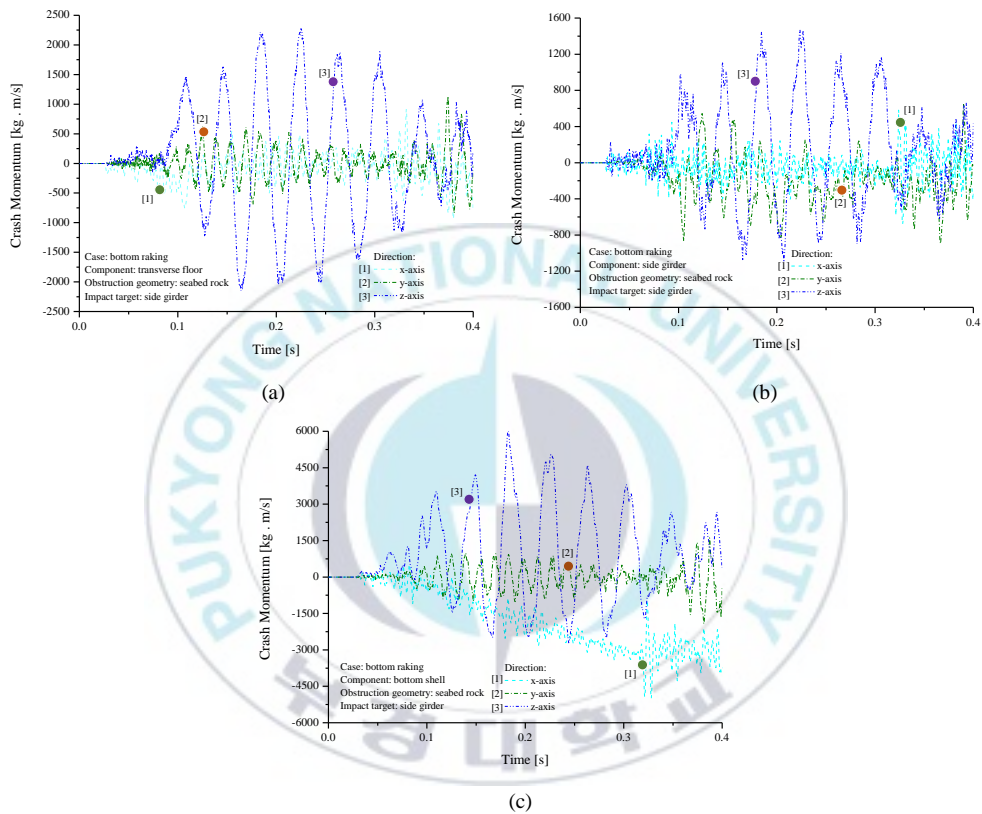
Figure 5.15. Crash momentum for component parts in the raking scenario: (a) floor, (b) girder and (c) shell.

Information of the crash momentum as a crashworthiness criterion on the structural impact was considered necessary to be observed. This criterion is useful to assess critical direction which is experienced by a structural member in grounding. Crash momentum is the criterion which reflects transfer-momentum behavior from the obstruction to the structure during impact. In Newtonian mechanics, momentum is the product of mass and velocity of an object. It is a three-dimensional vector quantity, possessing magnitude and direction. As presented in Figures 5.15 and 5.16 for the raking and stranding scenarios, grounding caused massive impact on the members in z-axis (according to the Cartesian coordinate system)

regardless the penetration mode. Even though the raking happened in longitudinal direction, critical direction was also shown in the vertical axis, same with the stranding case. The momentum concluded that during the structure crushing, the selected parts, namely floor, girder and shell was deformed in the z-axis. This result also confirmed the findings of Hu et al. (2011) regarding illustration of the plastic rolling process, which the plate was distorted in vertical axis due to advance movement of the indenter during ship grounding. Furthermore, crash momentum was satisfyingly validating other criterion, namely internal energy where the bottom plate was found received high level of momentum during impact which lead to experience major structural damage and high amount of the internal energy. Comparison with analytical theory by Simonsen (1997) which stated that the lowest part of the ship structure would experience the most damage in grounding, was successfully confirmed by the crashworthiness criteria presented in this study.
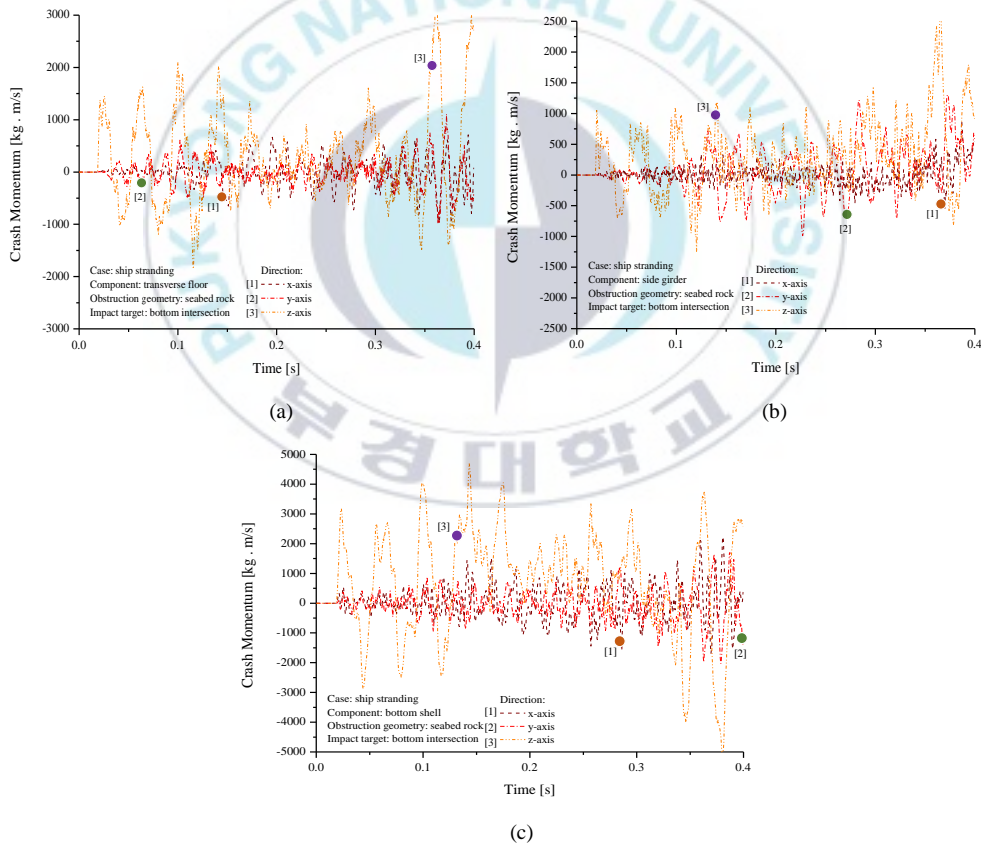
Figure 5.16. Crash momentum for component parts in the stranding scenario: (a) floor, (b) girder and (c) shell.

5. Concluding Remarks: Grounding Scenario

Main study was conducted to observe behavior of the double bottom structure against impact load. Grounding phenomena in forms of the raking and stranding were considered in this study. The internal energy criterion indicated that the raking was superior to the stranding case since it was capable to produce severe damage in longitudinal directions. However, in point of view for the cargo safety, the stranding required serious attention as in the end of simulation, the inner bottom shell was breached by the obstruction. During full-load condition, massive oil spillage can be expected as a chain reaction. Specific stranding case on the tank space between girders and floors was noted as critical scenario. This conclusion was taken after observation on the summary of damage extent and failure sequence for each component.

It was realized that evaluation on crashworthiness calculation method was necessary to keep the method in check in terms of its reliability. Besides laboratory test, empirical approach was also considered in this study. Results concluded that the present work was match with the mathematical expression for the low-energy phenomenon. Confirmation for the Minorsky formula to be applied for high-energy collision and grounding, was well-evidenced by comparison with developed formulas by Woisin and Zhang. Based on the results, it was also obtained that these two formulas presented better accuracy for the internal energy prediction than the Minorsky formula for the designated grounding scenarios. Verification of the current results was also conducted by presenting crash momentum for the raking and stranding cases, consecutively. This criterion was intended to observe direction of transfer momentum from the obstruction to the ship structure in grounding. Tendency indicated that the structural component was mostly damaged in the vertical direction. Evaluation on the crash momentum also concluded good correlation with tendency of other crashworthiness criteria. Furthermore, it was found that the bottom shell as the lowest component experienced the most damage in grounding according to energy, force, momentum and damage extent criteria. This result was satisfyingly match with the analytical theory by Simonsen which described that the lowest part on ship would experience major damage in grounding.

VI. Conclusions and Recommendations

The current benchmark analysis using explicit codes ANSYS LS-DYNA successfully produced satisfactory on terms of deformation pattern and crushing force, which satisfied structural aspect. After that, focus was addressed to assess proposed the element-length-to-thickness (ELT) ratio to obtain the most suitable mesh size and fastest simulation time without neglecting structural aspects. Conclusion of the test concluded that it was not necessary to deploy very fine mesh (below 20 mm) to obtain satisfactory structural response. It also clearly indicated that application of ELT ratio provided similar force tendency with the arbitrary fine mesh, while resulting remarkable faster time process. Furthermore, correct combination with failure criteria can be good solution in reaching convergence for nonlinear-dynamic analysis, such as collision and grounding.

Observation in collision parameters addressed two fundamental groups, namely external dynamics and internal mechanics. In the first group, impact location on side collision significantly affected the results during the selected locations had different structural preferences. Hull deck will act as longitudinal stiffener which provides more resistance against penetration of the striking ship. In terms of the striking angle, changes in β produced internal energy during ship-ship interaction. The perpendicular collision ($\beta=90°$) was evidenced more inferior than the oblique collisions. For the ship velocity, as expected in kinematic energy equation, higher velocity/speed will produce deeper penetration and finally inflicts more notable damage on the ship structure in collision.

For the second group, internal mechanics, structural design with stiffener and wider double hull reached was the best in terms of collision resistance, which was same conclusion as general ship structure theory. Besides macroscopic parameter, material-related properties was also included in discussion. Influence of material type was found significant especially for medium and high-carbon steels. Similar tendency was shared in terms of failure strain that increment of strain value will directly affect to energy and damage. Regarding the hardening input, only minor difference was spotted in implementation of hardening type, such more wrinkling on impacted structures applied by isotropic hardening.

Based on the deterministic analysis and assessment on the full-ship regions, it can be obtained that the recommended speed for the strait considered in this study is in range 5−10 kts when a crossing situation (reefer to COLREGS description) is expected to occur. Higher speeds can be used during clear conditions (good visibility and maneuverability) and when no crossing situations will take place. For crossing situations in clear conditions, an

operational speed limit of 10 kts can be applied. However, in bad weather when vision and maneuverability are restricted, the speed limit should be limited to 5 kts. This methodology can be possibly used as reasonable reference in designing various engineering instrument, such as impact absorber.

The conclusion of rebounding phenomena occurs after the striking ship experiences a zero-movement state in a side collision scenario. In this situation, the kinetic energy of the collision is completely absorbed by the struck ship. As applied material on the struck ship has elastic properties, the absorbed energy is deflected in the opposite direction, so that the striking ship undergoes rebounding. This is confirmed by the fact that kinetic energy rises again after the zero-movement state has been passed. The rebounding of the striking ship is obtained reach its farthest distance in one-velocity before rupture occurs (if tearing occurs in the 9 m/s, then the farthest distance will occur in the 8 m/s). This conclusion is summarized with the assumption the striking ship is applied by the rigid body. Considering that rebounding is reduced when rupture occurs, it can be estimated that when a deformable striking ship is deployed, the rebounding distance will be lower than it is in a scenario using a rigid striking ship.

Variation of ship grounding takes place has become serious attention of involved parties in shipbuilding and marine structures. Notable difference during the seabed penetration on double bottom invites a comparative study to provide complete crashworthiness assessment on dangerous carrier, such as tanker. Related to the structural resistance, it was found that the bottom shell and girder were vital in providing resistance in case of the double bottom experienced ship grounding. Perspective of the double bottom arrangement would be different for the raking and stranding cases, which led to variety of crashworthiness tendency. In global form, this distinction could be observed in terms of the crushing force, which in the initial contact, the raking produced significant force increment as affected by the contact surface on the transverse floor was strengthened by the stiffener, girder and floor in same time. While the stranding case presented gradual force increment which it reached the ultimate point when the obstruction fully entered the structure. Extended study on the obstruction topology concluded that the steeper angular distance and baseline length were the main parameter which directly contributed to structural damage. The shoal model emerged as worse obstruction than the rock in raking analyses.

Conventional methodology in benchmarking structural analysis has been developed through a series of test which considers time simulation. This findings is highly suggested for further analysis related to impact phenomena as developed verification method, especially

when advance computational instrument cannot be used in numerical calculation. It will allow users to obtain good structural results within more reasonable time process.

Related to ship collision, more criteria are recommended to be used in effort to develop the speed-limit regulation, especially consideration to ship maneuverability. As addition, deployment of probabilistic method to analyze ship collision (e.g. using Monte Carlo simulation) can be considered as good topic in future study. Findings of the rebounding phenomena are highly encouraged to be adopted in other impact analysis. It was realized that evaluation on crashworthiness calculation method was necessary to keep the method in check in terms of its reliability. Besides ship collision, application of mathematical expression for rapid energy estimation based on grounding damage is judged well enough. To provide more convincing research result, calculation using empirical formula can also be used in grounding benchmark to complete such general techniques, i.e. test and FE method.

Ultimately, compiled researches in the dissertation were previously performed using fundamental assumptions of structure-structure and structure-rock interactions for collision and grounding, consecutively. Consideration for fluid effect is neglected, since calculation time using numerical techniques will be explicably larger. Furthermore, effect of surrounding water has been successfully quantified in pioneer work, which concluded dissipation 20% of kinetic energy by water during structural impact. Future study is encouraged to conduct research of to compare the current findings with new designed analysis by involving fluid-structure interaction strategy in finite element method.

충돌 및 좌초 사고 시 선박 구조의 내구성 평가

Aditya Rio Prabowo

부경대학교 대학원 마린융합디자인협동과정

국문요약

본 논문에서는 선박 구조물의 건전성을 평가하고 사고 하중 시 예상되는 손상을 구조해석을 통해 검토하고자 한다. 여객선의 경우, 구조 손상은 인명피해와 재정적 손실을 야기하기에 사전 검토가 필수적이다. 또한, 산적화물선과 유조선의 경우, 언급된 피해와 더불어 화물 유출로 인한 심각한 해양환경 피해를 초래한다.

19 세기 중반 이후부터는 해양 사고의 위험성에 대비하여 선박 및 해양구조물의 안전과 관련된 국제 규정개발이 이루어지고 있다. 따라서, 선박은 설계초기단계부터 국제법규에서 규정된 사고로 인한 위험성을 고려하여 개발이 이루어져야 한다

본 연구는 빈번히 발생하는 사고 하중 중 충돌과 좌초에 대해 비선형 유한요소법 (NLFEM)을 사용 하여 강판구조물의 구조응답을 분석하였다. 우선적으로, 중형 유조선의 축소모델 (1 side-frame panel) 에 대한 실험과 결과 비교를 통해 수치적 해석방법의 적합성을 검토하였다. 실험과 수치적 방법에서의 구조적 응답의 유사성을 확인하였으며, 수치해석 방법도 확립하였다.

첫 장에서는 충돌사고 시 선박의 구조응답인 변형에너지와 내부 충돌력을 검토하였다. Ship-ship 충돌 시 구조물의 상태를 예측하기 위해, 수치해석에는 외부 역학적 요인인 위치, 각도, 속도와 내부 역학적 요인인 부재 및 구조적 유형에 따른 매개변수를 설정하였다. 이후 분석은 발생한 구조적 손상의 struck ship 에 근거하여 Sunda strait 의 제한 속도 규정을 합리적으로 참조할 수 있도록 재안하였다. 분석에 따르면, crossing 상황 (Collision Regulation - COLREGS 을 고려)이 발생할 경우 해협에서의속도는 5~10kts 범위로 권장된다. 추가적으로 리바운딩(rebounding) 시 충돌 내구성에 미치는 효과도 포함되었다.

두 번째 파트에서는 좌초 사고시나리오를 이중 선저에 대한 길이방향 손상인 raking 과 수직방향 손상인 stranding 로 가정하여 선박 구조물의 내구성을 평가하였다. Stranding 시 구조물의 흡수 에너지 및 내부 충돌력의 응답 크기가 작다는 점을

고려하여, 이중 바닥 구조물이 raking 보다 stranding 에 더 약하다는 것이 밝혀졌다. 또한, 본 장에서는 다양한 형태의 충돌체(obstruction)가 이중 선저에 미치는 영향을 검토하였다. 충돌체의 기선에 대한 길이 및 충돌 각이 주요 변수였으며, 두 변수가 커질수록 이중 선저에 더 큰 손상이 발생하였다.

본 논문에서 고찰된 결과는 해양 구조물의 충돌 및 좌초사고 시 손상평가에 합리적인 자료로 사용될 것이다.

키워드: 충돌 및 좌초, 충돌 내구성, 유한요소법 (FEM), 비선형 수치해석, 외부와 내부 역학, 제한 속도 규정, striking ship 의 리바운드 효과, raking-stranding 현상.

Reference

AbuBakar, A., Dow, R.S., 2013. Simulation of ship grounding damage using the finite element method. International Journal of Solids and Structures 50, pp. 623-636.

Amdahl J., 1995. Side collision. The 22nd WEGMT Graduate School, Accidental Loadings on Marine Structures: Risk and Response, Lyngby, Denmark.

Allianz, 2012. *Safety and shipping 1912-2012, From Titanic to Costa Concordia*. Allianz Global Corporate & Specialty, Munich, Germany.

Allianz, 2017. *Safety and Shipping, Review 2017*. Allianz Global Corporate & Specialty, Munich, Germany.

Alsos, H.S., Amdahl, J., 2007. On the resistance of tanker bottom structures during stranding. Marine Structures 20, pp. 218-237.

Alsos, H.S., Amdahl, J., 2009. On the resistance of penetration of stiffened plates, Part I – Experiments. International Journal of Impact Engineering 36, pp. 799-807.

Alsos, H.S., Amdahl, J., Hopperstad, O.S., 2009. On the resistance of penetration of stiffened plates, Part II – Numerical analysis. International Journal of Impact Engineering 36, pp. 875-887.

ANSYS, 2017. *ANSYS LS-DYNA User's Guides*. ANSYS Inc., Pennsylvania, US.

Baek, S.J., Sohn, J.M., Paik, J.K., Kim, S.J., 2018. Development of a method for prediction of residual strength for prevention of secondary accidents on large oil tankers subjected to collisions. Journal of the Society of Naval Architects of Korea 55, pp. 144.152 (in Korean).

Bae, D.M., Prabowo, A.R., Cao, B., Sohn, J.M., Zakki, A.F., Wang, Q., 2016a. Numerical simulation for the collision between side structure and level ice in event of side impact scenario. Latin American Journal of Solids and Structures 13, pp. 2991-3004.

Bae, D.M., Prabowo, A.R., Cao, B., Zakki, A.F., Haryadi, G.D., 2016b. Study on collision between two ships using selected parameters in collision simulation. Journal of Marine Science and Application 15, pp. 63-72.

Bathe, K.J., 1996. *Finite Element Procedures*. Prentice Hall, New Jersey, US.

Calle, M.A.G., Oshiro, R.E., Alves, M., 2017. Ship collision and grounding: scaled experiments and numerical analysis. International Journal of Impact Engineering 103, pp. 195-210.

Callister Jr., W.D., 2007. *Material Science and Engineering; An Introduction, Seventh Ed*. John Wiley & Sons (Publisher), Inc., New Jersey, US.

Christensen, N.I., 1996. Poisson's ratio and crustal seismology. Journal of Geophysical Research 101, pp. 3139-3156.

Cho, S.R., Park, J.Y., Song, S.U., Park, S.H., 2018. Scale effects on the structural behavior of steel unstiffened plates subjected to lateral collision. Journal of the Society of Naval Architects of Korea 55, pp. 178-186 (in Korean).

Cockroft, M.G., Latham, D.J., 1968. Ductility and the workability of metals. Journal of the Institute of Metals 96, pp. 33-39.

Fang, C., Das, P.K., 2005. Survivability and reliability of damaged ships after collision and grounding. Ocean Engineering 32, pp. 293–307.

GL, 2003. *Development of Explanatory Notes for Harmonized SOLAS Chapter II-1*. International Maritime Organization, London, UK.

Goerlandt, F., Kujala, P., 2014. On the reliability and validity of ship-ship collision risk analysis in light of different perspectives on risk. Safety Science 62, pp. 348–365.

Haag, S.R., 2017. *Ship Grounding Damage*. Delft University of Technology, Delft, The Netherlands.

Haris, S., Amdahl, J., 2013. Analysis of ship-ship collision damage accounting for bow and side deformation interaction. Marine Structures 32, pp. 18–48.

Heinvee, M., Tabri, K., 2015. A simplified method to predict grounding damage of double bottom tankers. Marine Structures 43, pp. 22-43.

Hu, Z., Amdahl, J., Hong, L., 2011. Verification of a simplified analytical method for predictions of ship groundings over large contact surfaces by numerical simulations. Marine Structures 24, pp. 436-458.

IMO, 1972. *International Regulations for Preventing Collision at Sea (as amended by Resolution A464(XII), A626(15), A678(16) and A736(18))*. International Maritime Organization, London, UK.

IMO, 2008. *Report of the Maritime Safety Committee on Its Eighty-Fourth Session (MSC 84/24Add.1 - Annex 1)*. International Maritime Organization, London, UK.

Kitamura, O., 2002. FEM approach to the simulation of collision and grounding damage. Marine Structures 15, pp. 403-428.

Lamb, T., 2003. Ship Design and Construction. Society of Naval Architects and Marine Engineers, New Jersey, US.

Leheta, H.W., Badran, S.F., Elhanafi, A.S., 2015. Ship structural integrity using new stiffened plates. Thin-Walled Structures 94, pp. 545-561.

Lehmann, E., Peschmann J., 2002. Energy absorption by the steel structure of ships in the event of collisions. Marine Structures 15, pp. 429-441.

Liu, B., Soares, C.G., 2015. Simplified analytical method for evaluating web girder crushing during ship collision and grounding. Marine Structures 42, pp. 71-94.

Liu, B., Villavicencio, R., Zhang, S., Soares, C.G., 2017a. A simple criterion to evaluate the rupture of materials in ship collision simulations. Marine Structures 54, pp. 92-111.

Liu, B., Zhu, L., Chen, L., 2017b. Numerical assessment of the resistance of ship double-hull structures in stranding. The 6th International Conference on Marine Structures (MARSTRUCT), Lisbon, Portugal.

Marine Traffic, Dharma Ferry 3, ⟨www.marinetraffic.com⟩, accessed in the 2 January 2017.

Minorsky, V.U., 1958. An analysis of ship collision with reference to protection of nuclear power ships. Journal of Ship Research 3, pp. 1-4.

National Government, 1983. *Indonesian Economic Exclusive Zone (UU 5/1983)*. Government of Indonesia, Jakarta, Indonesia.

Ozguc, O., Das, P.K. and Barltrop, N., 2005. A comparative study on the structural integrity of single and double skin bulk carriers under collision damage. Marine Structures 18, pp. 511-547.

Paik, J.K., Hyun, M.K., Lee, T.L., 1994. On the grounding damage of ship bottom stiffened platings (Part I: Experiment). Transaction of the Society of Naval Architects of Korea 31, 121-131 (in Korean).

Paik, J.K., Lee, M.S., 2005. A semi-analytical method for the elastic-plastic large deflection analysis of stiffened panels under combined biaxial compression/tension, biaxial in-plane bending, edge shear, and lateral pressure loads. Thin-Walled Structures 43, pp. 375-410.

Paik, J.K., Pedersem, P.T., 1995. Collision strength analysis of double hull tanker. Transaction of the Society of Naval Architects of Korea 32, 103-117 (in Korean).

Paik, J.K., Pedersen, P.T., 1996. Modelling of the internal mechanics in ship collisions. Ocean Engineering 23, pp. 107–142.

Paik, J.K., Seo, J.K., 2007. A method for progressive structural crashworthiness analysis under collision and grounding. Thin-Walled Structures 45, pp. 15-23.

Paik, J.K., Thayamballi, A.K., 2003. A concise introduction to the idealized structural unit method for nonlinear analysis of large plated structures and its application. Thin-Walled Structures 41, pp. 329-355.

Patuzi, D., 2015. The concept of the economic exclusive zone. Academic Journal of Bussiness, Administration, Law and Social Science 1, pp. 149-159.

Peschmann, J., Kulzep, A., 2000. *Final Report for BMBF Life-Cycle Design, Part D2A: Side Collision of Skin Ship*. Technical University of Hamburg, Hamburg, Germany.

Prabowo, A.R., Baek, S.J., Cho, H.J., Byeon, J.H., Bae, D.M., Sohn, J.M., 2017a. The effectiveness of thin-walled hull structures against collision impact. Latin American Journal of Solids and Structures 14, pp. 1345-1360.

Prabowo, A.R., Baek, S.J., Byeon, J.H., Bae, D.M., Cho, J.H., Sohn, J.M., 2017i. Investigation on the structural damage of a double-hull ship, Part I – Ship collision. Procedia Structural Integrity 5, pp. 935-942.

Prabowo, A.R., Baek, S.J., Lee, S.G., Bae, D.M., Sohn, J.M., 2017f. Investigation of impact phenomena on the marine structures: Part II - Internal energy of the steel structure applied by selected materials in the ship-ship collision incidents. Journal of Physics: Conference Series 953, article no. 012002.

Prabowo, A.R., Bae, D.M., Sohn, J.M., Cao, B., 2016b. Energy behavior on side structure in event of ship collision subjected to external parameters. Heliyon 2, article no. e00192.

Prabowo, A.R., Bae, D.M., Sohn, J.M., Zakki, A.F., Cao, B., Cho, J.H., 2017m. Effects of the rebounding of a striking ship on structural crashworthiness during ship-ship collision. Thin-Walled Structures 115, pp. 225-239.

Prabowo, A.R., Bae, D.M., Sohn, J.M., Zakki, A.F., Cao, B., Wang, Q., 2017c. Analysis of structural damage on the struck ship under side collision scenario. Alexandria Engineering Journal, *in production*.

Prabowo, A.R., Bae, D.M., Sohn, J.M., Zakki, A.F., Cao, B., Wang, Q., 2017n. Analysis of structural behavior during collision event accounting for bow and side structure interaction. Theoretical and Applied Mechanics Letters 7, pp. 6-12.

Prabowo, A.R., Bae, D.M., Sohn, J.M., Zakki, A.F., Cao, B., 2017l. Development in calculation and analysis of collision and grounding on marine structures and ocean engineering fields. Journal of Aquaculture and Marine Biology 5, article no. 00116.

Prabowo, A.R., Bae, D.M., Sohn, J.M., Zakki, A.F., Cao, B., 2017o. Rapid prediction of damage on a struck ship accounting for side impact scenario models. Open Engineering 7, pp. 91-99.

Prabowo, A.R., Bae, D.M., Sohn, J.M., Zakki, A.F., 2016a. Evaluating the parameter influence in the event of a ship collision based on the finite element method approach. International Journal of Technology 4, pp. 592-602.

Prabowo, A.R., Bae, D.M., Sohn, J.M., 2017k. Behavior prediction of ship structure due to side impact scenario by dynamic-nonlinear finite element analysis. Applied Mechanics and Materials 862, pp. 253-258.

Prabowo, A.R., Bahatmaka, A., Cho, J.H., Sohn, J.M., Bae, D.M., Samuel, S., Cao, B., 2017h. Analysis of structural crashworthiness on a non-ice class tanker during stranding accounting for the sailing routes. The 17th International Congress of the Maritime Association of the Mediterranean (IMAM), Lisbon, Portugal.

Prabowo, A.R., Cao B., Bae, D.M., Bae, S.Y., Zakki, A.F., Sohn, J.M., 2017d. Structural analysis of the double bottom structure during ship grounding by finite element approach. Latin American Journal of Solids and Structures 14, pp. 1-18.

Prabowo, A.R., Cho, H.J., Byeon, J.H., Bae, D.M., Sohn, J.M., 2017e. Investigation of impact phenomena on the marine structures: Part I - On the behaviour of thin-walled double bottom tanker during rock-structure interaction. Journal of Physics: Conference Series 953, article no. 012003.

Prabowo, A.R., Cho, H.J., Lee, S.G., Bae, D.M., Sohn, J.M., Cho, J.H., 2017j. Investigation on the structural damage of a double-hull ship, Part II – Grounding impact. Procedia Structural Integrity 5, pp. 943-950.

Prabowo, A.R., Sohn, J.M., Bae, D.M., Cho, J.H., 2017b. Performance assessment on a variety of double side structure during collision interaction with other ship. Curved and Layered Structures 4, pp. 255-271.

Prabowo, A.R., Sohn, J.M., Byeon, J.H., Bae, D.M., Zakki, A.F., Cao, B., 2017g. Structural analysis for estimating damage behavior of double hull under ice-grounding scenario models. Key Engineering Materials 754, pp. 303-306.

Rice, J., Tracey, D., 1969. On the ductile enlargement of voids in triaxial stress fields. Journal of Mechanics and Physics of Solids 17, pp. 201-217.

Rosato, D.V., Rosato, D.V., (2003). *Plastic Engineered Product Design*. Elsevier: Oxford, UK.

Simonsen, B.C., Hansen, P.F., 2000. Theoretical and statistical analysis of ship grounding accidents. Journal of Offshore Mechanics and Arctic Engineering 122, pp. 200-207.

Simonsen, B.C., Wierzbicki, T., 1998. Plasticity, fracture and friction in steady state plate cutting. International Journal of Impact Engineering 21, pp. 387-411.

Simonsen, B.C., 1997a. Ship grounding on rock – I. Theory. Marine Structures 10, pp. 519-562.

Simonsen, B.C., 1997b. Ship grounding on rock – II. Validation and application. Marine Structures 10, pp. 563-584.

Sormunen, O.V.E., Kõrgesaar, M., Tabri, K., Heinvee, M., Urbel, A., Kujala, P., 2016. Comparing rock shape models in grounding damage modelling. Marine Structures 50, pp. 205–223.

Törnqvist, R., 2003. *Design of Crashworthy Ship Structures*. Technical University of Denmark, Lyngby, Denmark.

Wiśniewski, K., Kołakowski, P., 2003. The effect of selected parameters on ship collision results by dynamic FE simulations. Finite Elements in Analysis and Design 39, pp. 985-1006.

Woisin, G., 1979. Design against collision. Schiff & Hafen 31, pp. 1059-1069.

Yeom, C.W., Nho, I.S., 2015. Redudancy analysis of stiffened panel with plastic deformation due to collision. Journal of the Society of Naval Architects of Korea 52, pp. 161-169 (in Korean).

Yip, T.L., Talley, W.K., Jin, D., 2011. The effectiveness of double hulls in reducing vessel accident oil spillage. Marine Pollution Bulletin 62, pp. 2427–2432.

Yu, Z., Hu, Z., Wang, G., 2015. Plastic mechanism analysis of structural performances for stiffeners on bottom longitudinal web girders during a shoal grounding accident. Marine Structures 40, pp. 134–158.

Zhang, S., 1999. *The Mechanics of Ship Collisions.* Technical University of Denmark, Lyngby, Denmark.

Zhang, J., Zhang, D., Yan, X., Haugen, S., Soares, C.G., 2015a. A distributed anti-collision decision support formulation in multi-ship encounter situations under COLREGs. Ocean Engineering 105, pp. 336-348.

Zhang, S., 1999. *The Mechanics of Ship Collisions.* Technical University of Denmark, Lyngby, Denmark.

Zhang, W., Goerlandt, F., Montewka, J., Kujala, P., 2015b. A method for detecting possible near miss ship collisions from AIS data. Ocean Engineering 107, pp. 60-69.

Acknowledgements